THE MINISTRY OF SCIENCE AND HIGHER EDUCATION OF THE RUSSIAN FEDERATION

ISSN 2687-0517

Computing, Telecommunications and Control

Vol. 19, No. 1
2026

Peter the Great St. Petersburg
Polytechnic University
2026

The journal is included in the List of Leading PeerReviewed Scientific Journals and other editions to publish major findings of PhD theses for the research degrees of Doctor of Sciences and Candidate of Sciences.

Open access journal is to publish articles of a high scientific level covering advanced experience, research results, theoretical and practical problems of informatics, electronics, telecommunications, and control.

The journal is indexed by Ulrich's Periodicals Directory, Google Scholar, EBSCO, ProQuest, Index Copernicus, VINITI RAS Abstract Journal (Referativnyi Zhurnal), VINITI RAS Scientific and Technical Literature Collection, Russian Science Citation Index (RSCI) database Scientific Electronic Library and Math-Net.ru databases.

The journal is registered with the Federal Service for Supervision in the Sphere of Telecom, Information Technologies and Mass Communications (ROSKOMNADZOR). Certificate ЭЛ No. ФС77-77378 issued 25.12.2019.

Editorial office

Dr. Sc., Professor A.S. Korotkov – Editor-in-Chief;

Ph.Ch.S. Bastian – literary editor, proofreader; G.A. Pyshkina – editorial manager; A.A. Kononova – computer layout; I.E. Lebedeva – English translation.

Address: 195251 Polytekhnicheskaya Str. 29, St. Petersburg, Russia.

+7 (812) 552-6216, e-mail: infocom@spbstu.ru

Release date: 31.03.2026

МИНИСТЕРСТВО НАУКИ И ВЫСШЕГО ОБРАЗОВАНИЯ РОССИЙСКОЙ ФЕДЕРАЦИИ

ISSN 2687-0517

Информатика, телекоммуникации и управление

Том 19, № 1
2026

Санкт-Петербургский политехнический
университет Петра Великого
2026

ИНФОРМАТИКА, ТЕЛЕКОММУНИКАЦИИ И УПРАВЛЕНИЕ

Журнал с 2002 года входит в Перечень ведущих рецензируемых научных журналов и изданий, в которых должны быть опубликованы основные результаты диссертаций на соискание ученой степени доктора и кандидата наук.

Сетевое издание открытого доступа публикует статьи высокого научного уровня, освещающие передовой опыт, результаты НИР, теоретические и практические проблемы информатики, электроники, телекоммуникаций, управления.

Сведения о публикациях представлены в Реферативном журнале ВИНИТИ РАН, в международной справочной системе «Ulrich`s Periodical Directory», в Российской государственной библиотеке. В базах данных: Российский индекс научного цитирования (РИНЦ), Google Scholar, EBSCO, Math-Net.Ru, ProQuest, Index Copernicus.

Журнал зарегистрирован Федеральной службой по надзору в сфере информационных технологий и массовых коммуникаций (Роскомнадзор). Свидетельство о регистрации ЭЛ № ФС77-77378 от 25.12.2019.

Учредитель и издатель: Санкт-Петербургский политехнический университет Петра Великого, Санкт-Петербург, Российская Федерация.

Редакция журнала

д-р техн. наук, профессор А.С. Коротков – главный редактор;

Ф.К.С. Бастиан – литературный редактор, корректор; Г.А. Пышкина – ответственный секретарь, выпускающий редактор;

А.А. Кононова – компьютерная вёрстка; И.Е. Лебедева – перевод на английский язык.

Адрес редакции: Россия, 195251, Санкт-Петербург, ул. Политехническая, д. 29.

Тел. редакции +7(812) 552-62-16, e-mail редакции: infocom@spbstu.ru

Дата выхода: 31.03.2026

Contents

Содержание

MONETEC 2026

The international Science and Technology Conference «Modern Network Technologies, MoNeTec-2026»

CALL FOR PAPERS

https://monetec.ru/

Oct 24-30, 2026

Moscow, Russia

Российская Академия Наук

ОТДЕЛЕНИЕ МАТЕМАТИЧЕСКИХ НАУК

SPRINGER NATURE

CONFERENCE

The MoNeTec conference gathers specialists of the international scientific community, research departments of corporations, start-ups, representatives of industry and business, development institutions, and public authorities to discuss promising and relevant technologies in the field of computer networks, virtualization of network resources, and cloud computing. VI International Conference MoNeTec-2026 will be dedicated to the 100th anniversary of Lev Korolev – patriarch of system programming in the USSR. Under his leadership, the first operating system for the famous Russian computer, BESM-6, was created in 1968.

TOPICS

- Computation Centric Network as a network with “Computation on Demand” as a service: Architecture, Protocols, Models
- Quality of Service in networking: monitoring and control methods and tools
- Computation Workload allocation, scheduling and control in Computation Centric Networks: methods and tools
- Languages for application modeling and specification
- Mathematical models and methods for resource control and management in Computation Centric Network
- IoT integration with Computation Centric Network
- Problems of Resource disaggregation paradigm: how to dynamically “compose” a logical server for application needs
- High-speed routing and switching devices: architecture, mathematical models and simulation
- Cell-free cellular network and Scalable MIMO

PAPER SUBMISSION

Papers may be submitted in English or in Russian. Peer-reviewed, accepted and presented papers in English will be published in the Springer CCIS series. Peer-reviewed, accepted and presented papers in Russian will be published in eLibrary.ru and indexed in RSCI.

IMPORTANT DATES

- **May 01, 2026** • Extended Abstract Submission
- **May 15, 2026** • Preliminary Acceptance Notification
- **June 15, 2026** • Paper Submission
- **September 05, 2026** • Acceptance Notification
- **October 05, 2026** • Camera Ready Paper Submission
- **October 24-30, 2026** • MoNeTec-2026 Conference incl. Tutorials

In-person and online participation

ORGANIZERS

Московский государственный университет имени М.В. Ломоносова

CONSORTIUM NETWORK AND CLOUD TECHNOLOGIES

Центр прикладных исследований компьютерных сетей

MEDIA PARTNERS

Научная Россия

Издательский дом Юр-ВАК

Спектр

Издательский Дом «ГУБКИН»

INJOIT

ИНФОРМАТИК@

Журнал “ИСУП”

ИНФОРМАЦИОННЫЕ ТЕХНОЛОГИИ

Computing, Telecommunication and Control, 2026, Vol. 19, No. 1, Pp. 8–15.
Информатика, телекоммуникации и управление. 2026. Том 19, № 1. С. 8–15.

Intelligent Systems and Technologies, Artificial Intelligence

Интеллектуальные системы и технологии, искусственный интеллект

Research article
DOI: https://doi.org/10.18721/JCSTCS.19101
UDC 004.932.72

CROSS-DOMAIN DEEP TRANSFER LEARNING FOR BRANCHING STRUCTURE SEGMENTATION

F. Shariaty ✉, *V.A. Pavlov*, *E.A. Medvedeva*

Peter the Great St. Petersburg Polytechnic University,
St. Petersburg, Russian Federation

✉ shariaty3@gmail.com

Abstract. Segmentation of thin, branching structures in volumetric imaging is a challenging computer vision task due to low contrast, strong class imbalance, and large variability in scale and topology. This work investigates a cross-domain deep transfer learning strategy that exploits morphological similarity between vascular-like branching patterns in different imaging modalities. Models are first pre-trained on the data-rich FIVES retinal vessel dataset and then fine-tuned on a subset of the NSCLC-Radiogenomics chest CT dataset containing annotations of branching structures. We evaluate four U-Net-based architectures – U-Net, Attention U-Net, R2 U-Net and Dense U-Net – and compare them with DeepLabV3 models using ResNet50 and ResNet101 backbones. A unified training pipeline with multi-stage intensity and contrast normalization is employed, along with a 10-fold stratified cross-validation protocol. Performance is assessed using accuracy, precision, Dice (F1 score), and area under the ROC curve (AUC). Cross-domain transfer learning leads to a substantial improvement over training from scratch: Dice scores increase from near-zero values to above 0.48 for the best-performing models. Attention U-Net achieves the highest Dice score of 0.4814, while DeepLabV3 (ResNet50) attains the highest AUC of 0.9621. Dense U-Net also provides competitive results, whereas R2 U-Net benefits less from the proposed transfer scheme. The results demonstrate that leveraging cross-domain morphological priors is an effective way to enhance segmentation of branching structures in data-scarce CT scenarios. The proposed framework provides a strong, reproducible baseline for future research on transfer learning and fine-structure segmentation in volumetric images.

Keywords: branching structure segmentation, cross-domain transfer learning, deep learning, U-Net, DeepLabV3

Acknowledgements: The research was supported by the Russian Science Foundation grant No. 24-25-00204 “Integrating genomic analysis and medical imaging to accurately predict and predict cancer characteristics and treatment outcomes in early-stage non-small cell lung cancer”. Available online: https://rscf.ru/project/24-25-00204/.

Citation: Shariaty F., Pavlov V.A., Medvedeva E.A. Cross-domain deep transfer learning for branching structure segmentation. Computing, Telecommunications and Control, 2026, Vol. 19, No. 1, Pp. 8–15. DOI: 10.18721/JCSTCS.19101

Научная статья
DOI: https://doi.org/10.18721/JCSTCS.19101
УДК 004.932.72

МЕЖДОМЕННОЕ ГЛУБОКОЕ ТРАНСФЕРНОЕ ОБУЧЕНИЕ ДЛЯ СЕГМЕНТАЦИИ РАЗВЕТВЛЕННЫХ СТРУКТУР

Ф. Шариати ✉ , *В.А. Павлов* , *Е.А. Медведева*

Санкт-Петербургский политехнический университет Петра Великого,
Санкт-Петербург, Российская Федерация

✉ shariaty3@gmail.com

Аннотация. Сегментация тонких разветвленных структур в объемной визуализации является нетривиальной задачей компьютерного зрения из-за низкого контраста, выраженного дисбаланса классов и большой вариативности в масштабе и топологии. В данной работе исследуется подход междоменного глубокого трансферного обучения, использующий морфологическое сходство сосудистоподобных разветвленных структур в разных модальностях визуализации. Модели предварительно обучаются на богатом данными наборе FIVES для сегментации сосудов сетчатки, после чего дообучаются на подмножестве набора данных NSCLC-Radiogenomics с КТ-изображениями грудной клетки и аннотациями разветвленных структур. Оцениваются четыре архитектуры на основе U-Net (стандартная U-Net, Attention U-Net, R2 U-Net и Dense U-Net), а также модели DeepLabV3 с базовыми сетями ResNet50 и ResNet101. Применяется единый конвейер обучения, включающий многоэтапную нормализацию интенсивностей и контраста, а также 10-кратную стратифицированную перекрестную проверку. Качество сегментации измеряется метриками Accuracy, Precision, Dice (F1-мера) и площадью под ROC-кривой (AUC). Междоменное трансферное обучение приводит к существенному улучшению по сравнению с обучением «с нуля»: значения Dice увеличиваются с почти нулевых до 0,48 и более для лучших моделей. Модель Attention U-Net достигает максимального значения Dice 0,4814, тогда как DeepLabV3 (ResNet50) демонстрирует наивысшее значение AUC – 0,9621. Dense U-Net показывает сопоставимые результаты, в то время как R2 U-Net в меньшей степени выигрывает от предложенной схемы трансфера. Полученные результаты показывают, что использование междоменных морфологических априорных знаний является эффективным способом повышения качества сегментации разветвленных структур в условиях дефицита размеченных КТ-данных. Предложенная методология формирует воспроизводимую базу для дальнейших исследований в области трансферного обучения и сегментации тонких древовидных структур в объемной визуализации.

Ключевые слова: сегментация разветвленных структур, междоменное трансферное обучение, глубокое обучение, U-Net, DeepLabV3

Финансирование: Исследование выполнено за счет гранта Российского научного фонда в рамках реализации проекта «Интеграция геномного анализа и медицинской визуализации для точного прогнозирования и предсказания характеристик рака и результатов лечения при ранней стадии неклеточного рака легкого» (Соглашение №24-25-00204, https://rscf.ru/project/24-25-00204/).

Для цитирования: Shariaty F., Pavlov V.A., Medvedeva E.A. Cross-domain deep transfer learning for branching structure segmentation // Computing, Telecommunications and Control. 2026. Т. 19, № 1. С. 8–15. DOI: 10.18721/JCSTCS.19101

Introduction

Segmentation of thin, branching vascular structures in chest computed tomography (CT) images is a challenging problem in image analysis and computer vision. These structures exhibit large variation in scale, complex topology and often low contrast with respect to surrounding tissue, which makes

robust extraction difficult [1–5]. In addition, the foreground (vessels) typically occupies only a small fraction of the image volume, leading to strong class imbalance and making learning-based methods sensitive to overfitting [6].

Classical image processing techniques, such as thresholding, region growing and edge-based methods, have been widely used for vessel extraction [7, 8]. Although these approaches are conceptually simple and computationally efficient, their performance is highly dependent on hand-crafted parameters and they struggle with noise, partial volume effects and the wide range of vessel calibers present in CT images. The emergence of deep learning, and in particular convolutional neural networks (CNNs), has significantly advanced the state of the art in segmentation of complex anatomical and vascular structures [9, 10]. Encoder–decoder architectures with skip connections, such as U-Net, have become a *de facto* standard due to their ability to combine high-level semantic information with fine-grained spatial detail.

A key limitation in many volumetric segmentation tasks, however, is the scarcity of large, pixel-level annotated datasets, especially for small or hard-to-label structures. Training deep architectures from scratch on such limited data often results in poor generalization. Transfer learning provides an effective strategy to alleviate this problem by reusing features learned in a data-rich source domain to initialize models in a data-scarce target domain [11]. When there is morphological similarity between structures in the source and target domains – such as tree-like vascular networks – transfer learning can be particularly beneficial, since the learned feature hierarchies capture reusable patterns of branching geometry and local appearance.

In this work, we investigate a cross-domain transfer learning strategy for segmentation of branching vascular structures in chest CT images. Our hypothesis is that the intricate, tree-like morphology of retinal vessels, for which large annotated datasets are available, can serve as a suitable source domain for learning generic vessel features. These features are then transferred and fine-tuned for segmenting morphologically similar, but anatomically different, vascular structures in CT volumes. To evaluate this idea, we consider several U-Net-based architectures: standard U-Net, Attention U-Net [12], R2 U-Net [13] and Dense U-Net [14], and compare them with DeepLabV3 models equipped with ResNet backbones [15].

Materials and methods

This study applies a cross-domain transfer learning methodology using two distinct datasets. For pre-training, the Fundus Image Dataset for AI-based Vessel Segmentation (FIVES) [16] dataset was used. This dataset contains 800 high-resolution (2048×2048) fundus images with pixel-wise vessel annotations designed for data-driven vessel segmentation. For fine-tuning, we used the NSCLC-Radiogenomics collection from The Cancer Imaging Archive (TCIA) [17], which provides 286754 chest CT slices from 211 volumes. A subset of this collection with annotations of branching vascular structures was employed as the target domain.

A multi-stage image preprocessing pipeline was implemented to enhance vessel-like feature extraction and standardize input data. All images were converted to grayscale, followed by Z-normalization $(x-\mu)/\sigma$ and Min–Max normalization (scaled to [0, 255]). Contrast Limited Adaptive Histogram Equalization (CLAHE, clip limit 2.0) was then applied to improve local contrast, followed by gamma correction ($\gamma = 1.2$) to emphasize darker structures.

The transfer learning procedure consisted of two phases:

1) pre-training on FIVES using binary cross-entropy loss and the Adam optimizer to learn general vessel-like features;

2) fine-tuning on the NSCLC-Radiogenomics subset with encoder weights initialized from the pre-trained models, a reduced learning rate and a cosine annealing schedule to adapt the representations to CT-domain branching structures.

Both datasets were evaluated using 10-fold stratified cross-validation for robust assessment of generalization. Model performance was measured using accuracy, precision, Dice (F1 score) and Area Under the Receiver Operating Characteristic Curve (AUC). Statistical comparisons included p-values and 95% confidence intervals (CI). Hyperparameters included a batch size of 16, an initial learning rate of 10^{-4} (decayed via cosine annealing) and training for 100 epochs on an NVIDIA RTX 2080 Ti GPU.

Results and discussion

Both the FIVES retinal vessel dataset and the NSCLC-Radiogenomics CT dataset were systematically divided into 10 folds for stratified cross-validation. For the FIVES dataset (800 images), each fold contained a proportional split for training, validation and testing. Similarly, the CT branching-structure dataset (100 images) was divided into 10 folds, ensuring a representative distribution across training, validation and testing sets within each fold. For each fold, models were trained on the training subset and evaluated on the held-out test subset, and the reported metrics are averages over all CT test folds.

The performance of the models on the retinal vessel segmentation task (pre-training phase, trained and tested on the FIVES dataset) is summarized in Table 1.

Table 1

Performance comparison of deep learning models for retinal vessel segmentation

Model	Accuracy	Precision	Dice (F1-Score)	AUC
U-Net	0.9867	0.9386	0.8974	0.9843
Attention U-Net	0.9872	0.9142	0.9038	0.9871
Dense U-Net	0.9865	0.9269	0.8969	0.9834
R2 U-Net	0.9232	0.4058	0.3453	0.8300
DeepLabV3 (ResNet50)	0.9640	0.7503	0.7234	0.9772
DeepLabV3 (ResNet101)	0.9628	0.7405	0.7138	0.9763

As shown in Table 1, the U-Net variants generally achieve high performance on the retinal vessel segmentation task. Attention U-Net demonstrates the highest Dice (F1 score) of 0.9038 and the best AUC of 0.9871, closely followed by U-Net and Dense U-Net. This indicates that the attention mechanism effectively enhances the model's ability to focus on relevant features for segmenting thin vessel structures. R2 U-Net performs noticeably worse across all metrics (Dice 0.3453, AUC 0.8300), suggesting that its recurrent residual structure may be suboptimal for this setting or require different hyperparameter tuning. DeepLabV3 models also show strong performance, particularly in AUC, but remain slightly behind the best U-Net variants in terms of Dice. The ROC curves for these models are presented in Fig. 1, visually confirming the superior classification performance of Attention U-Net and Dense U-Net on the FIVES dataset.

After pre-training on FIVES, all models were fine-tuned on the CT branching-structure dataset. Segmentation performance on CT images was computed on the CT test subsets of each fold, using pixel-wise accuracy, precision, recall, Dice and AUC. The averaged results over 10 folds are presented in Table 2.

The transfer learning approach reveals a dramatic improvement in performance across all models on CT images, particularly in Dice (F1 score) and AUC. For example, the Dice score for U-Net

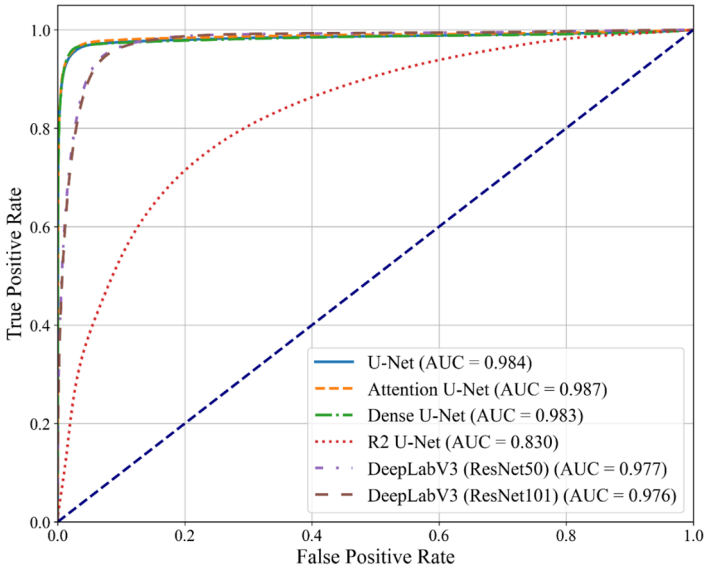

Fig. 1. ROC curves for U-Net, Attention U-Net, R2 U-Net, Dense U-Net, DeepLabV3 (ResNet50/ ResNet101) trained and tested on FIVES dataset

Table 2

Performance comparison of deep learning models for pulmonary vessel segmentation

Model	Accuracy	Precision	Recall	Dice
U-Net	0.9583	0.5377	0.4371	0.4822
Attention U-Net	0.9582	0.5356	0.4445	0.4858
Dense U-Net	0.9525	0.4654	0.4663	0.4608
R2 U-Net	0.9586	0.8648	0.08	0.1465
DeepLabV3 (ResNet50)	0.9584	0.5399	0.4294	0.4783

increases from 0.0028 (training from scratch on CT only) to 0.4802 with cross-domain pre-training, while for Attention U-Net the Dice rises from 0.0088 to 0.4814. This large gain demonstrates the effectiveness of the proposed cross-domain transfer learning strategy for branching structure segmentation in CT data.

Among the U-Net variants with transfer learning, Attention U-Net achieves the highest Dice (F1 score) of 0.4814, indicating superior foreground delineation on CT images. DeepLabV3 (ResNet50) also performs very well, with a Dice of 0.4760 and the highest AUC of 0.9621, which reflects strong discriminative power at the pixel level. Dense U-Net attains a competitive Dice of 0.4592. R2 U-Net, while showing improvement compared to its non-transfer counterpart, still lags significantly behind the other models with a Dice of 0.1465, reinforcing its observed limitations for this type of segmentation task.

The ROC curves for the models after transfer learning are shown in Fig. 2 and illustrate the improved classification performance in the CT domain. Qualitative analysis is provided in Fig. 3. Fig. 3, *d* (Attention U-Net) demonstrates visibly more accurate and complete segmentation of fine branching structures compared to other models and the original CT slice (Fig. 3, *a*). This visual evidence supports the quantitative results and confirms that Attention U-Net, leveraging its attention mechanisms, is particularly effective for delineating complex and subtle branching patterns in chest CT images.

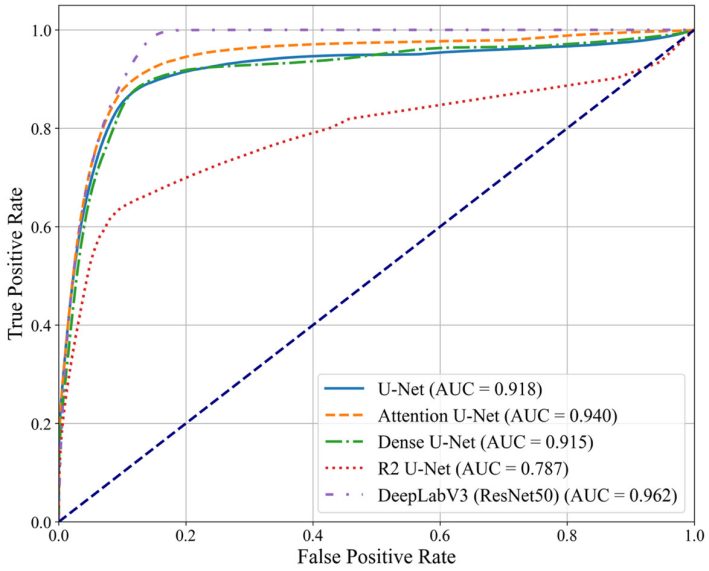

Fig. 2. ROC curves for U-Net, Attention U-Net, R2 U-Net, and Dense U-Net, DeepLabV3 (ResNet50) (pretrained on FIVES dataset) trained and tested on LUNG dataset

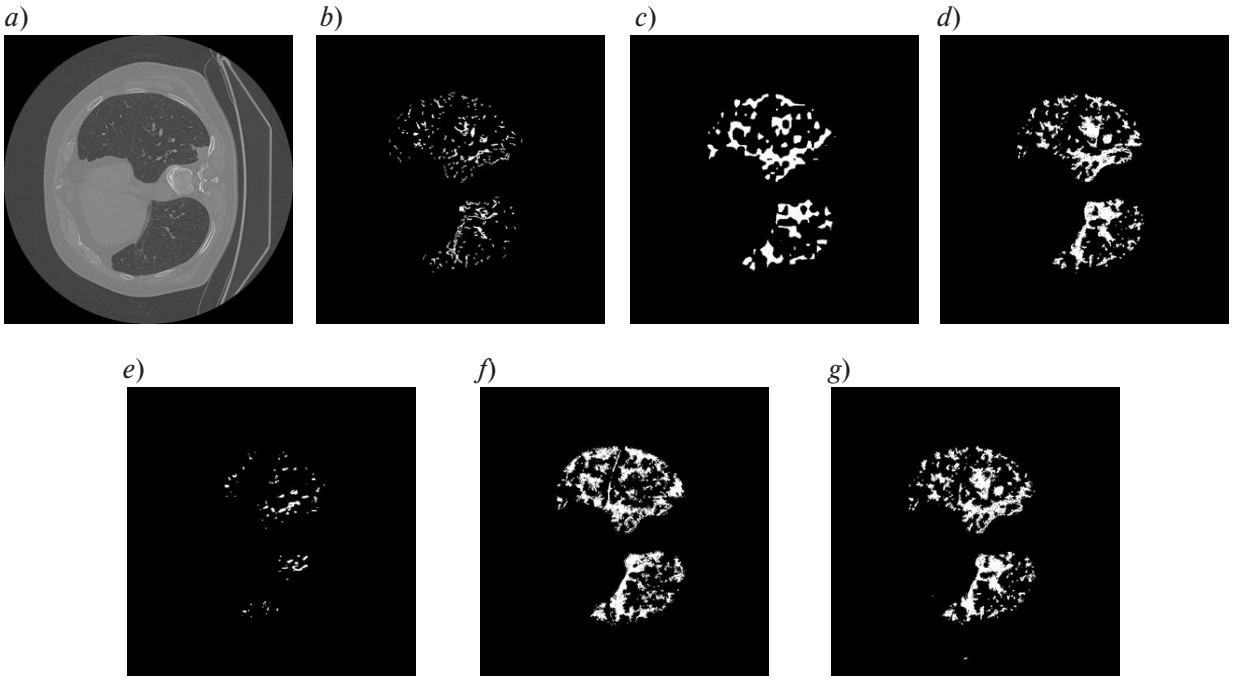

Fig. 3. Visual analysis of vessel segmentation in CT images. Original CT (*a*); Annotation (*b*); DeepLabV3 (ResNet50) (*c*); Attention U-Net (*d*); R2 U-Net (*e*); Dense U-Net (*f*); U-Net (*g*)

Conclusion

This study investigated a cross-domain deep transfer learning strategy for segmentation of branching vascular structures in chest CT images. By exploiting morphological similarity between retinal and CT vascular patterns, the proposed approach effectively mitigates the data-scarcity problem in the target CT domain. Experimental results demonstrate a substantial improvement in segmentation

performance for all evaluated architectures when pre-training on the FIVES retinal dataset is followed by fine-tuning on the CT dataset.

Among the U-Net variants, Attention U-Net and Dense U-Net emerged as the most effective models, with Attention U-Net achieving the highest Dice score of 0.4814, indicating superior delineation of fine branching structures. DeepLabV3 (ResNet50) also showed strong performance, attaining the highest AUC value of 0.9621 and thus providing excellent discriminative capability at the pixel level. These findings confirm that cross-domain transfer from a data-rich vascular segmentation task is a viable and powerful strategy for improving performance on data-limited CT segmentation tasks.

Overall, the proposed framework offers a robust, reproducible baseline for branching structure segmentation in volumetric images and highlights the advantages of attention mechanisms and dense connectivity in this context. It can be readily extended to other applications involving thin, tree-like structures and limited annotated data.

REFERENCES

1. **Wu Y., Qi S., Wang M., Zhao S., Pang H., Xu J., Ren H.** Transformer-based 3D U-Net for pulmonary vessel segmentation and artery-vein separation from CT images. *Medical & Biological Engineering & Computing*, 2023, Vol. 61, Pp. 2649–2663. DOI: 10.1007/s11517-023-02872-5

2. **Shariaty F., Zavjalov S. V., Pavlov V. A., Pervunina T. M., Orooji M.** Inf-Seg: Automatic segmentation and quantification method for CT-based COVID-19 diagnosis. *Computing, Telecommunications and Control*, 2022, Vol. 15, No 3, Pp. 7–21. DOI: 10.18721/JCSTCS.15301

3. **Lenin Marksia U., Yesubai Rubavathi C.** Accurate segmentation of COVID-19 infected regions in lung CT scans with deep learning. *Neural Computing and Applications*, 2024, Vol. 36, Pp. 22511–22531. DOI: 10.1007/s00521-024-10336-6

4. **Skalunova M., Shariaty F., Rozov S., Radmard A.R.** Personalized Chemotherapy Selection for Lung Cancer Patients Using Machine Learning and Computed Tomography. *2023 International Conference on Electrical Engineering and Photonics* (*EExPolytech*), 2023, Pp. 128–131. DOI: 10.1109/EExPolytech58658.2023.10318700

5. **Shariaty F., Pavlov V.A., Fedyashina S.V., Serebrennikov N.A.** Integrating deep learning and explainable AI for non-invasive prediction of EGFR and KRAS mutations in NSCLC: A novel radiogenomic approach. *2024 V International Conference on Neural Networks and Neurotechnologies* (*NeuroNT*), 2024, Pp. 32–35. DOI: 10.1109/NeuroNT62606.2024.10585441

6. **Shariaty F., Zavjalov S.V., Pavlov V.A., Pervunina T.M., Orooji M.** Inf-Seg: Automatic segmentation and quantification method for CT-based COVID-19 diagnosis. *Computing, Telecommunications and Control*, 2022, Vol. 15, No. 3, Pp. 7–21. DOI: 10.18721/JCSTCS.15301

7. **Deng X., Li W., Yang Y., Wang S., Zeng N., Xu J., Hassan H., Chen Z., Liu Y., Miao X., Guo Y., Chen R., Kang Y.** COPD stage detection: leveraging the auto-metric graph neural network with inspiratory and expiratory chest CT images. *Medical & Biological Engineering & Computing*, 2024, Vol. 62, No. 6, Pp. 1733–1749. DOI: 10.1007/s11517-024-03016-z

8. **Khan A., Garner R., La Rocca M., Salehi S., Duncan D.** A novel threshold-based segmentation method for quantification of COVID-19 lung abnormalities. *Signal, Image and Video Processing*, 2023, Vol. 17, No. 4, Pp. 907–914. DOI: 10.1007/s11760-022-02183-6

9. **Sasidhar B.** Segmentation of Lung Regions for the Detection of Juxta-Pleura Nodules in CT scan. *Intelligent Computing and Communication* (*ICICC 2022*), 2023, Vol. 1447, Pp. 233–239. DOI: 10.1007/978-981-99-1588-0_21

10. **Shariaty F., Mousavi M., Moradi A., Oshnari M.N., Navvabi S., Orooji M., Novikov B.** Semi-automatic segmentation of COVID-19 infection in lung CT scans. *International Youth Conference on Electronics,*

Telecommunications and Information Technologies, 2022, Vol. 268, Pp. 67–76. DOI: 10.1007/978-3-030-81119-8_7

11. **Dhanwanth B., Vivek B., Shobana P., Sineghamathi G., Joshi A.** Advanced machine learning techniques for precise lung cancer detection from CT scans. *Technology: Toward Business Sustainability*, 2024, Vol. 925, Pp. 328–349. DOI: 10.1007/978-3-031-54019-6_30

12. **Galdran A., Anjos A., Dolz J., Chakor H., Lombaert H., Ben Ayed I.** State-of-the-art retinal vessel segmentation with minimalistic models. *Scientific Reports*, 2022, Vol. 12, Art. no. 6174. DOI: 10.1038/s41598-022-09675-y

13. **Oktay O., Schlemper J., Le Folgoc L., Lee M., Heinrich M., Misawa K., Mori K., McDonagh S., Hammerla N.Y., Kainz B., Glocker B., Rueckert D.** Attention U-Net: Learning where to look for the pancreas. *arXiv:1804.03999*, 2018. DOI: 10.48550/arXiv.1804.03999

14. **Alom M.Z., Hasan M., Yakopcic C., Taha T.M., Asari V.K.** Recurrent Residual Convolutional Neural Network based on U-Net (R2U-Net) for Medical Image Segmentation. *arXiv:1802.06955*, 2018. DOI: 10.48550/arXiv.1802.06955

15. **Zhou Z., Siddiquee M.M.R., Tajbakhsh N., Liang J.** UNet++: A Nested U-Net Architecture for Medical Image Segmentation. *Deep Learning in Medical Image Analysis and Multimodal Learning for Clinical Decision Support*, 2018, Vol. 11045, Pp. 3–11. DOI: 10.1007/978-3-030-00889-5_1

16. **Chen L.-C., Papandreou G., Kokkinos I., Murphy K., Yuille A.L.** DeepLab: Semantic Image Segmentation with Deep Convolutional Nets, Atrous Convolution, and Fully Connected CRFs. *IEEE Transactions on Pattern Analysis and Machine Intelligence*, 2018, Vol. 40, No. 4, Pp. 834–848. DOI: 10.1109/TPAMI.2017.2699184

17. **Jin K., Huang X., Zhou J., Li Y., Yan Y., Sun Y., Zhang Q., Wang Y., Ye J.** FIVES: A fundus image dataset for artificial intelligence based vessel segmentation. *Scientific Data*, 2022, Vol. 9, Art. no. 475. DOI: 10.1038/s41597-022-01564-3

18. **Clark K., Vendt B., Smith K., Freymann J., Kirby J., Koppel P., Moore S., Phillips S., Maffitt D., Pringle M., Tarbox L., Prior F.** The Cancer Imaging Archive (TCIA): Maintaining and operating a public information repository. *Journal of Digital Imaging*, 2013, Vol. 26, Pp. 1045–1057. DOI: 10.1007/s10278-013-9622-7

INFORMATION ABOUT AUTHORS / СВЕДЕНИЯ ОБ АВТОРАХ

Faridoddin Shariaty
Шариати Фаридоддин
E-mail: shariaty3@gmail.com
ORCID: https://orcid.org/0000-0002-7060-8826

Vitalii A. Pavlov
Павлов Виталий Александрович
E-mail: pavlov_va@spbstu.ru
ORCID: https://orcid.org/0000-0003-0726-6613

Ekaterina A. Medvedeva
Медведева Екатерина Александровна
E-mail: tato_ks@mail.ru
ORCID: https://orcid.org/0000-0003-0473-5007

Submitted: 29.08.2025; Approved: 19.02.2026; Accepted: 17.03.2026.
Поступила: 29.08.2025; Одобрена: 19.02.2026; Принята: 17.03.2026.

Computing, Telecommunication and Control, 2026, Vol. 19, No. 1, Pp. 16–25.
Информатика, телекоммуникации и управление. 2026. Том 19, № 1. С. 16–25.

Research article
DOI: https://doi.org/10.18721/JCSTCS.19102
UDC 004.85

ENHANCING BOUNDARY STABILITY IN DECISION TREES AND RANDOM FORESTS: A WEIGHTED SAMPLE DUPLICATION APPROACH

A.V. Konstantinov[1], *A.P. Elizarova*[2], *L.V. Utkin*[1] ✉

[1] Peter the Great St. Petersburg Polytechnic University, St. Petersburg, Russian Federation;

[2] National Research University Higher School of Economics, St. Petersburg branch, St. Petersburg, Russian Federation

✉ lev.utkin@gmail.com

Abstract. Decision trees and their ensemble extensions, such as random forests, are widely used as classification models due to their simplicity and interpretability. However, in many real-world tasks where class labels overlap in the feature space, standard decision trees rely on hard splits that create fragile decision boundaries. In these regions, small perturbations in the input values can lead to misclassification, reducing the reliability of the model. To address this issue, we propose a localized data duplication mechanism that modifies the standard CART algorithm by duplicating samples located near the chosen split threshold into both child nodes. To prevent these duplicated samples from overpowering the nodes, they are assigned a reduced weight based on a smoothly decaying function relative to their distance from the threshold. This approach allows both child nodes to learn from ambiguous regions, preserving information about uncertainty while maintaining the axis-aligned deterministic structure of classical decision trees. When applied within a random forest framework, the duplication process also increases ensemble diversity. Experimental evaluation on 11 real-world datasets with varying degrees of class overlap demonstrates that the proposed modification consistently improves ROC-AUC scores and boundary stability while keeping computational costs low.

Keywords: machine learning, decision trees, random forest, classification, data duplication

Acknowledgements: The research was supported by the Russian Science Foundation grant No. 25-21-00103 “New methods and models of multivariate learning in medical diagnostics”. Available online: https://rscf.ru/project/25-21-00103/.

Citation: Konstantinov A.V., Elizarova A.P., Utkin L.V. Enhancing Boundary Stability in Decision Trees and Random Forests: A Weighted Sample Duplication Approach. Computing, Telecommunications and Control, 2026, Vol. 19, No. 1, Pp. 16–25. DOI: 10.18721/JCSTCS.19102

Научная статья
DOI: https://doi.org/10.18721/JCSTCS.19102
УДК 004.85

ПОВЫШЕНИЕ УСТОЙЧИВОСТИ ГРАНИЦ В ДЕРЕВЬЯХ РЕШЕНИЙ И СЛУЧАЙНЫХ ЛЕСАХ: ПОДХОД С ИСПОЛЬЗОВАНИЕМ ВЗВЕШЕННОГО ДУБЛИРОВАНИЯ ВЫБОРКИ

А.В. Константинов[1], *А.П. Елизарова*[2], *Л.В. Уткин*[1] ✉

[1] Санкт-Петербургский политехнический университет Петра Великого, Санкт-Петербург, Российская Федерация;

[2] НИУ ВШЭ, Санкт-Петербургский филиал, Санкт-Петербург, Российская Федерация

✉ lev.utkin@gmail.com

Аннотация. Деревья решений и их ансамблевые расширения, такие как случайные леса, широко используются в качестве моделей классификации благодаря своей простоте и интерпретируемости. Однако во многих реальных задачах, где метки классов перекрываются в пространстве признаков, стандартные деревья решений полагаются на жесткие разбиения, которые создают слабые границы принятия решений. В этих областях небольшие возмущения входных значений могут привести к неправильной классификации, снижая надежность модели. Для решения этой проблемы мы предлагаем механизм локализованного дублирования данных, который модифицирует стандартный алгоритм CART (Classification and Regression Tree) путем дублирования образцов, расположенных вблизи выбранного порога разбиения, в оба дочерних узла. Чтобы предотвратить перегрузку узлов этими дублированными образцами, им присваивается уменьшенный вес на основе плавно убывающей функции относительно их расстояния от порога. Такой подход позволяет обоим дочерним узлам обучаться на неоднозначных областях, сохраняя информацию о неопределенности, одновременно поддерживая выровненную по осям детерминированную структуру классических деревьев решений. При применении в рамках случайного леса процесс дублирования также увеличивает разнообразие ансамбля. Экспериментальная оценка на 11 реальных наборах данных с различной степенью перекрытия классов показывает, что предложенная модификация последовательно улучшает показатели ROC-AUC и устойчивость границ, сохраняя при этом низкие вычислительные затраты.

Ключевые слова: машинное обучение, деревья решений, случайный лес, классификация, дублирование данных

Финансирование: Исследование выполнено за счет гранта Российского научного фонда в рамках реализации проекта «Новые методы и модели многовариантного обучения в задачах медицинской диагностики» (Соглашение №25-21-00103, https://rscf.ru/project/25-21-00103/).

Для цитирования: Konstantinov A.V., Elizarova A.P., Utkin L.V. Enhancing Boundary Stability in Decision Trees and Random Forests: A Weighted Sample Duplication Approach // Computing, Telecommunications and Control. 2026. Т. 19, № 1. С. 16–25. DOI: 10.18721/JCSTCS.19102

Introduction

Decision trees and their ensemble extensions, such as random forests, are popular because they are simple, often perform well in practice, and offer interpretability. Each decision tree splits the feature space in a hierarchical way, which allows users to trace exactly how a prediction is made. Ensembles average over many trees, which tends to reduce variance and improve generalization.

In many real-world classification tasks, especially in medical or environmental settings, class-conditional distributions overlap in feature space. That means that for certain regions, observations from more than one class lie very close to each other in the features. In these overlapping regions, small perturbations of input values or small changes in the split thresholds can lead to different class predictions. This reduces predictive stability and increases variance near class boundaries. A standard decision tree uses hard splits: at each internal node it chooses a feature and a threshold that minimize impurity (such as Gini impurity or entropy). When classes overlap, small perturbations can lead to misclassification due to fragile decision boundaries. As trees grow deeper, the number of samples in each node tends to shrink, increasing sensitivity to small changes and decreasing robustness near class boundaries.

This work proposes a modification of tree construction that introduces a stochastic or softening element in handling samples near decision boundaries. Specifically, after a split is determined, samples whose values are close to the threshold (i.e., near the hyperplane defined by the feature and threshold) are duplicated into both child nodes. The influence of each duplicated sample decreases as its distance from the threshold increases. This duplication has two key effects: it preserves information about ambiguous or uncertain regions, and it increases diversity among trees when used in a random forest ensemble. The goal is to make decision boundaries more precise, reduce errors arising in overlapping class regions, and improve learning in difficult parts of feature space, while retaining much of the interpretability and simplicity of standard CART-style trees.

Related works

The problem of class overlap, uncertainty, and decision boundary instability has been extensively addressed in recent literature. Existing approaches can broadly be categorized into probabilistic tree modifications, fuzzy logic parameterizations, and data-level boundary interventions. These approaches help illustrate why the proposed method is needed.

The concept of soft or probabilistic splits replaces rigid decision boundaries with weighted contributions from both child branches. While foundational work demonstrated that soft thresholds reduce generalization error, soft decision trees (SDTs) have recently seen a massive resurgence as a means to balance deep learning's predictive power with interpretability [1]. For instance, the fusion of SDTs with concept-based convolutional models was used to create transparent classification systems in complex, overlapping spaces [3]. Recent advancements also include embedding spatial visual attention directly into the inner nodes of SDTs to ensure path-based interpretability [2]. Despite these improvements, SDTs fundamentally alter the standard tree routing mechanism by relying on fully differentiable gradient descent and sigmoid-based probability branching rather than classical hard splits [1, 2].

Fuzzy decision trees (FDTs) explicitly model uncertainty by mapping features to fuzzy membership functions [5, 7]. Recent advancements in this domain emphasize adaptability and scalability. Rabcan et al. (2025) proposed a dynamic FDT that uses cumulative mutual information to incrementally adapt to evolving, overlapping data streams [4]. FDT optimization has also been applied successfully in complex environments, such as personalized hybrid learning systems, utilizing cost-complexity pruning to prevent boundary overfitting [6]. Furthermore, FDTs are proven highly effective for regression and classification in uncertain physical environments, such as climate factor modeling [5]. However, these approaches introduce significant mathematical overhead: they require predefined triangular or trapezoidal membership functions and linguistic parameters that must be manually tuned, deviating from the algorithmic simplicity of axis-aligned crisp splits [4, 6].

Instead of modifying the tree structure probabilistically, several studies focus directly on the geometric boundaries and data overlap. Class overlap – where instances from different categories share the exact same feature space – is proven to degrade the performance and interpretability of predictive

models significantly [8]. To tackle this, novel decision rules based on boundary mixed attribute dependency have been introduced, allowing trees to factor the boundary region explicitly as a measure of knowledge uncertainty [9]. Additionally, when dealing with noisy class variables at the boundaries, random forest algorithms exhibit measurably higher robustness compared to standalone C4.5 or CART trees [10].

When individual tree boundaries fail to resolve class overlap, ensemble and distributed techniques provide an alternative. Coalition-based decision trees now use decision template fusion to manage conflicting or overlapping data sources across distributed networks [11]. In complex medical domains characterized by overlapping tumor classes, multiclass tree ensembles combining perfusion and spectroscopy data have achieved high accuracy by extracting precise, overlapping rule combinations [12]. Nevertheless, these techniques typically operate as global or post-hoc ensembles, not fundamentally altering how the individual underlying decision tree processes the ambiguous boundary during the split search.

Despite these advances, a critical gap remains. Current state-of-the-art methods either mandate computationally expensive gradient routing [1, 3], require complex fuzzy membership tuning [4, 6], or rely on global data-level interventions [8]. There is a distinct need for methods that preserve the clean CART structure, do not require extensive global parameter tuning, and maintain interpretability while dynamically improving robustness at class boundaries.

Method

The proposed method modifies the construction of standard decision trees in order to handle uncertain or overlapping class regions more effectively, as well as small sample size, while keeping the simplicity and interpretability of classical CART. The main idea is to duplicate samples that lie close to a chosen split threshold, so that both resulting child nodes can learn from data in ambiguous regions. This adjustment helps the model to better capture local structure near class boundaries and to become less sensitive to small variations in input data or threshold placement. Furthermore, it allows for a more precise determination of split thresholds if they are shared among child nodes with the same parent.

In a traditional decision tree, each node contains a subset of the training data and selects one feature, defined as x_j, and a threshold value, called t. The goal of this step is to find the split that best reduces impurity, for example measured by Gini impurity or entropy. Once the threshold is determined, all samples with feature values less than or equal to t are sent to the left child node, and the remaining points, i.e., those with values greater than t are sent to the right child node. The algorithm then continues recursively on both child nodes until a stopping criterion is met, such as a minimum node size or maximum depth.

Let D denote the current node dataset. At the root node, D is the whole dataset:

$$D = \left\{\left(x^{(i)}, y^{(i)}\right)\right\}_{i=1}^{N},$$

where each feature vector $x = (x_1, ..., x_f)$ is of size f. In classical CART algorithm, at the current node, when the split is found, D_L and D_R are subsets to which D is partitioned after splitting by feature x_j and threshold t:

$$D_L = \left\{(x, y) \in D \middle| x_j \le t\right\}, \quad D_R = \left\{(x, y) \in D \middle| x_j \rangle t\right\}.$$

The subset D_L is considered in the left child node, and D_R – in the right.

This deterministic splitting process works well when the classes are clearly separated, but it can be unreliable when the data contain regions of overlap, or the sample size within the node becomes

insufficient for reliable splitting threshold estimation. In such areas, some samples from different classes have very similar feature values, and even a small change in t or in the input values can send them to opposite sides of the split. As the tree grows deeper, each node contains fewer samples, which increases the instability of these boundaries, leading to possibly higher error rate.

To address this issue, we propose a localized weighted sample duplication mechanism. After the best split feature and threshold are found, the samples that lie close to the chosen threshold along the selected feature are selected (near-boundary samples), where closeness is defined by a distance between the feature value and the threshold and the number of samples that are nearest to the threshold. Once the near-boundary samples are identified, they are duplicated so that they appear in both child nodes. In other words, each of these samples contributes to learning in both branches of the split. This ensures that the information about uncertain regions is not lost. To prevent the duplication from overpowering the data in either node, each duplicated sample receives a reduced influence, which depends on how far it is from the threshold. Samples that are exactly at or very close to the threshold have the highest influence, and those further away have gradually smaller influence.

This mechanism preserves the deterministic structure of a standard decision tree. The split itself remains hard and axis-aligned, so the interpretability of the resulting model is unchanged. However, by allowing both child nodes to learn from near-boundary samples, the model becomes more robust. It no longer discards information from uncertain regions, and it gains a more stable decision boundary, less sensitive to small variations in the data.

When this method is used within a random forest, the duplication process also introduces additional diversity among trees. Because each tree in the ensemble is built from a bootstrap sample and may select different features and thresholds, the specific boundary samples that are duplicated vary between trees. This increases the variety of the ensemble members, which in turn improves generalization and reduces the correlation of their errors, especially in regions of class overlap.

A few practical considerations are important for implementation. Since duplicating samples changes the number of observations seen by each node, stopping criteria based on sample counts may need to account for the reduced influence or weight of duplicated points rather than counting them as separate full samples. It is also necessary to choose the width of the near-boundary region carefully: if it is too wide, unnecessary duplication may increase computational cost or overfit the boundary; if it is too narrow, the effect may be too small. Similarly, the decay rule for sample influence must ensure a smooth transition between duplicated and non-duplicated samples. Despite these considerations, the method remains simple to integrate into standard tree algorithms because it does not alter impurity calculations, prediction procedures, or the overall recursive structure.

In summary, the method retains the key advantages of CART, including simplicity, interpretability, and computational efficiency, while improving robustness in overlapping class regions. It achieves this by allowing both branches of a split to learn from data that lie close to uncertain boundaries, thereby reducing error sensitivity and enhancing the reliability of both individual trees and ensembles built from them.

This mechanism introduces randomized noise into sampling procedure for child node data, as shown in Fig. 1. By exposing subsequent splits to both sides of the uncertain region, the tree becomes less sensitive to exact threshold placement and gains resilience to perturbations.

Let the absolute distance from the decision boundary for sample i along the splitting feature j be defined as:

$$d_i = \left| x_{ij} - t \right|.$$

Let r be a user-defined parameter controlling the proportion of copied samples. The number of samples duplicated from the opposite branch is:

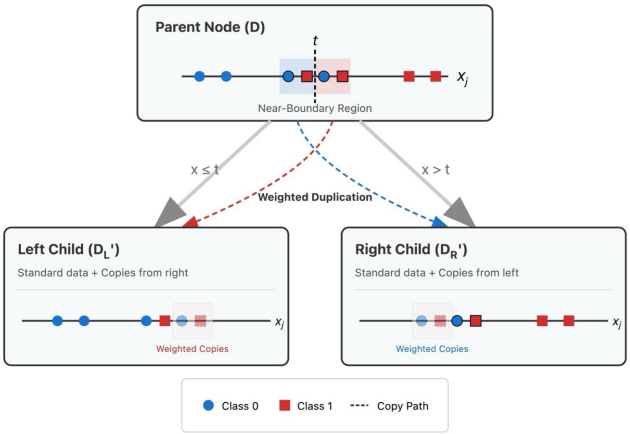

Fig. 1. Sample duplication near decision threshold

$$k = \left\lfloor r \cdot \min\left(|D_L|, |D_R|\right) \right\rfloor.$$

Select k samples with smallest d_i values from each side and duplicate them into the opposite child subset. Thus, final subsets become:

$$D_{L'} = D_L \cup \text{Copy}_R, \quad D_{R'} = D_R \cup \text{Copy}_L.$$

Each duplicated observation receives a weight reflecting its proximity to the decision boundary. We use a smooth decaying function:

$$w_i = e^{-a|d_i|}, \quad a > 0,$$

where a controls the decay rate. A larger a causes a rapid drop in weight for samples further from the boundary, while a smaller a allows a wider band of samples to influence the child nodes. Alternatively, a polynomial decay function can be utilized:

$$w_i = \left(1 + |d_i|\right)^{-a}.$$

This ensures that exact boundary samples have maximum weight (1), while farther ones contribute less.

These weights affect computation of Gini impurity and class assignment in leaves, defined as:

$$G = \frac{1}{W} \sum_c \left(\sum_{i \in C_c} w_i \right) \left(1 - \frac{\sum_{i \in C_c} w_i}{W} \right),$$

where W is the normalizing term representing the sum of all sample weights in the node, and C_c represents the subset of samples belonging to class c.

If a sample is duplicated across multiple splits (tree depth more than one), its influence must gradually diminish. Therefore, each time a sample is re-copied, its weight is updated recursively:

$$w_i^{(k+1)} = w_i^{(k)} \cdot e^{-ad_i}.$$

Duplication is only allowed up to a specified maximum copy depth δ to avoid exponential growth.

The proposed tree construction algorithm consists of the following steps:

1. For each node:
   - o Compute impurity for all possible splits.
   - o Select best feature x_j and threshold t.
2. Identify boundary-near samples using distances d_i.
3. Duplicate k closest samples into opposite nodes.
4. Assign weights via chosen decay function.
5. Recurse until stopping criteria (max depth, min sample size) are met.

The computational complexity of the proposed algorithm remains close to the original one. In a standard CART algorithm, finding the optimal split at a given node requires $O(f\,N\log N)$ operations, where f is the number of features and N is the number of samples in the node. The proposed modification introduces three additional operations per node: calculating the absolute distances d_i from the threshold for all samples ($O(N)$), identifying the k closest samples (which can be achieved in $O(N)$ time using selection algorithms), and copying and weighting these k samples ($O(k)$). Because k is much smaller than N and these additional steps scale linearly, the computational complexity of the node-splitting process remains dominated by the original $O(f\,N\log N)$ split search. While duplicating samples increases the effective N for subsequent child nodes, the strict enforcement of the maximum copy depth δ caps the duplication process, preventing exponential growth of the dataset. Consequently, the overall training time increases only by a bounded constant factor, preserving the efficiency and scalability of the baseline random forest framework.

Numerical experiments

The proposed method was evaluated on 11 publicly available datasets obtained from the UCI Machine Learning Repository and Kaggle. These datasets cover a range of application areas and data characteristics. Most of them are related to medical classification problems such as heart disease, diabetes, and cancer diagnosis. The datasets differ in size, ranging from 306 to 1484 samples, and in dimensionality, from 3 to 34 features. Full description of the used data is provided in Table 1. Basic preprocessing was applied to all datasets: missing values were removed and categorical features were encoded using label encoding.

Table 1

Description of data sets

Title	M	N	C
Breast Cancer Wisconsin (Original)	9	682	2
Haberman's Survival	3	306	2
Titanic	3	714	2
Heart Attack	13	303	2
Diabetes	8	768	2
Hepatitis C virus	14	615	5
Ecoli	7	336	8
Dermatology	34	366	6
Heart Failure	12	918	2
Yeast	8	1484	10
Cirrhosis	20	418	4

For quantitative evaluation, the standard classification metric independent of threshold choice, the area under the receiver operating characteristic curve (ROC-AUC), was used. Each metric value was obtained by averaging results from five-fold stratified cross-validation repeated ten times with different random seeds to ensure statistical reliability.

As a baseline, the standard random forest implementation based on the CART algorithm from the scikit-learn library was employed. The main hyperparameters of this baseline were selected as follows: the number of trees was set to 100, and the maximum depth of individual trees was limited to values between 5 and 10, depending on the dataset (the best parameters were selected via grid search with cross-validation). For the proposed modification, hyperparameters were also tuned using grid search, including the parameter r that determines the width of the near-boundary region, tested in increments between 0 and 0.9, the maximum tree depth at which sample duplication is applied (δ, ranging from 1 to 5), and parameters describing the weighting function. The weight decay parameter was fixed to $a = 1$ across all datasets.

Table 2

Experiment results on real data, ROC-AUC

Data set	Max tree depth	Baseline RF	Proposed RF		
		mean ± std	r	δ	mean ± std
Breast Cancer	8	0.993 ± 0.005	0.1	5	**0.994 ± 0.005**
Haberman's Survival	5	0.683 ± 0.049	0.4	3	**0.699 ± 0.052**
Titanic	5	0.859 ± 0.035	0.3	1	**0.860 ± 0.035**
Heart Attack	10	0.904 ± 0.034	0.8	6	**0.911 ± 0.030**
Diabetes	5	0.834 ± 0.034	0.1	3	**0.835 ± 0.034**
Hepatitis C virus	7	0.983 ± 0.009	0.5	3	**0.985 ± 0.007**
Ecoli	3	0.897 ± 0.017	0.5	2	**0.900 ± 0.013**
Dermatology	5	**0.998 ± 0.001**	0.1	1	0.998 ± 0.002
Heart Failure	4	**0.926 ± 0.014**	0.1	1	0.925 ± 0.014
Yeast	7	0.879 ± 0.016	0.1	1	**0.881 ± 0.016**
Cirrhosis	5	0.715 ± 0.049	0.4	4	**0.723 ± 0.041**

The results are provided in Table 2. Across the eleven datasets, the modified algorithm achieved higher ROC-AUC scores in 8 cases out of 11, with the strongest improvements observed on datasets known to contain overlapping or noisy class boundaries, such as Haberman's Survival, Heart Attack, and Cirrhosis. Statistical significance was confirmed using both the Wilcoxon signed-rank test, which produced a p-value of 0.005, and the paired t-test, with a p-value of 0.017. These results indicate that the improvements are consistent and unlikely to result from random variation.

Overall, the experimental results confirm that introducing sample duplication near decision boundaries improves the stability and predictive performance of decision-tree ensembles. The method consistently enhances ROC-AUC on most real datasets. These findings show that the proposed approach effectively strengthens robustness in uncertain regions while keeping computational cost and interpretability close to those of the standard random forest.

Conclusion

This paper introduced a simple yet effective modification of the decision tree learning process aimed at improving robustness in overlapping class regions. The method duplicates samples that lie

near splitting thresholds so that both child nodes can learn from uncertain regions, with each duplicated sample weighted according to its distance from the threshold. This design preserves the structure, interpretability, and efficiency of the standard CART algorithm while reducing sensitivity to small feature perturbations and unstable decision boundaries.

A comprehensive experimental study on real and synthetic datasets demonstrated that the proposed approach consistently improves classification performance and stability, especially in tasks characterized by high class overlap. Statistical tests confirmed that these improvements are significant. Importantly, the modification requires minimal changes to existing tree-based implementations and can be seamlessly integrated into standard random forest frameworks.

Future work will focus on theoretical bias-variance analysis, extension to regression and survival analysis tasks, evaluation on larger and higher-dimensional datasets, and exploration of adaptive weighting schemes that further optimize learning in uncertain regions.

REFERENCES

1. **Chen J., Wang Z., Wei Z., Huang C., Yang Y., Wei P., Li H., You Y., Zhang S., Dong Z. et al.** An Interpretable Attention Decision Forest Model for Surface Soil Moisture Retrieval. *Remote Sensing*, 2025, Vol. 17, No. 20, Art. no. 3468. DOI: 10.3390/rs17203468

2. **Yan J., Yamada S.** Learning Dual-Path Soft Decision Trees for Vision Prototype XAI. *IEEE Access*, 2025, in print. DOI: 10.1109/ACCESS.2025.3639412

3. **Rodríguez D.M., Cuéllar M.P., Morales D.P.** On the fusion of soft-decision-trees and concept-based models. *Applied Soft Computing*, 2024, Vol. 160, Art. no. 111632. DOI: 10.1016/j.asoc.2024.111632

4. **Rabcan J., Zaitseva E., Levashenko V., Kvassay M.** Incremental fuzzy decision tree based on cumulative mutual information. *Journal of Computational Design and Engineering*, 2025, Vol. 12, Pp. 116–130. DOI: 10.1093/jcde/qwaf088

5. **Habeeb A.S., Hasan H.A., Al-Sinjary A.M.** Fuzzy decision-tree regression model and its application to measure some climate change factors. *Frontiers in Applied Mathematics and Statistics*, 2026, Vol. 12, Art. no. 1732313. DOI: 10.3389/fams.2026.1732313

6. **Liu L., Yang S., Jiang K.** Fuzzy Decision Tree Optimization for Personalized Hybrid English Teaching in Smart Classrooms. *Journal of Circuits, Systems and Computers*, 2025, Vol. 34, No. 11, Art. no. 2550251. DOI: 10.1142/S0218126625502512

7. **Liu C.** Fuzzy decision tree based online precision marketing method for brand products on the internet. *International Journal of Product Development*, 2024, Vol. 28, No. 4, Pp. 241–256. DOI: 10.1504/IJPD.2024.143258

8. **Han H., Yu Q., Zhu Y., Cheng S., Zhang Y.** An Empirical Study of the Impact of Class Overlap on the Performance and Interpretability of Cross-Version Defect Prediction. International *Journal of Software Engineering and Knowledge Engineering*, 2024, Vol. 34, No. 12, Pp. 1895–1918. DOI: 10.1142/S0218194024500414

9. **Lin B., Liu C., Miao D.** An improved decision tree algorithm based on boundary mixed attribute dependency. *Applied Intelligence*, 2024, Vol. 54, Pp. 2136–2153. DOI: 10.1007/s10489-023-05238-4

10. **Alharbi A.A.** Classification Performance Analysis of Decision Tree-Based Algorithms with Noisy Class Variable. *Discrete Dynamics in Nature and Society*, 2024, Vol. 2024, Art. no. 6671395. DOI: 10.1155/2024/6671395

11. **Kusztal K., Przybyła-Kasperek M.** Distributed Data Classification with Coalition-Based Decision Trees and Decision Template Fusion. *Entropy*, 2025, Vol. 27, No. 12, Art. no. 1205. DOI: 10.3390/e27121205

12. **Vallée R., Vallée J.-N., Guillevin C., Lallouette A., Thomas C., Rittano G., Wager M., Guillevin R., Vallée A.** Machine learning decision tree models for multiclass classification of common malignant brain tumors using perfusion and spectroscopy MRI data. *Frontiers in Oncology*, 2023, Vol. 13, Art. no. 1089998. DOI: 10.3389/fonc.2023.1089998

INFORMATION ABOUT AUTHORS / СВЕДЕНИЯ ОБ АВТОРАХ

Andrei V. Konstantinov
Константинов Андрей Владимирович
E-mail: andrue.konst@gmail.com
ORCID: https://orcid.org/0000-0002-1542-6480

Anastasiya P. Elizarova
Елизарова Анастасия Павловна
E-mail: anastasiya.eliz@yandex.ru
ORCID: https://orcid.org/0000-0002-3796-4757

Lev V. Utkin
Уткин Лев Владимирович
E-mail: lev.utkin@gmail.com
ORCID: https://orcid.org/0000-0002-5637-1420

Submitted: 13.01.2026; Approved: 15.03.2026; Accepted: 27.03.2026.
Поступила: 13.01.2026; Одобрена: 15.03.2026; Принята: 27.03.2026.

Computing, Telecommunication and Control, 2026, Vol. 19, No. 1, Pp. 26–37.
Информатика, телекоммуникации и управление. 2026. Том 19, № 1. С. 26–37.

Circuits and Systems for Receiving, Transmitting and Signal Processing

Устройства и системы передачи, приема и обработки сигналов

Research article
DOI: https://doi.org/10.18721/JCSTCS.19103
UDC 004.942

APPLICATION OF REGULARIZATION TECHNIQUES TO IMPROVE FORECAST STABILITY IN NOISY DATA FOR INDUSTRIAL AUTOMATION

Ya.V. Ludishchev ✉

Peter the Great St. Petersburg Polytechnic University,
St. Petersburg, Russian Federation

✉ shariaty3@gmail.com

Abstract. The article explores modern approaches to the application of regularization methods – Ridge and LASSO – in problems of forecasting technological process parameters under industrial automation conditions. Special attention is given to addressing challenges associated with the high-dimensional feature spaces and the presence of noise in input data, which are typical in industrial environments. The theoretical foundations of these methods are presented, along with their specific characteristics and mechanisms that reduce model overfitting and enhance robustness under varying input data. An experimental evaluation of the effectiveness of regularized regression models is conducted using real industrial datasets, including time series with missing and distorted values. The results demonstrate improved forecasting accuracy, model stability, and, consequently, the reliability of automated monitoring and control systems. These methods help cope with data noise, avoid retraining, and highlight key parameters, which is especially important in conditions of limited computational resources and complex production systems.

Keywords: regularization, industrial automation, ridge regularization method, LASSO, industrial control systems, regression models

Citation: Ludishchev Ya.V. Application of regularization techniques to improve forecast stability in noisy data for industrial automation. Computing, Telecommunications and Control, 2026, Vol. 19, No. 1, Pp. 26–37. DOI: 10.18721/JCSTCS.19103

Научная статья
DOI: https://doi.org/10.18721/JCSTCS.19103
УДК 004.942

ИСПОЛЬЗОВАНИЕ МЕТОДИК РЕГУЛЯРИЗАЦИИ ДЛЯ ПОВЫШЕНИЯ СТАБИЛЬНОСТИ ПРОГНОЗОВ В УСЛОВИЯХ ШУМНЫХ ДАННЫХ В ПРОМЫШЛЕННОЙ АВТОМАТИЗАЦИИ

Я.В. Лудищев ✉

Санкт-Петербургский политехнический университет Петра Великого,
Санкт-Петербург, Российская Федерация

✉ ludishevyaroslav@mail.ru

Аннотация. В статье рассматриваются современные подходы к применению методов регуляризации – гребневого (Ridge) и лассо (LASSO) – в задачах прогнозирования параметров технологических процессов в условиях промышленной автоматизации. Особое внимание уделяется решению проблем, связанных с высокой размерностью признакового пространства и наличием шумов в исходных данных, характерных для производственной среды. Представлены теоретические основы указанных методов, их особенности и механизмы, позволяющие снижать переобучение моделей и обеспечивать их устойчивость при варьирующихся входных данных. Проведено экспериментальное сравнение эффективности регрессионных моделей с регуляризацией на основе реальных производственных выборок, включая временные ряды с пропущенными и искаженными значениями. Полученные результаты демонстрируют повышение точности прогнозов, устойчивости моделей и, как следствие, надежности работы автоматизированных систем мониторинга и управления. Эти методы помогают справляться с шумом в данных, избегать переобучения и выделять ключевые параметры, что особенно важно в условиях ограниченных вычислительных ресурсов и сложных производственных систем.

Ключевые слова: регуляризация, промышленная автоматизация, гребневый метод регуляризации, LASSO, алгоритмы оптимизации, регрессионные модели

Для цитирования: Ludishchev Ya.V. Application of regularization techniques to improve forecast stability in noisy data for industrial automation // Computing, Telecommunications and Control. 2026. Т. 19, № 1. С. 26–37. DOI: 10.18721/JCSTCS.19103

Introduction

Gas turbine plants (GTPs) play a key role in ensuring reliable and efficient electricity generation, particularly in the context of growing demands for power system stability and the reduction of operational costs. Under these conditions, methods for diagnosing and analyzing the performance of gas turbine equipment are of paramount importance, as they enable high operational reliability while reducing maintenance costs. Modern diagnostic approaches involve the use of advanced data processing techniques, which allow for addressing various malfunctions that occur during GTP operation [1].

One of the most critical tasks in GTP diagnostics is the processing and analysis of large volumes of data acquired from multiple sensors installed on various components of the power unit. Due to their nature, these data often contain gaps caused by failures in measurement equipment, instability of communication channels, or other technical issues. To ensure the accuracy of forecasting and diagnostics, it is necessary to develop and apply effective methods for imputing missing data [2]. Such methods restore the integrity of time series, ensuring the correct functioning of analytical algorithms and machine learning, which form the basis of modern approaches to forecasting and anomaly detection.

Thus, the development and implementation of methods for data imputation, signal filtering, measurement recovery, and the application of regularization represent an important direction in the field of diagnostics and performance analysis of gas turbine power units. These approaches lay the foundation for building high-precision predictive and diagnostic models, which, in turn, contributes to enhancing the reliability and efficiency of power unit operation, minimizing downtime and reducing operational expenditures [1, 3].

Modern GTP diagnostic methods are based on the use of machine learning and AI techniques. Among these, clustering, classification, regression analysis, and neural network algorithms can be distinguished [4]. The application of such methods allows not only for the identification of equipment operation anomalies but also for predicting the development of faults based on historical data and current system performance indicators. The use of hybrid approaches, combining physical-mathematical modeling and machine learning, plays a significant role [5].

A promising direction is the implementation of digital twins – virtual copies of physical equipment – which enable real-time monitoring of the system state, simulation of potential event scenarios, and the making of optimal decisions [6]. These technologies not only improve diagnostic accuracy but also contribute to the optimization of power unit operating regimes.

Particular attention is also paid to the development of methods for estimating the residual life of GTP components [7]. This task requires accounting for multiple factors, such as temperature, pressure, vibrations, and the chemical composition of the environment. Predictive analytics methods are used to solve this problem, allowing for the determination of the remaining equipment service life and the planning of repair or replacement activities [8].

Furthermore, significant attention is given to the issues of energy efficiency and environmental safety of GTPs. Modern approaches include the use of fuel combustion technologies with low emissions of nitrogen and carbon oxides, as well as the application of renewable fuels [9]. This helps reduce the carbon footprint of the power system and comply with international environmental standards.

Thus, a comprehensive approach to the diagnosis and optimization of GTPs, based on the use of modern technologies and methods, enables the achievement of a high level of reliability, energy efficiency, and environmental safety of power units [10].

An important addition to these approaches is the use of regularization techniques to enhance the robustness of predictive models in the presence of noisy data. Within the framework of this work, the following main propositions are put forward:

1) The application of L1 and L2 regularization methods reduces the impact of noise and missing data, which are characteristic of industrial monitoring systems;

2) Regularization contributes to increased robustness and generalization capability of regression models when forecasting technical parameters of gas turbine units (GTUs);

3) Integration of regularized models into industrial automation loops creates a foundation for the implementation of predictive diagnostics.

Industrial automation is characterized by complexity and a large number of distortions arising from data noise or the instability of measurement systems. Under such conditions, regularization plays a key role, preventing the overfitting of machine learning algorithms and ensuring the stability of their operation.

The necessity of conducting this research is due to the fact that under real-world GTU operating conditions, measurement data are characterized by high noise levels, the presence of outliers, and missing values, which significantly reduces the accuracy of predictive models and the effectiveness of monitoring systems. The application of regularization methods enables robust predictive analysis aimed at the early detection of equipment degradation, failure forecasting, and optimization of gas turbine unit operating regimes.

The aim of this work is to evaluate and experimentally confirm the effectiveness of applying L1 and L2 regularization methods to improve the robustness and accuracy of forecasting gas turbine unit

parameters under conditions of noisy, incomplete, and distorted data. The study intends to demonstrate that the use of regularization enhances the accuracy and robustness of predictive models, reduces the influence of noise and missing data in measurements, and improves the generalization capability of models when analyzing real operational data. To achieve this goal, the following research objectives are formulated:

- Analysis of modern methods for forecasting the technical condition of GTUs and identification of their limitations under noisy data conditions;
- Development and implementation of regression models for forecasting GTU parameters without regularization and with the application of Ridge and LASSO methods;
- Conducting an experimental study on archival data from a real gas turbine unit containing noisy data and missing values;
- Comparative evaluation of forecasting quality using metrics (MAE, RMSE, R^2);
- Comparison of the obtained results with those presented in the work of other authors, and formulation of conclusions regarding the feasibility of applying regularization for forecasting tasks in industrial automation.

The primary task is to develop solutions capable of effectively processing data, taking into account their characteristics and the specifics inherent in industrial conditions. Such solutions can significantly increase the operational stability of power units, minimizing the risks of unplanned shutdowns and optimizing operational costs.

Overview of regularization and its significance in forecasting tasks

Regularization is a technique in machine learning aimed at improving the generalization capability of models. The primary goal of regularization is to prevent overfitting, which occurs when a model adapts too closely to the training data, including noise and outliers, thereby losing its ability to accurately predict new, unseen data. Overfitting is particularly critical in tasks related to industrial automation, where data quality can vary significantly due to interference, technical failures, and other factors. Regularization helps balance the model, reducing the risk of overfitting and improving its stability in forecasting.

The problem of overfitting is often associated with excessive model complexity. The more parameters a model has, the higher the probability that it will begin to "memorize" random noise in the data. This leads to a decrease in prediction accuracy on new data and reduces the model's practical utility. Regularization addresses this problem by adding penalty terms to the error function, which constrain the values of the model coefficients or their number. This makes the model more robust to data variability and enhances its ability to identify general patterns.

There are two main types of regularization: L1 and L2. L1 regularization, known as Least Absolute Shrinkage and Selection Operator (LASSO), adds a penalty to the error function in the form of the sum of the absolute values of the model coefficients. This causes some coefficients to become exactly zero, effectively discarding insignificant features. This approach is useful for feature selection, which is particularly relevant when working with high-dimensional data. The main advantages of L1 regularization include model simplification and improved interpretability. However, it may be less effective when dealing with highly correlated features.

L2 regularization, also referred to as Ridge regression, adds a penalty to the error function in the form of the sum of the squares of the coefficients. Unlike L1, L2 does not zero out coefficients but only reduces their values, thereby mitigating the influence of noise and stabilizing the model. L2 regularization is particularly effective in tasks where all features are important and a balanced distribution of weight among them is required. However, this approach does not aid in explicit feature selection, which can be a limitation when working with data where only a small subset of parameters is meaningful.

A comparison of L1 and L2 regularization shows that both approaches have their advantages and limitations. L1 is well-suited for feature selection and creating simpler models but can yield unstable results in the presence of correlated variables. L2 provides a smoother distribution of weights and stability but does not simplify the model, as it does not zero out coefficients. These methods can be combined to leverage their joint benefits, as implemented in ElasticNet, which uses a linear combination of L1 and L2 penalties.

The LASSO method is actively used for selecting key parameters in complex systems, such as sensor data analysis in GTPs, where it is necessary to identify the most important characteristics from a multitude of available data. Ridge regression finds application in tasks requiring accurate prediction that accounts for the influence of all parameters, for example, in forecasting system energy consumption.

ElasticNet, combining the properties of LASSO and Ridge, represents a versatile approach well-suited for working with data where features may be both correlated and redundant. This method is actively used in industrial automation for creating predictive models robust to noise and outliers, thereby improving both prediction accuracy and model interpretability [11, 12].

Theoretical foundations of the methods

L2 regularization adds a penalty to the error function proportional to the square of the model coefficient values. This leads to the minimization of the following function:

$$J(\theta) = \sum_{i=1}^{n} (y_i - \hat{y}_i)^2 + \lambda \sum_{j=1}^{p} \theta_j^2, \quad (1)$$

where y_i is the real values, $\hat{y}_i$ is the predicted values, θ_j is the model coefficients, p is the number of features, λ is the regularization hyperparameter determining the degree of penalty.

The main idea of L2 regularization is to constrain the values of the coefficients, preventing their excessive growth, which can be caused by noise or multicollinearity in the data.

Ridge regression reduces the influence of features that contribute disproportionately to the model, especially if these features are associated with data noise. By smoothing the coefficients, the model becomes more stable and capable of identifying general patterns. This is particularly important in tasks related to forecasting in automation systems, where data can be highly noisy. In GTPs, Ridge can be used for predicting temperature, pressure, or vibration, providing stable results even in the presence of imperfections in the measurement data.

L1 regularization introduces a penalty proportional to the sum of the absolute values of the model coefficients. The objective function for LASSO is as follows:

$$J(\theta) = \sum_{i=1}^{n} (y_i - \hat{y}_i)^2 + \lambda \sum_{j=1}^{p} |\theta_j|. \quad (2)$$

Unlike L2 regularization, L1 leads to the zeroing of coefficients for some features, making it particularly useful for feature selection in tasks with high-dimensional data. Lasso automatically selects the most significant features, reducing the others to zero. This not only improves model interpretability but also allows for data dimensionality reduction, which is critical in systems where a large number of parameters are analyzed. In GTP condition monitoring systems, LASSO helps identify key parameters, such as vibration or rotational speed, while ignoring less significant data. This simplifies the interpretation of results and reduces the computational load.

ElasticNet combines the advantages of L1 and L2 regularization by adding a penalty to the error function that includes both the sum of squared coefficients (L2) and the sum of their absolute values (L1):

$$J(\theta) = \sum_{i=1}^{n} (y_i - \hat{y}_i)^2 + \alpha\lambda \sum_{j=1}^{p} \theta_j^2 + (1-\alpha)\lambda \sum_{j=1}^{p} |\theta_j|, \quad (3)$$

where α regulates the balance between the L1 and L2 components.

ElasticNet is particularly effective in situations where features are correlated with each other or when the data contain both relevant and irrelevant variables. Unlike LASSO, which tends to select one feature from a group of correlated ones, ElasticNet can retain several such features [13].

In forecasting tasks for equipment parameters, ElasticNet enables:

- Accounting for correlated parameters, such as pressure and temperature in power equipment systems;
- Selecting key features while maintaining model robustness to noise;
- Providing a better balance between accuracy and interpretability, especially when working with high-dimensional and noisy data.

For example, in GTP control systems, ElasticNet can be used for predicting component wear, where data is collected from dozens of sensors, many of which have interrelated measurements.

Application of regularization in PLC-based systems

Programmable Logic Controllers (PLCs) play a key role in industrial automation systems. Modern data analysis approaches, such as machine learning and predictive analytics, are increasingly being applied at the PLC level. However, the implementation of such technologies faces a number of unique constraints, including limited computational resources, strict processing time requirements, and the necessity of integration with existing systems. Regularization methods, such as L1 and L2, can be adapted for these conditions, ensuring algorithm robustness to noise and improving prediction accuracy [14].

Modern PLCs, such as Siemens SIMATIC or Allen-Bradley CompactLogix, support analytics and machine learning algorithms, including linear regression, time series forecasting, and anomaly recognition. However, most complex computations, such as neural network training, are performed on external devices, for instance, in the cloud or on local servers. PLCs are then integrated with these systems to perform real-time predictions [15].

To apply L1 and L2 regularization methods under constrained computational resources, it is necessary to adapt the algorithms. This may include:

- Model compression: Using pre-trained models where regularization was applied during the training phase, with a simplified version deployed on the PLC.
- Data dimensionality reduction: L1 regularization (e.g., via LASSO regression) allows for the exclusion of irrelevant features, minimizing the volume of data processed by the controller.
- Data preprocessing: Regularization can be used to stabilize predictive models on an external server, after which the optimized model is loaded into the PLC for executing predictions.

Regarding integration possibilities with existing automation systems, the integration of regularization methods with PLC systems can be achieved through the use of existing communication protocols (Modbus, OPC UA) and specialized libraries. For example:

- Using data from the PLC for preliminary processing on an external device and returning optimized parameters;
- Embedding regularized models (e.g., Ridge regression equations) directly into the PLC code written in IEC 61131-3 languages (ST or SCL).

Such integration minimizes modifications to the existing infrastructure and maximizes the use of analytics capabilities in real-time conditions.

Suppose a time series describing equipment temperature is being analyzed, where the data contains noise and outliers due to sensor malfunctions. Using Ridge regularization, probable deviations from

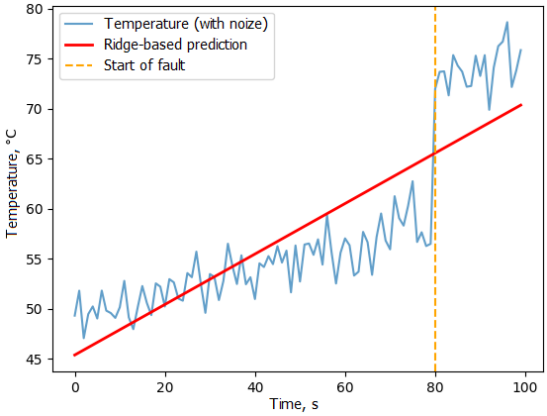

Fig. 1. Prediction of the best model

the norm can be forecast. Suppose a time series describing equipment temperature is being analyzed, where the data contains noise and outliers due to sensor malfunctions (Fig. 1). Using Ridge regularization, probable deviations from the norm can be forecast.

In a GTU diagnostic system, parameters must be adjusted under unstable data conditions using LASSO to identify the most significant parameters for optimization. LASSO effectively identifies key parameters by zeroing out insignificant ones. This helps focus on important features, minimizing model complexity and improving result interpretability.

The performance of the methods is analyzed using real data from a gas turbine engine within the framework of the research problem of reconstructing the time series of oil temperature at the GTU bearing outlet. It is assumed that the corresponding sensor has failed, and its readings need to be reconstructed based on measurements from other standard engine parameters. Time series of the following parameters are used as input features:

- Oil temperature readings in various GTU components;
- Fuel gas consumption;
- Power turbine rotational speed;
- Compressor turbine rotational speed;
- Vibration displacement;
- Oil pressure;
- Exhaust gas temperature;
- Air inlet pressure.

Some of these parameters are physically related to oil temperature. However, to complicate the task, features possessing weak or no correlation with the target variable are additionally introduced into the model. This creates a redundant feature space that includes irrelevant data. Furthermore, the experimental data contain noise due to measurement errors and outliers.

This problem formulation allows for demonstrating the impact of regularization under conditions of:

- Multicollinearity;
- Presence of irrelevant features;
- Noisy and unstable measurements;
- Risk of model overfitting.

The test set is formed from the last 20–30% of the time-series measurements, which corresponds to a real-world scenario of forecasting future values based on historical data.

To ensure experimental reproducibility, the pseudo-random number generators for Python, NumPy, and TensorFlow were fixed, and random shuffling of the training set was disabled.

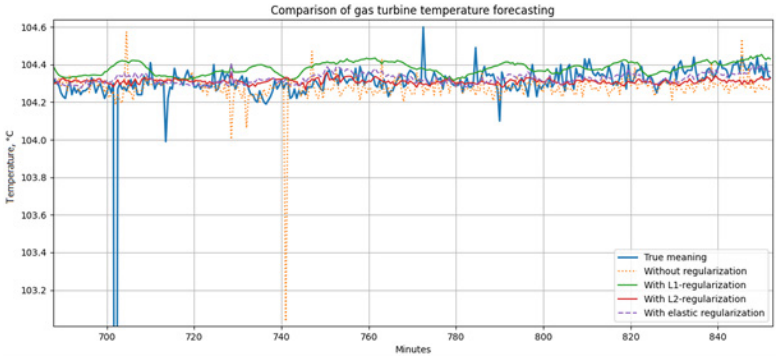

Fig. 2. Model prediction

To solve the problem, a regression-type neural network model with regularization is used: LASSO (L1), Ridge (L2), and ElasticNet (combination of L1 and L2). The obtained models are depicted in Fig. 2.

In the scikit-learn library implementation, the regularization parameter is denoted as α, which corresponds to the coefficient λ in the mathematical notation of formulas 1 and 2.

The parameter λ (α) determines the trade-off between approximation accuracy and model complexity. For small values of λ, the model seeks to minimize the error on the training set, which can lead to overfitting. For excessively large values of λ, the model becomes overly smoothed and loses its ability to adequately describe the data (underfitting).

The optimal value of λ cannot be determined analytically and depends on:

- Sample size;
- Level of noise in the data;
- Degree of feature correlation;
- Model complexity.

Increasing the data volume generally allows for a smaller λ, whereas a high noise level or the presence of numerous irrelevant features necessitates stronger regularization.

In this work, the optimal value of λ is selected through a grid search over a logarithmic scale (e.g., 10^{-6}–10^{-1}) using a validation set. The selection criterion is the minimum error on the validation data. The final quality assessment is conducted on the test set, which was not involved in hyperparameter tuning.

This approach ensures a correct assessment of the model's generalization capability and eliminates bias in the results.

For the investigated problem, the optimal λ value was selected through a grid search over a logarithmic scale from 10^{-6} to 10. The coefficient selection plots for the Ridge and LASSO methods are shown in Fig. 3. Based on this method, the following regularization coefficients were obtained: L1 – 0.0025, L2 – 0.04. Additionally, a heatmap was generated to find the optimal coefficients for the ElasticNet method (Fig. 4), yielding the following regularization coefficients: L1 – 10^{-5}, L2 – 0.023.

For this problem, the following model quality metrics were obtained (Table 1). Based on the presented results, a significant influence of regularization on the generalization capability of the neural network model can be concluded.

Analysis of the mean squared error (MSE) values shows that the model without regularization demonstrates the worst result. This indicates pronounced overfitting: the model approximates the training set too precisely but generalizes poorly to the test interval data.

The addition of regularization leads to a sharp decrease in error:

- with L1 regularization, the MSE value reduces to 0.021;

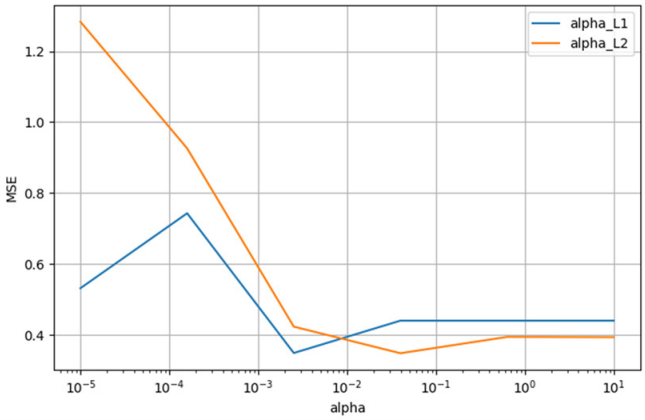

Fig. 3. Finding optimal L1 and L2 regularization coefficients for Ridge and LASSO methods

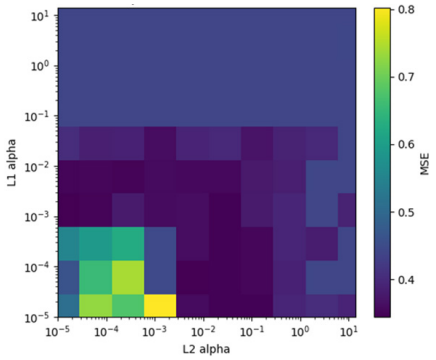

Fig. 4. Finding optimal L1 and L2 regularization coefficients for the ElasticNet method

Table 1

Training results

Model		MSE	MAE	R^2
Without regularization	train	0.015	0.059	0.734
	test	0.072	0.097	–2.752
L1 regularization	train	0.05	0.056	0.118
	test	0.021	0.054	–0.119
L2 regularization	train	0.051	0.057	0.1016
	test	0.019	0.045	–0.0079
ElasticNet	train	0.051	0.058	0.099
	test	0.02	0.045	–0.022

- with L2 regularization, the best result is achieved – 0.019;
- the ElasticNet (L1+L2) model shows a comparable value – 0.020.

A similar trend is observed for the MAE metric: a decrease from 0.097 (without regularization) to 0.045–0.054 when using penalty terms. The minimum MAE value (0.045) is achieved with L2 regularization and ElasticNet.

The coefficient of determination R^2 remains negative in all cases, indicating that the models are still inferior to a naive mean prediction. However, the addition of regularization significantly brings the model closer to an adequate description of the data: the R^2 value improves from −2.752 (without regularization) to −0.0079 with L2 regularization. This signifies the virtual elimination of the overfitting effect and a substantial increase in model robustness.

In a similar study [17], comparable results were obtained. The authors note that the application of L1 regularization allowed for a reduction in the number of initial features by 60–90%, which is consistent with the results obtained in the present work, where a significant decrease in the effective dimensionality of the input space is also observed.

Furthermore, study [17] showed that L2 regularization helps reduce the impact of multicollinearity among features and provides a 12–18% increase in prediction accuracy. In the present study, the application of L2 regularization also led to a significant improvement in model quality compared to the version without regularization, confirming its effectiveness for the considered time series reconstruction task.

Thus, the results confirm that for the task of reconstructing a sensor time series from indirect measurements, the application of regularization is a necessary condition for obtaining a robust model. In this experiment, L2 regularization proved to be the most effective, providing the minimum MSE and MAE values, as well as the best coefficient of determination.

The LASSO method demonstrates the ability for automatic feature selection. As the parameter α increases, some coefficients are zeroed out, leading to the exclusion of irrelevant parameters from the model. This is particularly effective under conditions of introduced redundant and weakly correlated features.

At small values of α, LASSO's behavior is close to that of ordinary linear regression. As α increases, a sequential zeroing of weights occurs, which reduces the influence of noise and enhances model interpretability. However, excessive regularization can lead to the removal of informative features and an increase in error.

The Ridge method smoothly reduces the values of coefficients, without bringing them to zero. This ensures smoothing of weights and model stability in the presence of multicollinearity among GTU parameters.

Ridge is better suited for tasks where most features contain useful information, but their influence needs to be constrained to prevent overfitting. Model predictions are characterized by greater stability on the test set.

ElasticNet combines the properties of L1 and L2 regularization and is an effective tool in the presence of correlated features and redundant data. Under the conditions of this experiment, this method simultaneously allows for reducing model dimensionality and smoothing coefficients, ensuring robustness to noise.

Advantages and limitations of regularization methods

Regularization methods, such as LASSO and Ridge, are powerful tools in machine learning and statistics. They find application in forecasting and data analysis tasks due to their ability to improve model generalization capability and combat the problem of overfitting. The advantages of these methods include the reduction of overfitting, increased model robustness to noise, and the ability to work with high-dimensional data. Various limitations arise. When working with high-dimensional data, finding a suitable α can be challenging due to the difficulty of assessing model generalization capability. This leads to specific requirements for hyperparameter tuning. ElasticNet, combining L1 and L2 regularization, is often used to overcome the shortcomings of LASSO and Ridge. However, the interpretation of coefficients becomes more complex, as the model includes components from two different methods. There is also a dependency on the quality of the initial data and sensitivity to the scale of the data (requiring feature normalization).

Conclusion

The conducted experiment on reconstructing the oil temperature time series under sensor failure demonstrated that regularization methods significantly enhance model robustness under conditions of noise, redundant, and weakly correlated features. Methods for finding regularization coefficients (α) for industrial systems were also addressed, and recommendations for finding optimal model regularization hyperparameters were proposed.

L1 regularization is effective when automatic selection of significant parameters is necessary, whereas L2 regularization ensures more stable model behavior in the presence of multicollinearity. The optimal value of the parameter α is determined experimentally through validation and depends on the data structure and noise level.

The practical application of L1 and L2 regularization methods in diagnostic and parameter reconstruction tasks for gas turbine units confirms their feasibility for industrial automation, where data are characterized by noise, correlation, and the potential redundancy of measured parameters.

REFERENCES

1. **Kolmogorova S.S., Golubyatnikova N.O.** On the application of big data structure regularization in a distributed evaluation system for emergency parameters. *The Bulletin of Voronezh State Technical University*, 2022, Vol. 18, No. 5, Pp. 91–99. DOI: 10.36622/VSTU.2022.18.5.012

2. **Kostychev V.I., Fedin V.D.** The using of L2 regularization to improve the accuracy of data forecasting in industrial factories. *Chelovek, obshchestvo, tekhnologii: aktual'nye voprosy vzaimodeistviia: sbornik statei IV Mezhdunarodnoi nauchno-prakticheskoi konferentsii* [*Man, society, technology: current issues of interaction: Proceedings of the IV International scientific and practical conferenc*e], 2024. Pp. 82–88.

3. **Tazhikova G.D., Alimova A.A., Kuanyshbaeva L.D.** Algoritmy obucheniia pri rabote s zadannymi naborami dannykh [Training algorithms for working with given data sets]. *Proceedings of the 15th International Scientific and Practical Conference "Scientific Horizon in the Context of Social Crises"*, 2024, Vol. 198, Pp. 128–132.

4. **Nazarenko I.V., Nikolaichuk N.Ya., Kozovik N.I.** Modelirovanie rezhimov raboty gazoperekachivaiushchikh agregatov na osnovanii metoda gruppovogo ucheta argumentov [Modeling of operating modes of gas pumping units based on the method of group accounting of arguments], *Young Scientist*, 2014, Vol. 66, No. 7, Pp. 162–171.

5. **Melkumova L.E., Shatskikh S.Ya.** Comparing Ridge and LASSO estimators for data analysis. *Procedia Engineering*, 2017, Vol. 201, Pp. 746–755. DOI: 10.1016/j.proeng.2017.09.615

6. **Alekseev A.P., Efremov V.A.** Tsifrovoi dvoinik v kiberfizicheskikh sistemakh: analiticheskie prediktivnye prilozheniia [Digital twin in cyber-physical systems: analytical predictive applications.]. *Tekhnologicheskaia perspektiva v ramkakh evraziiskogo prostranstva: novye rynki i tochki ekonomicheskogo rosta* [*Technological perspectives within the Eurasian space: new markets and points of economic growth*], 2019, Pp. 171–178.

7. **Potekhin V.V., Liadskii D.D., Bolotov S.V.** Ispol'zovanie metodov mashinnogo obucheniia dlia prediktivnogo analiza pri ekspluatatsii proizvodstvennykh system [Using Machine Learning Methods for Predictive Analysis in the Operation of Production Systems]. *Voprosy sistemnogo tekhnologicheskogo perekhoda* [*Issues of systemic technological transitio*n], 2023, Pp. 90–100.

8. **Gordievskaya K.Y., Khalimov D.N., Gorbenko O.N., Rozhkova A.A.** The analysis of methods for forecasting the state of technical equipment. *Modeling, Optimization and Information Technology*, 2014, Vol. 2, No. 4.

9. **Mikhailov S.A., Petrova E.V.** Regularization in Machine Learning: Application in Industrial Automation. Management systems and information technologies, 2021, No 2, Pp. 45–53.

10. **Ibragimov B.L., Gusev G.G.** Optimizing stochastic gradient boosting with out-of-sample evaluation metrics. *Proceedings of MIPT*, 2024, Vol. 16, No. 3, Pp. 49–56.

11. **Voronina V.V., Mikheev A.V., Iarushkina N.G., Sviatov K.V.** *Teoriia i praktika mashinnogo obucheniia* [*Theory and practice of machine learning*]. Ulyanovsk: UlGTU, 2017.

12. **Nguyen T.V., Kravets A.G.** Forecasting technological trends based on the heterogeneous data analysis. *Software and Systems*, 2022, Vol. 35, No. 3, Pp. 396–412. DOI: 10.15827/0236-235X.139.396-412

13. **Vrabie I., Spesivtsev P., Kaipov E., Syresin D., Lomukhin A., Romashkin S., Kulyatin O.** Digital Twin for Downhole Pressure Gauges: Model and Field Case Study. *SPE Russian Petroleum Technology Conference*, 2020. DOI: 10.2118/201926-MS

14. **Hastie T., Tibshirani R., Friedman J.** *The Elements of Statistical Learning: Data Mining, Inference, and Prediction*, 2nd ed. NY: Springer, 2009. DOI: 10.1007/978-0-387-84858-7

15. **Novikov A.A., Budzinskaya E.O., Kaneva O.N.** Analysis of time series forecasting methods. *Informatsionnyi biulleten' Omskogo nauchno-obrazovatel'nogo tsentra OmGTU i IM SO RAN v oblasti matematiki i informatiki* [*Information bulletin of the Omsk Scientific and Educational Center of OmskSTU and the Institute of Mathematics of the Siberian Branch of the Russian Academy of Sciences in the field of mathematics and computer science*], 2020, Pp. 37–43.

16. **Sabitov B.R., Almasbekova Z., Karagulov Sh.K.** The use of machine learning in applied tasks. *Bulletin of the Kyrgyz National University named after J. Balasagyn*, 2019, No. S1, Pp. 154–157.

17. **Deulin N.V.** Regularization in machine learning: Control over retraining. *Science and technologies – 2025*, 2025, Pp. 83–92.

INFORMATION ABOUT AUTHOR / СВЕДЕНИЯ ОБ АВТОЕ

Yaroslav V. Ludishchev
Лудищев Ярослав Вадимович
E-mail: ludishevyaroslav@mail.ru

Submitted: 07.11.2025; Approved: 11.03.2026; Accepted: 19.03.2026.
Поступила: 07.11.2025; Одобрена: 11.03.2026; Принята: 19.03.2026.

Computing, Telecommunication and Control, 2026, Vol. 19, No. 1, Pp. 38–45.
Информатика, телекоммуникации и управление. 2026. Том 19, № 1. С. 38–45.

Research article
DOI: https://doi.org/10.18721/JCSTCS.19104
UDC 621.37

SIGNAL DISTORTION IN POLAR ARCHITECTURE TRANSMITTERS USING CLASS E RF POWER AMPLIFIERS

H.D. Pham ✉ , *V.A. Sorotsky, N.A. Treimut*

Peter the Great St. Petersburg Polytechnic University,
St. Petersburg, Russian Federation

✉ phamduc2511997@gmail.com

Abstract. The trend towards increasing the energy efficiency of transmitters used in radio and telecommunications systems focuses the attention of equipment developers on finding optimal solutions when transitioning from linear power amplifiers (PAs) to amplifiers operating in switching mode. It is shown in the paper that signal distortion level along with high energy efficiency must be considered as an important parameter of PA. Reasons of signal distortions in class E switched-mode PA used in polar architecture transmitters are given. It is shown that most sufficient distortion is caused by phase shift of the load current, which results from the nonlinear change of transistors' output capacitance when amplifying signals with a non-constant envelope. The results of calculations of the error vector magnitude when using multilevel spectrally efficient modulation types, in particular quadrature amplitude modulation (QAM) and amplitude-phase shift keying (APSK), are presented. The results confirmed that for class E PA the most sufficient type of distortion is phase distortion. The results of analytical model are confirmed by simulation. It is shown that for 16-QAM at bit error rate = 10^{-4}, the energy loss is 0.5 dB, while for 16-APSK its value increases to 2.2 dB. The results presented in the paper can be used in the development of signal predistortion methods for switching class E PAs, ensuring a reduction in signal distortions.

Keywords: switched-mode power amplifier, envelope amplifier, class E, AM/AM, AM/PM, EVM

Citation: Pham H.D., Sorotsky V.A., Treimut N.A. Signal distortion in polar architecture transmitters using class E RF power amplifiers. Computing, Telecommunications and Control, 2026, Vol. 19, No. 1, Pp. 38–45. DOI: 10.18721/JCSTCS.19104

Научная статья
DOI: https://doi.org/10.18721/JCSTCS.19104
УДК 621.37

НЕЛИНЕЙНЫЕ ИСКАЖЕНИЯ СИГНАЛОВ В УСИЛИТЕЛЯХ МОЩНОСТИ КЛАССА E, ПРИМЕНЯЕМЫХ В ТРАНСМИТТЕРАХ С ПОЛЯРНОЙ АРХИТЕКТУРОЙ

Х.Д. Фам ✉ , *В.А. Сороцкий, Н.А. Треймут*

Санкт-Петербургский политехнический университет Петра Великого,
Санкт-Петербург, Российская Федерация

✉ phamduc2511997@gmail.com

Аннотация. Тенденция к повышению энергетической эффективности трансмиттеров, применяемых в системах радиосвязи и телекоммуникаций, фокусирует внимание разработчиков аппаратуры на поиске оптимальных решений при переходе от использования линейных усилителей мощности к усилителям, работающим в ключевом режиме. В работе показано, что при этом необходимо не только оценивать достигаемый выигрыш по КПД, но и учитывать увеличение уровня нелинейных искажений сигналов. Рассмотрены механизмы, приводящие к появлению искажений сигналов в усилителях мощности класса E, применяемых в трансмиттерах с полярной архитектурой. Показано, что при усилении сигналов с изменяющейся огибающей наиболее заметное влияние на искажение сигналов оказывает паразитный фазовый сдвиг тока в нагрузке усилителя мощности, обусловленный изменением выходной емкости транзистора. Приведены результаты расчетов амплитуды векторной ошибки при использовании многоуровневых спектрально эффективных видов модуляции, в частности квадратурной амплитудной модуляции и амплитудно-фазовой модуляции, которые подтвердили, что фазовые искажения оказывают превалирующее влияние на ухудшение свойств сигналов. Этот вывод подтверждается результатами расчета вероятности битовой ошибки. Показано, что для 16-QAM при BER = 10^{-4} энергетический проигрыш составляет 0,5 дБ, а для 16-APSK его значение увеличивается до 2,2 дБ. Представленные в работе результаты могут быть использованы при разработке методов предыскажений сигналов в ключевых усилителях мощности класса E, обеспечивающих снижение искажений сигналов.

Ключевые слова: ключевой усилитель мощности, усилитель огибающей, класс E, AM/AM, AM/PM, амплитуда векторной ошибки

Для цитирования: Pham H.D., Sorotsky V.A., Treimut N.A. Signal distortion in polar architecture transmitters using class E RF power amplifiers // Computing, Telecommunications and Control. 2026. Т. 19, № 1. С. 38–45. DOI: 10.18721/JCSTCS.19104

Introduction

Today the most important tasks for telecommunication and radio systems engineers are data rate and energy efficiency improvement. However, it is challenging to fulfill both of these tasks. To provide data rate improvement, signals with different quadrature amplitude modulation (QAM) types are widely used [1, 6, 13]. These types of signals could be characterized by relatively big constellation size and high spectral efficiency compared to simple analog modulation or manipulation. Despite positive qualities, such signals could be characterized with high dynamic ranges, and high distortion sensitivity. As a result, relatively small nonlinearities in power amplifier (PA) transfer characteristics could cause severe rise in error vector magnitude (EVM) in the transmitter, as well as in bit error rate (BER). These circumstances have led to a significant increase in the requirements for the linearity of PAs.

The use of signals with complicated types of modulation, in addition to increasing the PA linearity, requires its efficiency rising. The main problem here is that amplifying signals with a high peak to

average power ratios using linear mode PAs usually decreases the efficiency to 25–30% [2, 3] and this level sufficiently can be increased only by using a switched-mode PA, for example, class E mode [4, 5]. At the same time, it must be remembered that switched-mode PAs are fundamentally nonlinear and its use may be accompanied by an increase in signal distortion.

In well-known publications devoted to the analysis of class E PA characteristics, the authors limit themselves to considering the case of a constant voltage in the transistor supply circuit [4, 5, 7, 8]. The main attention in these works is paid to providing the conditions necessary to eliminate switching losses, for example, switching the transistor at zero voltage at the drain-source terminals (zero voltage switching, ZVS) and zero current in the drain circuit (zero voltage derivative switching, ZVDS). At the same time, it is obvious that the ZVS and ZVDS conditions can only be implemented at a fixed frequency and are extremely sensitive to changes in load and supply voltage: any deviations from the nominal values change the dynamics of the output capacitance charging process, leading not only to an increase in switching power losses, but also to the appearance of amplitude changes which are linear distortions for PA. Moreover, if we consider that the output capacitance of the transistor does not remain constant when the drain voltage changes, as is commonly assumed in well-known class E models, but changes according to a nonlinear law [9], then it is appropriate to assume the appearance of phase distortions of the signals.

The purpose of this work is to study the effect of the nonlinear dependence of the output capacitance of a transistor on the voltage at the drain-source terminals on the distortion of signals with a non-constant envelope in a polar architecture transmitter.

Signal distortion estimation when assuming nonlinear output capacitance in class E PA

It is well-known that in order to amplify signals with a non-constant envelope using a switched-mode PA, the transmitter must be designed in accordance with the polar architecture (Fig. 1). In the RF channel, the amplitude-limited phase-modulated high-frequency signal $S_0(t)$ of the original RF signal $S(t)$, and the envelope channel provides amplification of signal's envelope $S_{env}(t)$, which then enters the power supply chain of the class E PA.

During this work we will assume that the envelope amplifier (EA) does not introduce distortions into the signal and distortions are caused only by the properties of the class E PA. The equivalent circuit of PA, taking into account the specifics of its operation as part of a polar architecture transmitter, is shown in Fig. 2. It has fundamental differences from the well-known class E PA models [4, 5]. As noted above, the voltage in the drain circuit of the transistor is not constant and its behavior can be taken into account using the voltage source $V_{dd}(t)$. With this in mind, the output capacitance of the transistor (the capacitance of the forming contour) is also not fixed and can increase or decrease in accordance with the law of voltage change $V_{dd}(t)$ [9].

The estimation of nonlinear distortions in the class E PA was carried out in two steps. On the first one, according to the diagram in Fig. 2, the voltage $V_{dd}(t)$ was changed and the amplitude and phase of the current in the load were fixed. During this measurement, the phase of the load current at the peak point – when the voltage $V_{dd}(t)$ reaches the maximum value of $V_{dd\ \max}$ and the PA operates in soft switching mode with ZVS and ZVDS conditions – was taken as the initial one. A low-pass filter was used as the load, the parameters of which were determined from the condition for ensuring the frequency overlap coefficient $K_f = f_{\max}/f_{\min} \approx 1.6$ [11]. The evaluation showed that with a decrease in voltage in the range from 1.0 $V_{dd\ \max}$ to 0.1 $V_{dd\ \max}$, the output capacitance of the transistor increases by 3.9 times.

The amplitude (AM/AM) and amplitude-phase (AM/PM) characteristics of the PA depend on the relative voltage $V_{dd\ \max}$ are shown in Figs. 3, 4.

As follows from the analysis of these dependencies, the most noticeable effect of the nonlinearity of the transistor capacitance in a class E PA in a transmitter with a polar architecture is on the

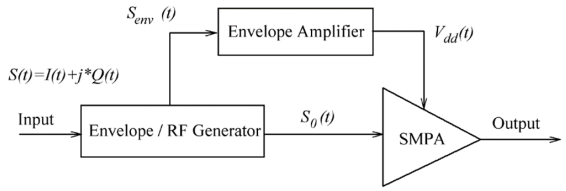

Fig. 1. PA with polar architecture

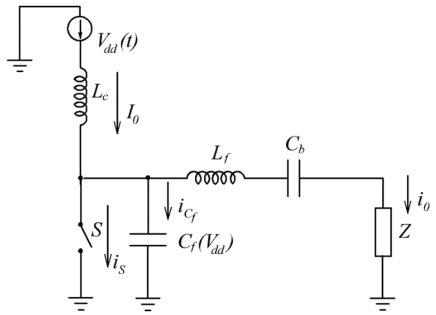

Fig. 2. Equivalent class E schematic

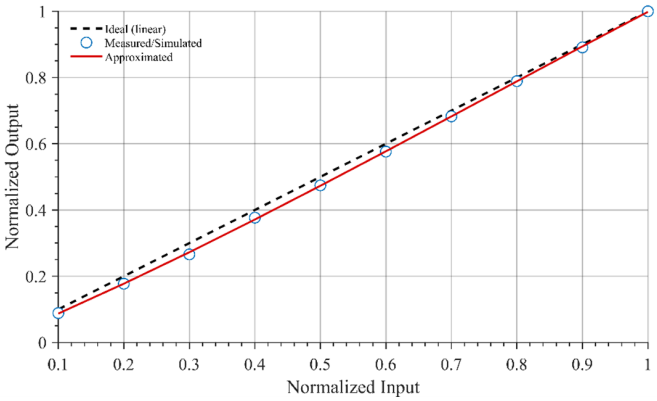

Fig. 3. AM/AM characteristic

amplitude-phase response, leading to a noticeable additional phase shift, which, with the indicated change in the output capacitance of the transistor $C_{max}/C_{min} = 3.9$, reaches 20 degrees.

At the second stage of the research, the EVM was estimated using simulation modeling. During modelling signals with QAM and amplitude-phase shift keying (APSK) were used. These results are shown in Table 1. Here, for comparison, the EVM values, calculated analytically using AM/AM (Fig. 3) and AM/PM (Fig. 4) characteristics are presented.

From the analysis of the results presented in table 1, we can conclude that the difference between the results of the EVM values obtained on the basis of analytical calculations and by simulation modeling does not exceed 1%. Considering that the analytical approach is much simpler to implement, it can be recommended as an estimation of the upper boundary of the EVM value.

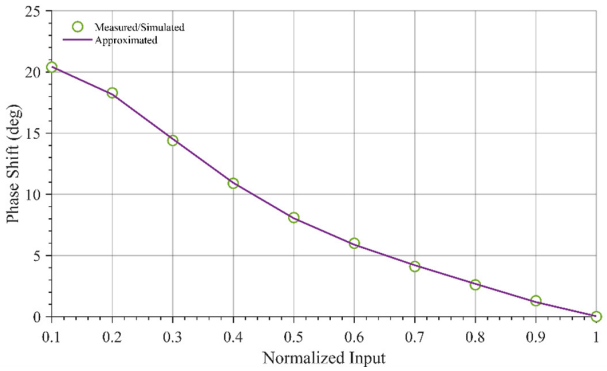

Fig. 4. AM/PM characteristic

a) *b*)

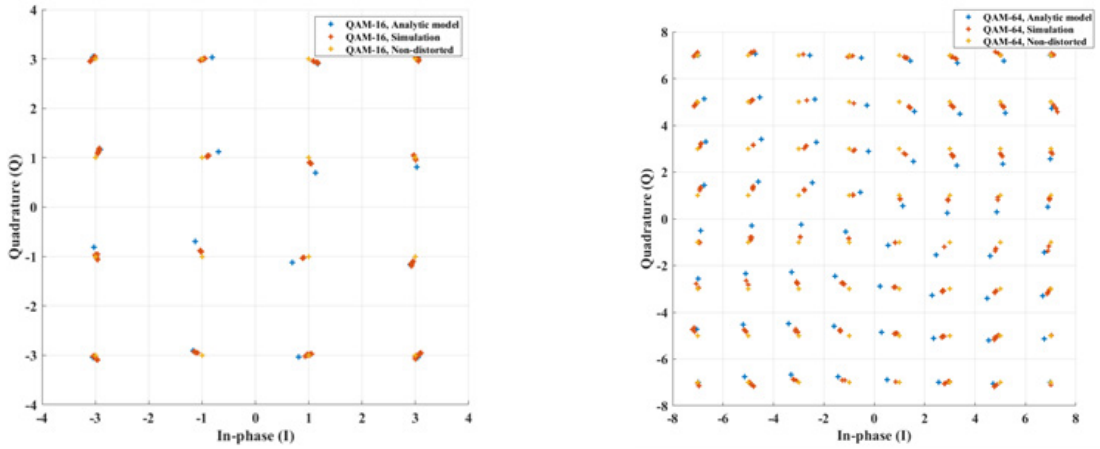

Fig. 5. Constellation diagrams of the PA output signal using different constellation sizes

Table 1

EVM for different modulation types

Modulation	Analytic model, %	Simulation, %
16-QAM	6.77	6.54
64-QAM	8.56	7.89
256-QAM	9.58	8.66
16-APSK	8.15	8.13
64-APSK	8.44	8.67

The impact of nonlinear distortion introduced by the class E PA on the constellation diagram can be evaluated from the positions of the received signal points for 16-QAM and 64-QAM modulated signals. These effects are clearly illustrated in the constellation diagrams presented in Fig. 5, which allow direct visual assessment of the scattering and displacement of the constellation points caused by the amplifier's nonlinear behavior.

Analyzing the relative contribution of amplitude and phase distortions in class E PA to the EVM value, it should be noted that the influence of the second type of distortion is much more noticeable.

a) *b*)

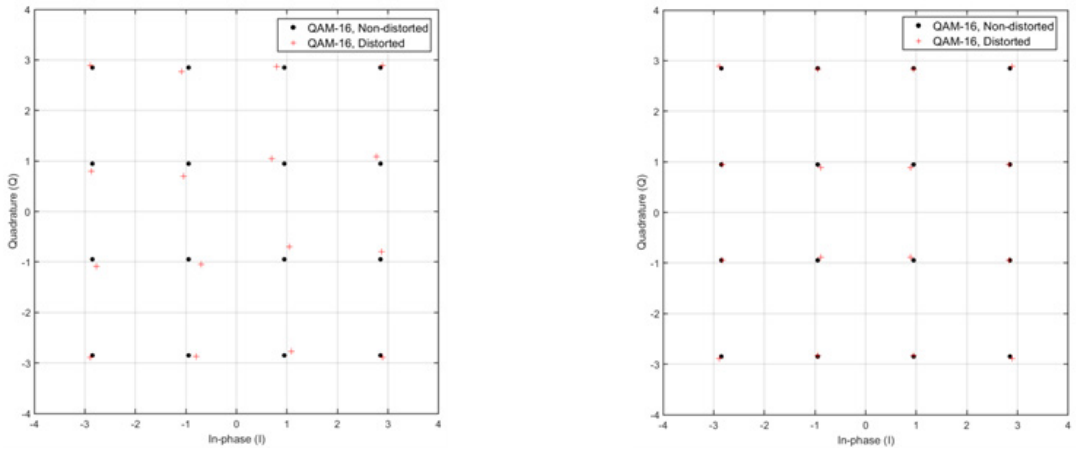

Fig. 6. Constellation diagram for 16-QAM with (*a*) and without (*b*) phase distortion

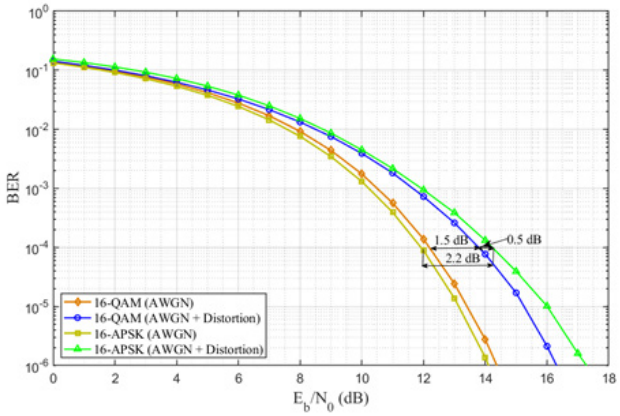

Fig. 7. BER performance of 16-QAM and 16-APSK

This, in particular, can be seen from a comparison of the dependencies in Figs. 3 and 4. A more detailed analysis showed that if it were possible to exclude a parasitic phase shift of the PA output current due to a change in the transistor capacitance, then in this case the EVM would be much smaller and amounted 1.82%. This result is in good agreement with diagrams of constellations shown in Fig. 6 corresponding to 16-QAM in the presence and absence of phase distortions.

Let us evaluate the effect of distortion in Class E PA on the probability of BER depending on the ratio of bit energy to spectral noise density using 16-QAM and 16-APSK signals as examples. The BER performance is evaluted in a channel with additive white Gaussian noise in the presence and absence of nonlinear distortions in the PA (Fig. 7).

From the analysis of the diagrams in Fig. 7, it can be seen that at BER = 10^{-4}, the distortions introduced by the class E PA in the case of signals with 16-QAM lead to an energy loss of 0.5 dB, and with 16-APSK, the loss increases to 2.2 dB. The stronger sensitivity of APSK signals to nonlinear distortions is due to the fundamental structure differences of their constellation's geometry [12], as well as the fact that phase distortions have stronger effect than amplitude ones in class E PA.

Conclusion

Summarizing the results obtained in this paper, we note the following:

1. It is shown that when applying amplifiers operating in switching mode, it is necessary not only to evaluate the efficiency gain achieved in this case, but also to take into account the increase in the level of nonlinear signal distortions.

2. One of the main reasons for the increase in the level of nonlinear distortions in the case of class E PA in a transmitter with a polar architecture is the appearance of a parasitic phase shift of the load current caused by a change in the output capacitance of the transistor when amplifying signals with a non-constant envelope. In particular, it is shown that for the GaN transistor used in the study, the change in the output capacitance of the device can reach 3.9 times, and the parasitic phase shift caused by this effect reaches 20 degrees.

3. Evaluation of the EVM in class E PA based on analytical approach, as well as using simulation modeling, showed that both methods provide approximately the same accuracy, moreover, difference in the EVM value does not exceed 1%. Needless to say, the analytical method is characterized by significantly less labor intensity.

4. When assessing the relative contribution of amplitude and phase distortions to the EVM value, it was found that the second type of distortion is predominant in class E PA. Therefore, in the case of signals with 16-QAM, the presence of amplitude distortion leads to an EVM value of 1.82%, and in the case of simultaneous action of both types of distortion, EVM = 6.77%.

5. The results of evaluating the effect of signal distortion in class E PA on the probability of bit error showed that at BER = 10^{-4} in the case of signals with 16-QAM energy loss is 1.5 dB, and when using 16-APSK signals, the loss increases to 2.2 dB.

REFERENCES

1. **Asif S.Z.** *5G Mobile Communications: Concepts and Technologies*, 1st ed. Boca Raton: CRC Press, 2018. DOI: 10.1201/9780429466342

2. **Cripps S.C.** *Advanced techniques in RF power amplifier design*. Boston/London: Artech House, 2002.

3. **Del Corso D., Camarchia V., Quaglia R., Bardella P.** *Telecommunication Electronics*. Boston/London: Artech House, 2020.

4. **Kamizierczuk M.K.** *RF Power Amplifiers*, 2nd ed. Chichester (UK): John Wiley & Sons Ltd., 2015.

5. **Grebennikov A.** *RF and Microwave Power Amplifier Design*, 2nd ed. Columbus (USA): McGraw-Hill, 2015.

6. **Prasad R.** *OFDM for wireless communication systems*. Boston/London: Artech House, 2004.

7. **Zhang P.** Analysis of Class E Push-Pull Power Amplifier for Low Power Wireless Energy Transmission. *2019 IEEE 4th Advanced Information Technology, Electronic and Automation Control Conference* (*IAEAC*), 2019, Pp. 2503–2506. DOI: 10.1109/IAEAC47372.2019.8997919

8. **Tong Z., Rivas-Davila J.M.** Wideband Push-Pull Class E Amplifier for RF Power Delivery. *2023 IEEE 24th Workshop on Control and Modeling for Power Electronics* (*COMPEL*), 2023, Pp. 1–7. DOI: 10.1109/COMPEL52896.2023.10220982

9. **Pham H.D., Sorotsky V., Zudov R., Treimut N., Pergushev A., Tung D.V.** The Impact of the Capacitance-Voltage Dependence on the Performance of Switched-Mode Power Amplifier. *2025 International Conference on Electrical Engineering and Photonics* (*EExPolytech*), 2025, Pp. 64–66. DOI: 10.1109/EExPolytech66949.2025.11252210

10. **Pham H.D., Sorotsky V.A.** Characteristics of Class E power amplifier with complex impedance load. *Computing, Telecommunications and Control*, 2025, Vol. 18, No. 1, Pp. 72–84. DOI: 10.18721/JCSTCS.18106

11. **Pham H.D., Zudov R.I., Sorotsky V.A.** Sintez fil'truiushchee-soglasuiushchei tsepi dlia raboty usilitelia moshchnosti klassa E v polose chastot [Synthesis of a filtering and matching network for the operation of a

Class E power amplifier in a frequency band]. *Vserossiiskaia konferentsiia "Nedelia nauki IEiT"* [*All-Russian Conference Science Week of IE&T*], 2025, Pp. 3–5.

12. **Suhartomo A., Vincent V.** Comparison of BER Performance for M-ary QAM and PSK on DWT-based OFDM System with PTS Technique Through AWGN Channel. *2020 IEEE International Conference on Sustainable Engineering and Creative Computing* (*ICSECC*), 2020, Pp. 5–10. DOI: 10.1109/ICSECC51444.2020.9557556

13. **Baldi M., Chiaraluce F., Cancellieri G.** Finite-Precision Analysis of Demappers and Decoders for LDPC-Coded M-QAM Systems. *IEEE Transactions on Broadcasting*, 2009, Vol. 55, No. 2, Pp. 239–250. DOI: 10.1109/TBC.2009.2016498

INFORMATION ABOUT AUTHOR / СВЕДЕНИЯ ОБ АВТОЕ

Huu Duc Pham
Фам Хыу Дык
E-mail: phamduc2511997@gmail.com
ORCID: https://orcid.org/0009-0004-1628-1772

Vladimir A. Sorotsky
Сороцкий Владимир Александрович
E-mail: sorotsky@mail.spbstu.ru

Nikita A. Treimut
Треймут Никита Александрович
E-mail: treimut2013@yandex.ru

Submitted: 25.12.2025; Approved: 19.03.2026; Accepted: 24.03.2026.
Поступила: 25.12.2025; Одобрена: 19.03.2026; Принята: 24.03.2026.

Computing, Telecommunication and Control, 2026, Vol. 19, No. 1, Pp. 46–56.
Информатика, телекоммуникации и управление. 2026. Том 19, № 1. С. 46–56.

Software and Hardware of Computer, Network, Telecommunication, Control, and Measurement Systems

Компьютерные сети, вычислительные, телекоммуникационные, управляющие и измерительные системы

Research article
DOI: https://doi.org/10.18721/JCSTCS.19105
UDC 004.056.5+519.237

METHOD FOR SELECTING THE STRENGTH OF UNSHARP MASKING PRE-FILTER USED TO ENHANCE THE DETECTION RATE OF DCT-DOMAIN IMAGE WATERMARKS

V.A. Anzhin ✉

Tomsk State University, Tomsk, Russian Federation

✉ viktor.anjin@gmail.com

Abstract. This work investigates the improvement of digital watermark detection robustness by applying image sharpening prior to the detection stage for an algorithm through the use of DCT-domain for both embedding and detection. Watermark detection is treated as a binary classification problem, enabling the use of the recall metric to evaluate the quality of detection. The recall metric is calculated on a set of test images by embedding and detecting the watermark with unsharp masking applied as a pre-filtering step. A method for selecting the optimal sharpening strength coefficient is proposed, based on maximizing the recall metric under fixed embedding and detection parameters. Computational experiments across a range of distortions demonstrate that pre-filtering with the optimal sharpening strength coefficient determined by the proposed method increases the true positive detection rate for most tested distortions without increasing the number of false positive detections.

Keywords: digital watermark, discrete cosine transform, unsharp masking, recall, content protection
Citation: Anzhin V.A. Method for selecting the strength of unsharp masking pre-filter used to enhance the detection rate of DCT-domain image watermarks. Computing, Telecommunications and Control, 2026, Vol. 19, No. 1, Pp. 46–56. DOI: 10.18721/JCSTCS.19105

Научная статья
DOI: https://doi.org/10.18721/JCSTCS.19105
УДК 004.056.5+519.237

МЕТОД ОПРЕДЕЛЕНИЯ КОЭФФИЦИЕНТА УВЕЛИЧЕНИЯ РЕЗКОСТИ ИЗОБРАЖЕНИЯ, ПОЗВОЛЯЮЩИЙ ПОВЫСИТЬ УСТОЙЧИВОСТЬ ЦИФРОВЫХ ВОДЯНЫХ ЗНАКОВ, ВСТРОЕННЫХ В ДКП-ОБЛАСТИ

В.А. Анжин ✉

Национальный исследовательский Томский государственный университет,
Томск, Российская Федерация

✉ viktor.anjin@gmail.com

Аннотация. В данной работе исследуется повышение устойчивости обнаружения цифровых водяных знаков (ЦВЗ) путем увеличения резкости изображения перед этапом обнаружения для алгоритма, использующего при встраивании и обнаружении область коэффициентов дискретного косинусного преобразования. Задача обнаружения ЦВЗ рассматривается как задача бинарной классификации, что позволяет использовать метрики качества бинарных классификаторов, в частности метрику полноты. Значение метрики полноты вычисляется на наборе тестовых изображений путем встраивания и последующего обнаружения ЦВЗ с предварительным увеличением резкости. Предложен метод выбора оптимального коэффициента увеличения резкости, основанный на максимизации значения метрики полноты при фиксированных параметрах встраивания и обнаружения. Результаты вычислительного эксперимента показывают, что предварительное увеличение резкости изображения перед обнаружением ЦВЗ с использованием коэффициента, выбранного предложенным методом, повышает число истинно положительных обнаружений для большинства протестированных искажений и не приводит к увеличению количества ложно положительных срабатываний.

Ключевые слова: цифровой водяной знак, дискретно косинусное преобразование, нерезкое маскирование, полнота, защита от несанкционированного копирования

Для цитирования: Anzhin V.A. Method for selecting the strength of unsharp masking pre-filter used to enhance the detection rate of DCT-domain image watermarks // Computing, Telecommunications and Control. 2026. Т. 19, № 1. С. 46–56. DOI: 10.18721/JCSTCS.19105

Introduction

A digital watermark is information embedded into host digital content (a container). The purpose of watermarking includes copyright protection, authentication, and traceability of digital media [1]. Over the past decades, a wide range of watermarking algorithms has been proposed [2, 3]. In this work, we focus on algorithms designed for digital images.

During the embedding stage the watermark is inserted into the container. Watermark embedding is paired with a detection algorithm, designed to verify the presence of a specific watermark within the analyzed container. Between the embedding and detection stages, the container can be modified by a range of distortions. These distortions may arise from unintentional factors such as signal processing operations occurring during transmission or losses in communication channels, as well as from attempts to remove the watermark.

Within a broad class of algorithms [4], the digital watermark is a pseudo-random sequence embedded into the container. Watermark detection is performed by calculating the correlation between the tested container and the watermark. The container is marked as watermarked when the correlation exceeds the selected detection threshold.

The correlation calculated between watermark and watermarked container for a watermark embedding and detection algorithm depends on both the embedding parameters and the distortions affecting the container. Distortions often decrease the correlation [5], resulting in undetected watermarks and reduced detection rates. However, certain types of distortions can increase the correlation, which improves detection performance. As described in [6–8], the use of sharpening filters as a pre-filtering step during the watermark detection stage improves the performance of the detection process.

In [6], the authors propose applying a linear unsharp masking filter before the watermark extraction in a spatial-domain correlation based watermarking scheme. The authors experimentally test the proposed method on a few images under several distortions and show that applying linear unsharp masking filtering prior to the extraction leads to better visual quality of the recovered watermark compared to the baseline method.

In [7], the authors propose using adaptive unsharp masking as a pre-filtering step before watermark detection. The proposed method adjusts the sharpening strength locally based on the contrast levels of the image. The authors demonstrate that using the proposed method can improve objective quality metrics for watermarking algorithm operating in the Discrete Cosine Transform (DCT) domain.

In [8], the authors propose a pre-filtering step applied before watermark extraction in a DCT-domain watermarking scheme. The pre-filtering process involves using an unsharp masking filter in combination with a Laplacian of Gaussian filter. The authors demonstrate that the proposed pre-filtering improves the quality of the extracted watermark compared to schemes without pre-filtering.

In our work we consider the use of an unsharp masking [9] which is a one of classical sharpening filters as a pre-filter applied to the watermarked container on the detection stage. The sharpened image is then used for watermark detection. Sharpening can be applied with different strength coefficients. In this paper, the impact of the sharpening strength coefficient to detection performance is evaluated. A method is proposed for determining the optimal sharpening strength coefficient through computational experiments with a software implementation of a watermarking algorithm. The founded optimal coefficient is then evaluated by testing detection rates on a set of images and range of distortions.

Methods

DCT-domain image watermarking

For embedding the watermark by the DCT based watermarking algorithm [10], the original image is divided into blocks of 8x8 pixels. A DCT is applied to each block. The transformed block of DCT coefficients is then converted into a sequence of 64 elements using ZigZag scanning [11], which reorders the DCT coefficients from low to high frequencies. In each sequence, the most significant low-frequency DCT coefficients are discarded. The remaining DCT coefficients are concatenated into a single sequence C_o. The length of C_o is n. The watermark W_r is a sequence of length n with elements generated according to the normal distribution $N(0, 1)$. The watermark W_r is embedded into the sequence C_o by equation (1). The modified blocks are transformed by inverse DCT to obtain the watermarked image.

$$C_w = C_o + \alpha W_r, \tag{1}$$

where $C_w, C_o, W_r \in R_n, n \in N, \alpha \in R$.

To detect the watermark W_r the normalized correlation (2) is calculated between W_r and the sequence of DCT coefficients C extracted from image.

$$\tilde{C}[i] = \frac{C[i]}{\sqrt{\sum_{j=1}^{n} C[j]^2}}, \quad \tilde{W}_r[i] = \frac{W_r[i]}{\sqrt{\sum_{j=1}^{n} W_r[j]^2}}, \quad Z_{nc}(C, W_r) = \sum_{i=1}^{n} \tilde{C}[i]\tilde{W}_r[i], \tag{2}$$

where $C, W_r \in R_n, n \in N$.

To determine the watermark W_r present in the image C the equation (3) with selected threshold detection threshold $\theta \in R$ is used:

$$Z_{nc}\left(C, W_r\right) > \theta. \tag{3}$$

Unsharp masking filter

Sharpening is a filtering method used in image processing and digital photography [9]. The primary goal of sharpening is to increase the contrast between adjacent pixels in the image. Sharpening is achieved by amplifying high-frequency components which correspond to high-intensity parts of the image, while leaving low-frequency regions unaffected. Unsharp masking is a classical tool for sharpening enhancement.

The process of unsharp masking involves generating a low-frequency (blurred) version of the image, which is used as a low-pass image approximation. Subtracting low-pass image approximation from the original image produces the high-frequency part of the image. The unsharp masked image is obtained by adding a high-frequency part scaled by sharpening strength coefficient to the original image.

In our work, the unsharp filter implemented in FFmpeg[1] is used for unsharp masking. The code of unsharp masking filter is based on the blurring algorithm described in [12]. The unsharp filter in FFmpeg has a sharpening strength coefficient limited to a maximum value of 5. For testing unsharp masking on higher sharpening strength coefficients, it is necessary to remove this restriction. The patch of FFmpeg code for removing this restriction can be found in the repository[2].

Method for selecting the optimal sharpening strength for watermark detection

Digital watermark detection can be considered as a binary image classification problem, which allows using the binary classification metrics to evaluate performance of detection. In this work, the optimal sharpening strength coefficient is determined by maximizing the recall metric [13] calculated by equation (4). The choice of this metric is motivated by the fact (as will be demonstrated in the following experiment) that changes in sharpening strength coefficient affect the number of correctly classified actual positives (true positive detections), while having no impact on the number of incorrectly classified actual negatives (false positive detections). This allows avoiding the need to prepare images for false positive detection analysis, thereby reducing the overall computational cost of the experiment.

$$\text{Recall} = \frac{TP}{TP + FN}, \tag{4}$$

where TP is the number of watermarked images in which the watermark was detected, FN is the number of watermarked images in which the watermark was not detected.

To perform the experiment for evaluating the quality of sharpening strength coefficient, it is needed to select a detection threshold θ. For the following experiments, the detection threshold is selected as the value below which false positive watermark detections begin to occur. To select this threshold, a computational experiment on the image set is conducted. A random watermark is embedded into each image in the set, and the correlation is calculated between the watermarked image and another watermark that was not embedded into that image. The maximum value from these calculated correlations is selected as the detection threshold.

[1] A complete, cross-platform solution to record, convert and stream audio and video. [online] Available: http://ffmpeg.org (Accessed 01.11.2025)

[2] GitHub – anjin-viktor/detect-with-unsharp: This repository contains Python scripts, C++ implementation of watermarks, and evaluation results used in the paper "Selecting the optimal unsharp masking strength for DCT-domain watermark detection via Recall metric optimization" · GitHub. [online] Available: https://github.com/anjin-viktor/detect-with-unsharp (Accessed 25.11.2025)

Although the detection threshold selected by the described algorithm was chosen to avoid false positives on the used set of images, the selected detection threshold can produce false positives on other images or randomly generated watermarks.

To evaluate the quality of sharpening strength and calculate recall metric, the experiment is conducted on a set of images. Random watermarks are generated and embedded into every image in the set. Since the detection rate is high for undistorted watermarked images, all watermarked images are distorted using a selected filter. After distortion, each image is processed by an unsharp masking filter with the evaluated sharpening strength. Watermark detection is then performed on the unsharp masked images, and the count of true positive detections is calculated. After processing all images in the set, the recall metric is calculated.

The recall metric calculated by the described algorithm for a watermarking algorithm with fixed embedding and detection parameters depends on the set of images, the filter applied to introduce distortions, and the sharpening strength coefficient used in the unsharp masking pre-filtering. The set of images and the distortion filter are selected once before the experiment. As a result, after all other parameters are fixed, the recall metric can be considered as a function of the sharpening strength coefficient.

The optimal value of sharpening strength is determined by maximizing the recall metric calculated by the described algorithm. This can be done by iterating through values of sharpening strength starting from 0 (which correspond to no unsharp masking) up to the point where a stable decrease in the recall metric is observed. When recall metric calculated by described algorithm has a single extremum, the methods for optimizing unimodal functions [14] can be used to select optimal value of sharpening strength.

Method for evaluating watermark detection performance with unsharp masking pre-filtering at selected optimal sharpening strength coefficient

To evaluate the selected sharpening strength coefficient, an experiment is conducted on a set of images. During the experiment, the counts of true and false positive detections are calculated with and without pre-filtering using the selected optimal sharpening strength coefficient.

A random watermark is generated and embedded into each image in the set. Filters are applied to the watermarked images to introduce distortions. The distorted by filters watermarked images are used for watermark detection, both with and without pre-filtering by unsharp masking at the selected optimal sharpening strength coefficient. The watermark detection is performed using detection thresholds selected while finding optimal value of sharpening strength. To evaluate false positive detections, watermark detection is performed using a different watermark that was not embedded in the images. The result of the experiment is the number of true positive and false positive detections.

Results and discussion

The C++ implementation of the watermarking algorithm, along with the Python scripts for running the experiments, plotting the figures and the obtained results, are available in the repository[3].

The computational experiments were conducted using the DCT-domain watermarking algorithm [10] with an embedding coefficient $\alpha = 0.5$, $\alpha = 1$ and $\alpha = 3$. All of these coefficients can be described as robust enough. The coefficient of $\alpha = 0.5$ introduces very small distortions that are imperceptible to the human eye after embedding. The coefficient $\alpha = 1$ produces minor distortions that are slightly noticeable. The coefficient $\alpha = 3$ produces distortions which are visible on some regions of images, but these distortions do not interfere with the overall perception of the image. Table 1 presents the average objective quality metrics PSNR [16] and VMAF [17], calculated between the original and watermarked images on set with 2500 images.

[3] GitHub – anjin-viktor/detect-with-unsharp: This repository contains Python scripts, C++ implementation of watermarks, and evaluation results used in the paper "Selecting the optimal unsharp masking strength for DCT-domain watermark detection via Recall metric optimization" · GitHub. [online] Available: https://github.com/anjin-viktor/detect-with-unsharp (Accessed 25.11.2025)

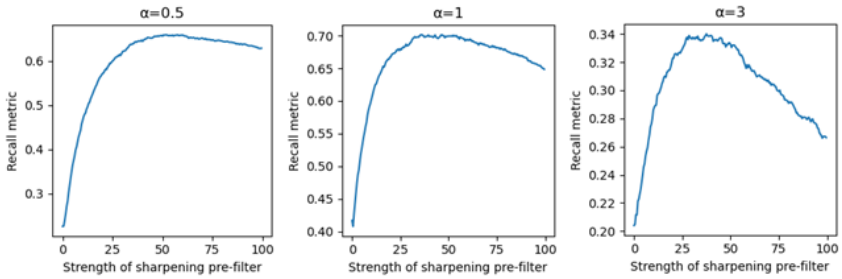

Fig. 1. Recall metrics calculated on 2500 images

Table 1

The average objective quality metrics of distortions introduced by watermarking

α	PSNR	VMAF
0.5	52.8	97.39
1	50.5	97.36
3	43.4	97.15

The computational experiment for selecting the detection thresholds was conducted using 2500 images from Flickr8K [15]. The detection threshold values $2.02*10^{-8}$, $1.64*10^{-8}$ and $2.03*10^{-8}$ were selected for $\alpha = 0.5$, $\alpha = 1$ and $\alpha = 3$ accordingly.

With these detection thresholds, the algorithm for selecting optimal value of sharpening strength coefficient was conducted using 2500 images from Flickr8K [15]. For introducing distortion to the watermarked images, the dctdnoiz filter from FFmpeg[4] was used with the filtering strength 7, 15, 45 for embedding coefficient $\alpha = 0.5$, $\alpha = 1$ and $\alpha = 3$ accordingly.

The results of the experiment are presented as a plot in Fig. 1. The X-axis represents the sharpening strength coefficient, varying from 0 (no sharpening) to 100. The Y-axis represents the recall metric calculated during experiments for corresponding sharpening strength coefficient.

The results of the experiment of evaluating the recall metric show that applying unsharp masking as pre-filtering step before watermark detection improves watermark detection performance. In the experiment with $\alpha = 0.5$ the recall value without sharpening (strength = 0) is 0.22. As the sharpening strength increases, the recall metric rises and reaches a maximum value of 0.66 at sharpening strength 52. Beyond this point, the recall value declines slowly. In the experiment with $\alpha = 1$ the recall metric without pre-filtering by unsharp masking is 0.43, and the maximum of recall is 0.70 which is achieved at the sharpening strength coefficient 35.5. Beyond this point, the recall decreases more rapidly compared to the $\alpha = 0.5$. For $\alpha = 3$ the value of recall metric without pre-filtering is 0.20, and the maximum recall is 0.34 which is achieved at the sharpening strength coefficient 37. Beyond this point, the recall metric also declines.

Based on the results of experiment, it can be observed that applying a unsharp masking as pre-filtering step before watermark detection improves detection performance up to an optimal sharpening strength coefficient, beyond which additional sharpening degrades detection accuracy. The optimal sharpening strength coefficient varies depending on the embedding coefficient α. The results also show that recall metric calculated over 2500 images has several local extremums, which prevents the use of fast optimization methods [14] designed for unimodal functions. Increasing the number of

[4] A complete, cross-platform solution to record, convert and stream audio and video. [online] Available: http://ffmpeg.org (Accessed 01.11.2025)

images can make plot of recall metric smoother and make the function unimodal, but this will lead to increasing the computational cost of experiment.

The obtained optimal sharpening strength coefficients were used to evaluate the performance of watermark detection with unsharp masking pre-filtering. The evaluation was performed using the Flickr30K [18] dataset which contains 31783 images. During the evaluating, the selected earlier detection thresholds were used ($2.02*10^{-8}$, $1.64*10^{-8}$ and $2.03*10^{-8}$ for $\alpha = 0.5$, $\alpha = 1$ and $\alpha = 3$ accordingly). The results of the experiment are presented in Table 2.

The following FFmpeg[5] filters were used to introduce distortions into watermarked images:

- Blurring: "unsharp=7:7:-1:7:7:-1";
- Denoising using the Non-Local Means: "nlmeans=s=15";
- Pixelization: "pixelize=w=2:h=2";
- JPEG transcoding with quantizer 10;
- Contrasting: "colorlevels=rimin=0.3:gimin=0.3:bimin=0.3:rimax=0.7:gimax =0.7:bimax=0.7";
- Noising: "noise=alls=100:allf=u".

In Table 2, the first column “Filter” specifies the FFmpeg filter used to introduce distortion in images. The column “Embedding coefficient α” specifies the value of embedding coefficient α. The “Unsharp masking pre-filter” column describes whether unsharp masking pre-filtering with the optimal sharpening strength coefficient was applied or not during watermark detection. The column “True positive (%)” contains the percentage of correctly detected watermarks for the corresponding configuration. The “False positive” column contains the number of false positive detections obtained under the corresponding configuration.

The results of the experiment show that applying an unsharp masking as pre-filter before watermark detection with the optimal sharpening strength coefficient selected by the proposed method improves the true positive rate in most cases. For low embedding coefficient $\alpha = 0.5$, the percentage of true positive detections increases significantly under most distortions, except noising, where it decreases from 99.61% without pre-filtering to 79.90% with pre-filtering. For embedding coefficient $\alpha = 1$ sharpening pre-filtering also improves detection performance for most distortions, except blurring, where the performance slightly decreases. For embedding coefficient $\alpha = 3$, the effect of sharpening becomes negligible, because the percentage of true positive detections after introducing distortions by selected filters is close to 100% without pre-filtering. However, in this case slight degradation in accuracy is observed for distortions introduced by JPEG transcoding and blurring.

Across all tested conditions, the false positive rate remains low, indicating that improvements in detection accuracy do not come at the cost of an increased count of false positive detections.

The correlations obtained during watermark detections in the experiment were used to plot Receiver Operating Characteristic (ROC) curves [19]. The ROC curve is a tool for evaluating the performance of results of binary classification. It represents the trade-off between true positive and false positive detections. In other words, the ROC curve provides a tool for evaluation of watermark detection robustness by plotting how reliably watermarks can be detected. The ROC curves were generated using the roc_curve function from the scikit-learn library [20], based on the correlations calculated during experiment between the watermarked container and the embedded and non-embedded watermarks. The resulting curves were visualized using Matplotlib [21].

The ROC curves shown in Fig. 2 demonstrates that applying unsharp masking filter with the selected optimal sharpening strength coefficient as a pre-filter step at the watermark detection stage after distortion by Non-Local Means denoising improves the true positive detection rate for the same false positive rate. The plot for $\alpha = 3$ is zoomed in, since the true positive detection rate is high and the difference between the curves is not visible over the full [0, 1] range. The curve corresponding to pre-filtering (orange dashed line) is located above the curve corresponding detection without pre-filtering

[5] A complete, cross-platform solution to record, convert and stream audio and video. [online] Available: http://ffmpeg.org (Accessed 01.11.2025)

Table 2

Percentage of true positive and count of false positive detections for watermark detection under distortions with and without unsharp masking pre-filtering

Filter	Embedding coefficient α	Unsharp masking pre-filter	True positive (%)	False positive
Blurring	0.5	no	22.52	6
		yes	25.42	8
	1	no	93.11	18
		yes	92.53	18
	3	no	99.99	8
		yes	99.98	8
Denoising with Non-Local Means	0.5	no	9.25	13
		yes	47.0	10
	1	no	67.13	22
		yes	87.22	27
	3	no	99.07	15
		yes	99.69	11
Pixelization	0.5	no	27.51	6
		yes	96.81	7
	1	no	95.20	30
		yes	99.97	20
	3	no	100	9
		yes	100	9
JPEG transcoding	0.5	no	0.93	12
		yes	1.00	5
	1	no	23.93	21
		yes	25.90	23
	3	no	93.26	9
		yes	92.84	8
Contrasting	0.5	no	96.20	11
		yes	99.24	5
	1	no	99.82	21
		yes	99.97	17
	3	no	99.99	10
		yes	100	8
Noising	0.5	no	99.61	6
		yes	79.90	7
	1	no	100	24
		yes	99.99	22
	3	no	100	11
		yes	100	12

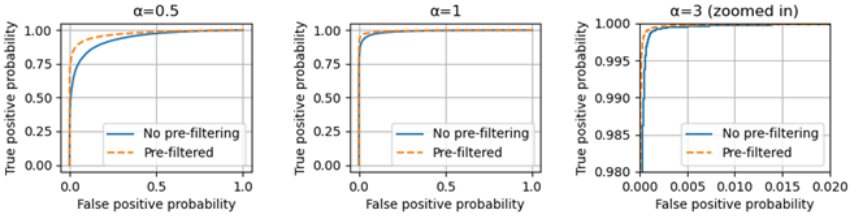

Fig. 2. ROC curves for detection with and without unsharp masking pre-filtering after Non-Local Means denoising

(blue solid line). This indicates that the use of unsharp masking as a pre-filtering step with optimal sharpening strength coefficient increases the watermark detection accuracy without introducing false positives in these cases.

An important observation is that pre-filtering does not introduce false positive detections. This suggests that a combined detection scheme that uses detection on both pre-filtered and non-filtered images can improve robustness across a wide range of distortions. When the detection modules with and without pre-filtering are considered as classifiers, the combined detection scheme can be implemented using classifier fusion [22]. An evaluation of such combined detection schemes is beyond the scope of the current paper.

Conclusion

This paper investigated the use of unsharp masking as a pre-filtering step during watermark detection in a DCT-domain correlation-based image watermarking algorithm [10]. A computational method was proposed for selecting the optimal sharpening strength coefficient by maximizing the recall metric of watermark detection on a set of images. The results of a computational experiment show that the recall metric increases with sharpening strength coefficient up to an optimal sharpening strength coefficient, beyond which unsharp masking degrades the accuracy of watermark detection. The optimal sharpening strength coefficient depends on the embedding coefficient α.

Evaluation of the sharpening strength coefficient selected by the proposed method for DCT-domain watermark embedding and detection algorithm confirmed that pre-filtering with the optimal sharpening strength improves the true positive detection rate across most of tested distortions without increasing the false positive rate. However, for some distortions (JPEG transcoding at high embedding coefficient α, noise at low embedding coefficient α), the detection rate decreases after pre-filtering.

ROC curve analysis of the data collected during optimal sharpening strength coefficient evaluation confirmed that sharpening pre-filtering enhances detection performance by increasing the true positive rate for the same false positive rate for most of tested distortions. These results demonstrate that unsharp masking on selected using the proposed method optimal sharpening strength coefficient improves the robustness of watermark detection when applied as pre-filtering step before watermark detection for DCT-domain watermark embedding and detection algorithm.

Since pre-filtering by unsharp masking on optimal sharpening strength coefficient does not introduce false positives detections, a combined detection scheme using both filtered and non-filtered images can be used to improve detection robustness across a wider range of distortions.

REFERENCES

1. **Rashid A.** Digital watermarking applications and techniques: A brief review. *International Journal of Computer Applications Technology and Research*, 2016, Vol. 5, No. 3, Pp. 147–150.

2. **Gribunin V.G., Okov I.N., Turintsev I.V.** *Tsifrovaia steganografiia* [*Digital steganography*]. Moscow: SOLON-PRESS, 2017.

3. **Wan W., Wang J., Zhang Y., Li J., Yu H., Sun J.** A comprehensive survey on robust image watermarking. *Neurocomputing*, 2022, Vol. 488, Pp. 226–247. DOI: 10.1016/j.neucom.2022.02.083

4. **Langelaar G.C., Setyawan I., Lagendijk R.L.** Watermarking digital image and video data. A state-of-the-art overview. *IEEE Signal Processing Magazine*, 2000, Vol. 17, No. 5, Pp. 20–46. DOI: 10.1109/79.879337

5. **Piva A., Barni M., Bartolini F., Cappellini V.** Threshold selection for correlation-based watermark detection. *Proceedings of COST254 Workshop on Intelligent Communications*, 1998, Vol. 254, Pp. 67–72.

6. **Amirgholipour S., Naghsh-Nilchi A.R., Sharifi A.M., Alirezanejad M., Arab M.** Application of unsharp mask in augmenting the quality of extracted watermark in spatial domain watermarking. *Journal of Mathematics and Computer Science*, 2014, Vol. 11, Pp. 137–146.

7. **Jane O., Ilk G.** Implementation of adaptive unsharp masking as a pre-filtering method for watermark detection and extraction. *Advances in Electrical and Electronic Engineering*, 2016, Vol. 14, No. 4, Pp. 429–436. DOI: 10.15598/aeee.v14i4.1827

8. **Amirgholipour S., Sharifi A.** A pre-filtering method to improve watermark detection rate in DCT based watermarking. *The International Arab Journal of Information Technology*, 2014, Vol. 11, No. 2, Pp. 178–185.

9. **Jain A.K.** *Fundamentals of digital image processing*. Englewood Cliffs, NJ (US): Prentice Hall, 1989.

10. **Cox I.J., Kilian J., Leighton F.T., Shamoon T.** Secure spread spectrum watermarking for multimedia. *IEEE Transactions on Image Processing*, 1997, Vol. 6, No. 12, Pp. 1673–1687. DOI: 10.1109/83.650120

11. **Wallace G.K.** The JPEG still picture compression standard. *IEEE Transactions on Consumer Electronics*, 1992, Vol. 38, No. 1, Pp. XVIII-XXXIV. DOI: 10.1109/30.125072

12. **Waltz F.M., Miller J.W.V.** Efficient algorithm for Gaussian blur using finite-state machines. *Machine Vision Systems for Inspection and Metrology VII*, 1998, Vol. 3521, Pp. 334–341. DOI: 10.1117/12.326976

13. **Powers D.M.W.** Evaluation: from precision, recall and F-measure to ROC, informedness, markedness and correlation. *arXiv:2010.16061*, 2020. DOI: 10.48550/arXiv.2010.16061

14. **Brent R.P.** *Algorithms for minimization without derivatives*. Englewood Cliffs, NJ (US): Prentice Hall, 1973.

15. **Rashtchian C., Young P., Hodosh M., Hockenmaier J.** Collecting image annotations using Amazon's Mechanical Turk. *Proceedings of the NAACL HLT 2010 Workshop on Creating Speech and Language Data with Amazon's Mechanical Turk*, 2010, Pp. 139–147.

16. **Horé A., Ziou D.** Image quality metrics: PSNR vs. SSIM. *2010 20th International Conference on Pattern Recognition*, 2010. Pp. 2366–2369. DOI: 10.1109/ICPR.2010.579

17. **Li Z., Bampis C., Novak J., Aaron A., Swanson K., Moorthy A., De Cock J.** VMAF: The journey continues, 2018. [online] Available: https://netflixtechblog.com/vmaf-the-journey-continues-44b51ee9ed12 (Accessed 17.03.2026)

18. **Plummer B.A., Wang L., Cervantes C.M., Caicedo J.C., Hockenmaier J., Lazebnik S.** Flickr30k entities: Collecting region-to-phrase correspondences for richer image-to-sentence models. *arXiv:1505.04870*, 2015. DOI: 10.48550/arXiv.1505.04870

19. **Fawcett T.** An introduction to ROC analysis. *Pattern Recognition Letters*, 2006, Vol. 27, No. 8, Pp. 861–874. DOI: 10.1016/j.patrec.2005.10.010

20. **Pedregosa F., Varoquaux G., Gramfort A., Michel V., Thirion B., Grisel O. et al.** Scikit-learn: Machine learning in Python. *The Journal of Machine Learning Research*, 2011, Vol. 12, Pp. 2825–2830.

21. **Hunter J.D.** Matplotlib: A 2D graphics environment. *Computing in Science & Engineering*, 2007, Vol. 9, No. 3, Pp. 90–95. DOI: 10.1109/MCSE.2007.55

22. **Kuncheva L.I.** *Combining pattern classifiers: methods and algorithms*. Hoboken, NJ (US): John Wiley & Sons, 2014.

INFORMATION ABOUT AUTHOR / СВЕДЕНИЯ ОБ АВТОРЕ

Viktor A. Anzhin
Анжин Виктор Андреевич
E-mail: viktor.anjin@gmail.com
ORCID: https://orcid.org/0009-0006-1273-6703

Submitted: 11.12.2025; Approved: 02.03.2026; Accepted: 17.03.2026.
Поступила: 11.12.2025; Одобрена: 02.03.2026; Принята: 17.03.2026.

Computing, Telecommunication and Control, 2026, Vol. 19, No. 1, Pp. 57–64.
Информатика, телекоммуникации и управление. 2026. Том 19, № 1. С. 57–64.

Simulations of Computer, Telecommunications and Control Systems

Моделирование вычислительных, телекоммуникационных и управляющих систем

Research article
DOI: https://doi.org/10.18721/JCSTCS.19106
UDC 621.375.026

ANALYSES OF A CLASS G POWER AMPLIFIER WITH CONTROLLED NONLINEAR DISTORTION FOR LTE-SIGNAL

E.V. Leontiev ✉

Peter the Great St. Petersburg Polytechnic University,
St. Petersburg, Russian Federation

✉ evgeniyleo888@mail.ru

Abstract. The work considers an analysis of nonlinear distortions in a class G power amplifier and an analysis of an envelope tracking power amplifier with a proposed combined envelope amplifier scheme for LTE cellular base stations. Both considered envelope amplifier schemes feature an additional shaping function to compensate for the AM-AM conversion of the power amplifier, as well as DPD correction for the AM-PM conversion of the amplifier. The analysis results showed that switching between 18 supply voltage levels in the class G power amplifier allows achieving an ACPR characteristic of the output LTE signal at an acceptable level of −50 dBc. Simulation has proved that a standard predistortion technique based on LUT or a Volterra series can be applied to a class G power amplifier at N = 18. The number of supply voltage levels can be reduced to N = 10 using the proposed combined scheme or by applying additional voltage supply filtration of the envelope amplifier.

Keywords: class G power amplifier, nonlinear distortions, drain efficiency, DPD, LTE

Citation: Leontiev E.V. Analyses of a class G power amplifier with controlled nonlinear distortion for LTE-signal. Computing, Telecommunications and Control, 2026, Vol. 19, No. 1, Pp. 57–64. DOI: 10.18721/JCSTCS.19106

Научная статья
DOI: https://doi.org/10.18721/JCSTCS.19106
УДК 621.375.026

АНАЛИЗ УСИЛИТЕЛЯ МОЩНОСТИ КЛАССА G С КОНТРОЛИРУЕМЫМ УРОВНЕМ НЕЛИНЕЙНЫХ ИСКАЖЕНИЙ ДЛЯ LTE-СИГНАЛА

Е.В. Леонтьев ✉

Санкт-Петербургский политехнический университет Петра Великого,
Санкт-Петербург, Российская Федерация

✉ evgeniyleo888@mail.ru

Аннотация. В работе показан анализ нелинейных искажений усилителя мощности класса G и усилителя мощности с непрерывным отслеживанием огибающей на основе предложенной комбинированной схемы усилителя огибающей для базовых станций сотовой связи стандарта LTE. Обе рассмотренные схемы усилителей огибающей имеют дополнительную формирующую функцию для компенсации AM-AM конверсии усилителя мощности, а также DPD коррекцию AM-ФМ конверсии усилителя. Результаты анализа показали, что коммутация между 18 уровнями напряжения питания в усилителе мощности класса G позволяется получить характеристику ACPR выходного LTE-сигнала на допустимом уровне −50 дБн. Моделированием доказано, что к усилителю мощности класса G возможно применить стандартную методику предыскажений на основе LUT или рядов Вольтерра при N = 18. Количество уровней возможно уменьшить, используя предложенную комбинированную схему усилителя огибающей до 10 или применить дополнительную фильтрацию выходного сигнала усилителя огибающей.

Ключевые слова: усилитель мощности класса G, нелинейные искажения, КПД, DPD, LTE

Для цитирования: Leontiev E.V. Analyses of a class G power amplifier with controlled nonlinear distortion for LTE-signal // Computing, Telecom-munications and Control. 2026. Т. 19, № 1. С. 57–64. DOI: 10.18721/JCSTCS.19106

Introduction

The widespread use of orthogonal frequency-division multiplexing (OFDM) signals with a high peak-to-average power ratio (PAPR) requires an improvement in radio frequency power amplifier (RFPA) schemes. Designing 4G base stations using OFDM technology requires high-efficiency LTE signal transmission. An envelope tracking power amplifier (ETPA) is a relevant solution to this problem in multiband applications.

An ETPA includes an envelope amplifier (EA) module (Fig. 1). The EA input ($U_{\text{in env}}$) receives an envelope detector signal with a maximum voltage 3.3 or 5 V. The EA output ($U_{\text{out env}}$) provides a variable supply voltage with a maximum value (e.g., 28 V) and the current required by the RFPA. Therefore, EA efficiency determines overall efficiency of the ETPA in many applications. Numerous studies [1–4] are devoted to improvements in the EA efficiency. An ETPA has maximum efficiency when the RFPA has a continuous supply voltage variation, as show in Fig. 3, *a*. Today, hybrid envelope amplifier (HEA) schemes, combining the pulse and linear parts (Fig. 2), are widely used. However, due to the presence of inductance (L_{th}) and other reactive elements, HEA efficiency is limited to 75–85% [4–7]. There are various modifications of HEA schemes [4], that can solve this problem, but improving HEA efficiency remains a relevant challenge.

There are EA schemes based on pulse-width modulated DC-DC power converters with an efficiency of over 90%. In such schemes, the high clock frequency of the pulse-width modulator makes

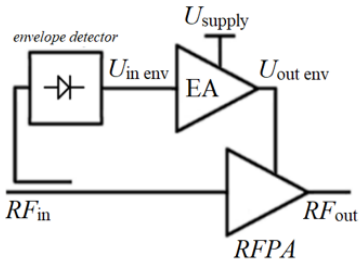

Fig. 1. ETPA

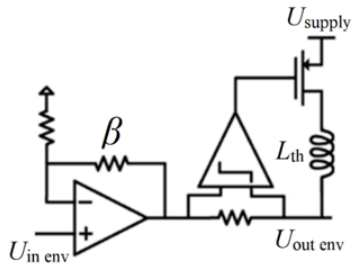

Fig. 2. HEA

it difficult to use these EA for signals with a bandwidth of over several tens of MHz. It is possible to reduce the clock frequency of this EA scheme by moving from continuous supply voltage variation (Fig. 2, *a*) towards discrete supply voltage switching (Fig. 2, *b*). An RFPA with discrete supply voltage switching is called a class G RFPA [8–11]. The disadvantage of class G RFPA is that the gain vs input power dependence has points of discontinuity. The presence of these points necessitates the use of non-standard digital pre-distortion (DPD) techniques.

Also, discrete supply voltage switching can be used to improve HEA efficiency. A supply voltage waveform for this scheme is shown in Fig. 2, *c*. The proposed scheme is called the combined envelope amplifier (CEA) and have better efficiency than HEA. An EA efficiency in a class G RFPA is 97% [11], and the HEA efficiency is only 60%. If the CEA switches the supply voltage discretely with a probability of 7/8 and continuously tracks the envelope with a probability of 1/8 using the HEA, then the total efficiency of such a CEA will be equal to 7/8·97% + 1/8·60% = 92.4%. With a probability of 15/16, the total CEA efficiency is 94.7%, which is only 2.3% lower than the class G RFPA efficiency. Therefore, the use of discrete supply voltages switching in the HEA can increase efficiency from 60% to 94.7%. This purpose of this study is to analyze the CEA and the class G EA to determine the optimal parameters for achieving minimal distortion of an LTE signal.

Analysis and synthesis of the EA for the class G RFPA or CEA involves finding the number of discrete supply voltages and their value, as well as the levels of U_{in} env at which the discrete supply voltages will switch. For example, the EA development for the class G RFPA in [11] showed that five discrete supply voltages are enough for achieving maximum efficiency. However, the analysis and synthesis of the EA for the class G RFPA can be considered in terms of nonlinear distortions rather that the efficiency of the class G RFPA and CEA. Adjacent channel power ratio (ACPR) is a useful RFPA characteristic showing the impact of nonlinear distortion on output signal. In this work, ACPR characteristic is used as a nonlinear RFPA distortion indicator. According to the 3GPP standard, the permissible ACPR level for an LTE signal should not exceed –50 dBc.

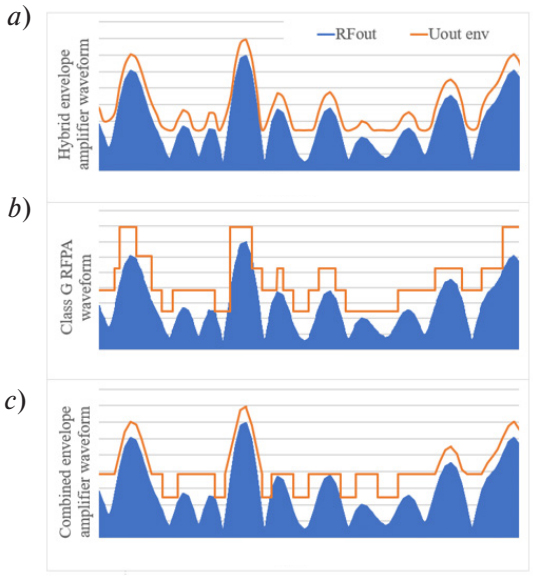

Fig. 3. Supply voltage waveform: ETPA with continuous supply voltage (*a*), class G RFPA (*b*), ETPA with CEA (*c*)

Thus, the article presents an analysis of two schemes: the EA for the class G RFPA and CEA. The schemes were analyzed using an LTE signal with a bandwidth of 20 MHz in the E-TM 3.1 test configuration. The work uses a nonlinear model of the main RFPA operating in the 700–1000 MHz frequency range, with a saturated power of 44.5 dBm at 28 V supply voltage; its measurement results are given in [10]. The analysis results show how the nonlinear distortions of the output LTE signal (reflected in ACPR) change under different configurations of these EA schemes.

Results

ACPR is influenced by several factors, such as AM-AM and AM-PM conversions, inertial effects of passive components etc. AM-AM and AM-PM conversions play a key role in increasing the nonlinear distortion level. It is possible to correct AM-AM conversion in an ETPA by using the shaping function module [12]. The shaping function compares $U_{\text{out env}}$ with $U_{\text{in env}}$. The gain coefficient β (Fig. 2) of an operational amplifier can be used as the shaping function in the HEA. Let us consider the operation principles of the shaping function using the ETPA model in CAD VSS and Microwave Office as an example (Fig. 4).

Fig. 4 shows the gain vs input power function at different supply voltages (dotted lines) for the nonlinear RFPA model. An increase in supply voltage leads to an increase in gain, resulting in AM-AM conversion in the ETPA. The shaping function should change supply voltage in such a way that the gain compression compensates for this gain increase. The gain vs input power function for the ETPA with the shaping function is shown in Fig. 4 (solid line). However, the shaping function cannot correct AM-PM conversion in the ETPA (Fig. 5). The standard DPD technic, using a look-up table (LUT) or Volterra series, can correct AM-PM conversion. Fig. 6 shows the power spectral density (PSD) of output signal with and without DPD (Fig. 6), which corrects only the AM-PM conversion in the ETPA with the shaping function. The use of DPD has improved ACPR by 13 dB from –42 dBc to –55 dBc. For cellular base stations, according to the 3GPP specification, the allowed ACPR level is –50 dBc. The shaping function for the class G RFPA defines a strict relationship between the supply voltage and the reference voltages of the comparators, which determines the moment of supply voltage switching, according to $U_{\text{in env}}$. Furthermore, this article assumes that at a certain supply voltage, the comparator reference voltage level will be calculated automatically, according to the shaping function.

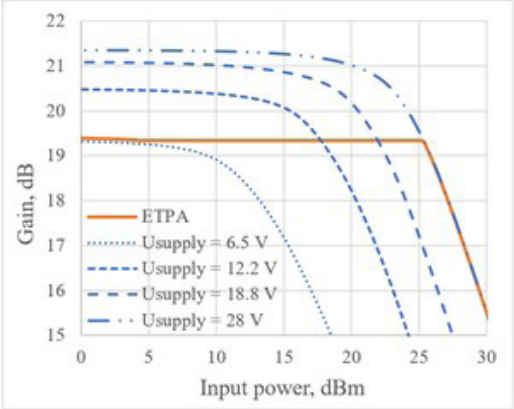

Fig. 4. AM-AM conversion

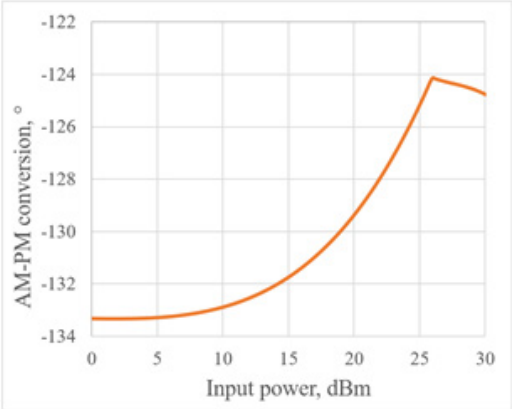

Fig. 5. AM-PM conversion

The class G RFPA model switches the nonlinear models of the main RFPA in CAD VSS. Each nonlinear model has a certain supply voltage from 6.5 V to 28 V, as shown in [10, 11]. Initially, the number of the nonlinear models is 55, the step between supply voltage is from 0.125 to 1 V, depending on the probability density function of LTE signal, which allowed to obtain ACPR of the output signal of −55 dBc. Each nonlinear model is analyzed using the APLAC harmonic balance method, which is more suitable for extremely nonlinear circuits analysis. Furthermore, the class G RFPA is analyzed with a different number of supply voltage levels (N) from 55 to 10. Using CAD LabVIEW [13], optimal supply voltage levels at which ACPR is minimal have been determined. The CEA analysis is similar to the class G RFPA analysis, with N reduced within the range of 6.5–12.2 V. The remaining maximum number of levels is between 12.2 and 28 V, simulating HEA.

The saturation power of the class G RFPA is 44.5 dBm; therefore, the minimum ACPR is achieved at an average power of 32.8 dBm when the output power is below saturation power by the PAPR value (11.7 dB for the LTE signal). In Fig. 7, ACPR degrade at powers below 33 dBm due to the nonlinear behavior of the main RFPA at a power supply voltage of 6.5 V, since it operates in class AB and has an individual type of AM-AM and AM-PM conversions, which are not taken into account by the shaping function and DPD. At $N = 18$, the ACPR of the output signal is equal to the acceptable value of −50 dBc.

The findings do not prove that the EA output voltage ($U_{\text{out env}}$) can be improved by RFPA supply voltage filtration [14, 15]. Of course, if a low-pass filter with a cutoff frequency equal to the signal

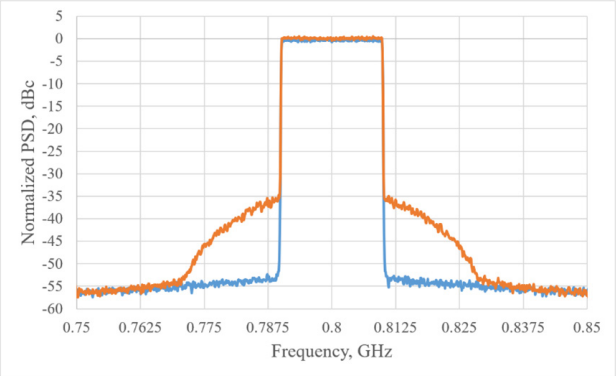

Fig. 6. Output signal specter

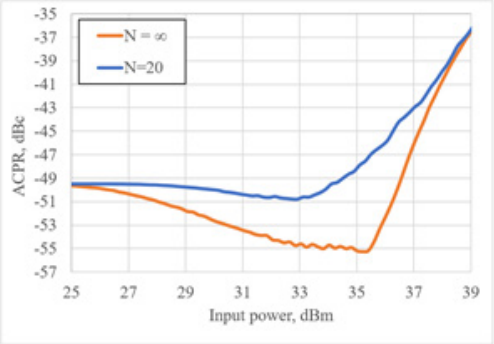

Fig. 7. ACPR vs output power

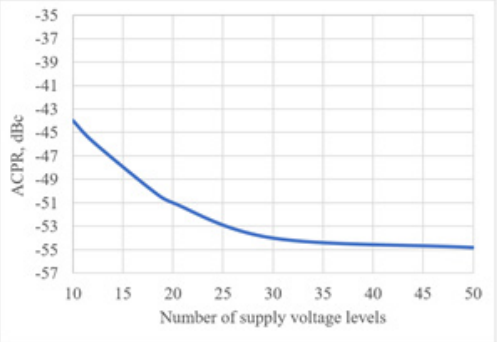

Fig. 8. ACPR vs N

bandwidth is applied, it is possible to achieve an optimal N less than 18. However, the use of filtering leads to the dependence of ACPR on signal bandwidth. Therefore, $N = 18$ is the optimal value for multiband applications where signal bandwidth varies.

Conclusion

This analysis has shown that the class G RFPA with the shaping function and a standard DPD based on LUT can provide an ACPR of –50 dBc at $N = 18$. The standard DPD technique, based on

a LUT or Volterra series, can be applied to the class G RFPA without the shaping function. In this case, the number of supply voltage levels required to achieve an ACPR of –50 dBc will be different. Moreover, the use of an additional filter can improve linearity for a fixed signal bandwidth. The previous work showed that five supply voltage levels are sufficient to achieve maximum efficiency in the class G RFPA. These five levels must be formed using highly efficient DC-DC pulse converters so that the total system efficiency remains at a high level. Therefore, it is enough to develop an 18-level class G RFPA with five DC-DC pulse converters, and to form the remaining 13 supply voltage levels using linear voltage converters. Also, the class G RFPA analysis showed that 10 of 18 supply voltage levels are in the voltage range from 6.5 to 12.2 V. An ETPA with the CEA can provide an ACPR of –50 dBc at N = 10. Therefore, CEA design is a challenging task, as it helps reduce the number of supply voltage levels by almost half.

Nomenclature

- OFDM – Orthogonal Frequency-Division Multiplexing;
- PAPR – Peak-to-Average Power Ratio;
- ETPA – Envelope Tracking Power Amplifier;
- EA – Envelope Amplifier;
- HEA – Hybrid Envelope Amplifier;
- DPD – Digital Pre-Distortion;
- CEA – Combined Envelope Amplifier;
- ACPR – Adjacent Channel Power Ratio;
- LUT – Look-Up Table;
- PSD – Power Spectral Density.

REFERENCES

1. **Anderson D.R., Cantrell W.H.** High-efficiency high-level modulator for use in dynamic envelope tracking CDMA RF power amplifiers. *2001 IEEE MTT-S International Microwave Symposium Digest* (*Cat. No.01CH37157*), 2001, Vol. 3, Pp. 1509–1512. DOI: 10.1109/MWSYM.2001.967189

2. **Huang H., Bao J., Zhang L.** A MASH-controlled multilevel power converter for high-efficiency RF transmitters. *IEEE Transactions on Power Electronics*, 2011, Vol. 26, No. 4, Pp. 1205–1214. DOI: 10.1109/TPEL.2010.2073721

3. **Cheshire A., Flaten P., Popović Z., Maksimović D.** High-frequency flying capacitor four-level drain supply modulator. *2025 IEEE Applied Power Electronics Conference and Exposition* (*APEC*), 2025, Pp. 682–688. DOI: 10.1109/APEC48143.2025.10977523

4. **Bhardwaj S., Moallemi S., Kitchen J.** A review of hybrid supply modulators in CMOS technologies for envelope tracking PAs. *IEEE Transactions on Power Electronics*, 2023, Vol. 38, No. 5, Pp. 6036–6062. DOI: 10.1109/TPEL.2022.3233441

5. **Chen C., Li X., Hu R., Cheng L.** A high-efficiency envelope-tracking supply modulator using a class-G linear amplifier and a single-inductor dual-input-dual-output converter for 5G NR power amplifier. *IEEE Journal of Solid-State Circuits*, 2024, Vol. 59, No. 12, Pp. 4101–4113. DOI: 10.1109/JSSC.2024.3481906

6. **Lopez J., Li Y., Popp J.D., Lie D.Y.C., Chuang C.-C., Chen K.** Design of highly efficient wideband RF polar transmitters using the envelope-tracking technique. *IEEE Journal of Solid-State Circuits*, 2009, Vol. 44, No. 9, Pp. 2276–2294. DOI: 10.1109/JSSC.2009.2022669

7. **Leng W., Abidi A.A., Mundlapdi S.R., Darabi H., Chowdhury D., Afsahi A.** Envelope tracking supply modulator with Trellis-search-based switching and 160-MHz capability. *IEEE Journal of Solid-State Circuits*, 2022, Vol. 57, No. 3, Pp. 719–733. DOI: 10.1109/JSSC.2021.3128394

8. **Wolff N., Heinrich W., Bengtsson O.** Highly efficient 1.8-GHz amplifier with 120-MHz class-G supply modulation. *IEEE Transactions on Microwave Theory and Techniques*, 2017, Vol. 65, No. 12, Pp. 5223–5230. DOI: 10.1109/TMTT.2017.2769089

9. **Jin Q., Ruan X., Ren X., Xi H.** High-efficiency switch-linear-hybrid envelope-tracking power supply with step-wave approach. *IEEE Transactions on Industrial Electronics*, 2015, Vol. 62, No. 9, Pp. 5411–5421. DOI: 10.1109/TIE.2015.2416690

10. **Leontiev E.V., Korotkov A.S., Matveev Y.A.** Class-G power amplifier for infocommunication systems. *Nanoindustry*, 2021, Vol. 14, No. S7 (107), Pp. 930–931. DOI: 10.22184/1993-8578.2021.14.7s.930.931

11. **Leontiev E.V.** Class G power amplifier synthesis based on the probability density function dependence of the transmitted signal. *Computing, Telecommunication and Control*, 2024, Vol. 17, No. 2, Pp. 17–23. DOI: 10.18721/JCSTCS.17202

12. **Zhu Y., Klimashov O.P., Jin B., Balteanu F., Drogi S., Bartle D.C.** Novel shaping function for envelope tracking linearization. *IEEE Asia Pacific Microwave Conference* (*APMC*), 2017, Pp. 402–405. DOI: 10.1109/APMC.2017.8251465

13. **Leontiev E.V., Korotkov A.S., Balashov E.V., Berezniak A.F.** Application of LabVIEW in the problems of computer-aided designing MMIC in Microwave office. *Nanoindustry*, 2017, Vol. 74, No. S, Pp. 531–533.

14. **Zhang Y., Rodríguez M., Maksimović D.** Output filter design in high-efficiency wide-bandwidth multi-phase buck envelope amplifiers. *2015 IEEE Applied Power Electronics Conference and Exposition* (*APEC*), 2015, Pp. 2026–2032. DOI: 10.1109/APEC.2015.7104627

15. **Xing L., Sun J.** Optimal damping of multi-stage EMI filters. *2011 Twenty-Sixth Annual IEEE Applied Power Electronics Conference and Exposition* (*APEC*), 2011, Pp. 1721–1728. DOI: 10.1109/APEC.2011.5744828

INFORMATION ABOUT AUTHOR / СВЕДЕНИЯ ОБ АВТОРЕ

Evgeniy V. Leontiev
Леонтьев Евгений Владимирович
E-mail: evgeniyleo888@mail.ru
ORCID: https://orcid.org/0000-0002-1477-3181

Submitted: 20.12.2025; Approved: 11.03.2026; Accepted: 23.03.2026.
Поступила: 20.12.2025; Одобрена: 11.03.2026; Принята: 23.03.2026.

Computing, Telecommunication and Control, 2026, Vol. 19, No. 1, Pp. 65–79.
Информатика, телекоммуникации и управление. 2026. Том 19, № 1. С. 65–79.

Research article
DOI: https://doi.org/10.18721/JCSTCS.19107
UDC 004.42

A LYAPUNOV-BASED DYNAMIC SCHEDULING ALGORITHM FOR HETEROGENEOUS COMPUTING CLUSTERS

Wang Shan , *I.V. Nikiforov* ✉

Peter the Great St. Petersburg Polytechnic University,
St. Petersburg, Russian Federation

✉ igor.nikiforovv@gmail.com

Abstract. The paper proposes a Lyapunov-based dynamic scheduling algorithm for heterogeneous computing clusters, targeting fine-grained resource control under bursty and latency-sensitive workloads. By constructing a quadratic Lyapunov function and applying a drift-plus-penalty framework, the scheduling problem is formulated as a two-criteria optimization problem balancing queue stability and scheduling delay. A dynamic control parameter V is introduced to quantitatively regulate the trade-off between backlog stability and delay minimization. Sensitivity analysis demonstrates an O(1/V) backlog and O(V) delay trade-off. Experiments conducted on the Alibaba GPU cluster trace dataset show that under burst-dominant workloads, the proposed method reduces average scheduling delay to 0.2663 seconds, while achieving a 0.5459 resource utilization and a 0.6489 fairness index. The method is particularly suitable for latency-sensitive and dynamically fluctuating environments.

Keywords: Lyapunov optimization, drift-plus-penalty, resource scheduling, cloud computing, two-criteria optimization

Citation: Wang Shan, Nikiforov I.V. A Lyapunov-based dynamic scheduling algorithm for heterogeneous computing clusters. Computing, Telecommunications and Control, 2026, Vol. 19, No. 1, Pp. 65–79. DOI: 10.18721/JCSTCS.19107

Научная статья
DOI: https://doi.org/10.18721/JCSTCS.19107
УДК 004.42

АЛГОРИТМ ДИНАМИЧЕСКОГО ПЛАНИРОВАНИЯ НА ОСНОВЕ ФУНКЦИИ ЛЯПУНОВА ДЛЯ ГЕТЕРОГЕННЫХ ВЫЧИСЛИТЕЛЬНЫХ КЛАСТЕРОВ

Ван Шань , *И.В. Никифоров* ✉

Санкт-Петербургский политехнический университет Петра Великого,
Санкт-Петербург, Российская Федерация

✉ igor.nikiforovv@gmail.com

Аннотация. В статье рассматривается алгоритм динамического планирования на основе функции Ляпунова для гетерогенных вычислительных кластеров, ориентированный на точное управление ресурсами при импульсных и чувствительных к задержкам рабочих нагрузках. Путем построения квадратичной функции Ляпунова и применения подхода *drift-plus-penalty* задача планирования формулируется как задача двухкритериальной оптимизации для стабильности очереди и задержки планирования. Вводится параметр динамического управления V для количественного регулирования компромисса между стабильностью очереди и минимизацией задержки. Анализ чувствительности демонстрирует компромисс между O(1/V) очереди и O(V) задержки. Эксперименты, проведенные на наборе данных трассировки кластера GPU Alibaba, показывают, что при импульсных рабочих нагрузках предложенный метод снижает среднюю задержку планирования до 0,2663 сек, при этом достигая коэффициента использования ресурсов 0,5459 и индекса справедливости 0,6489. Данный метод особенно хорошо подходит для чувствительных к задержкам и динамически изменяющихся рабочих окружений.

Ключевые слова: оптимизация Ляпунова, drift-plus-penalty, планирование ресурсов, облачные вычисления, двухкритериальная оптимизация

Для цитирования: Wang Shan, Nikiforov I.V. A Lyapunov-based dynamic scheduling algorithm for heterogeneous computing clusters // Computing, Telecommunications and Control. 2026. Т. 19, № 1. С. 65–79. DOI: 10.18721/JCSTCS.19107

Introduction

With the rapid development of cloud computing, big data analytics and AI technologies, computing clusters have become the core infrastructure supporting high-performance computing (HPC), large-scale data processing and distributed services. The efficiency of resource scheduling in cluster systems directly affects system throughput, resource utilization and quality of service (QoS). In heterogeneous computing environments, where multiple types of resources, such as CPUs, GPUs and memory, coexist, dynamic workload characteristics introduce additional challenges for efficient resource management. Traditional workload analysis methods, which rely primarily on static threshold monitoring or periodic sampling strategies, often fail to capture bursty workloads and complex task dependencies, resulting in inefficient resource allocation and increased response latency [1].

Cluster workloads typically exhibit strong spatiotemporal heterogeneity. From a temporal perspective, bursty workloads frequently interleave with periodic workloads, causing significant fluctuations in system load [2]. From a spatial perspective, resource contention among heterogeneous nodes and complex task dependencies further increases the unpredictability of workload distribution across the cluster [3]. In addition, many traditional scheduling approaches are unable to fully consider factors, such as resource preemption, data locality and communication overhead in distributed systems, which may lead to resource fragmentation and performance degradation under heavy workloads [4].

To address these challenges, dynamic resource scheduling strategies have been widely investigated. Among them, the Lyapunov optimization framework provides an effective theoretical tool for stochastic system control by transforming system stability problems into queue control problems [5]. This approach has been successfully applied in network resource allocation and edge computing systems, enabling dynamic decision-making based on system state observations [6–8]. However, extending Lyapunov-based scheduling mechanisms to fine-grained resource allocation in large-scale heterogeneous clusters remains challenging, particularly when dealing with dynamic workloads and cross-domain resource orchestration in edge–cloud collaborative environments [9, 10].

Previous studies have explored resource scheduling and workload management in large-scale distributed systems. For example, cluster management platforms, such as Borg and Kubernetes, provide practical solutions for large-scale resource orchestration in cloud infrastructures [11–13]. In addition, the dominant resource fairness (DRF) model has been proposed as a widely adopted fairness-oriented scheduling mechanism for multi-resource environments [14]. Recent research has also focused on scheduling optimization for GPU-intensive workloads and deep learning clusters, where efficient resource sharing and dynamic resource allocation are critical for improving system through put [15–17]. Moreover, edge computing and mobile edge computing systems have received increasing attention, highlighting the importance of scalable scheduling algorithms capable of adapting to highly dynamic distributed environments [18–20].

Despite these advances, many existing approaches either focus primarily on fairness-oriented allocation strategies or rely on static scheduling policies that are not well suited for highly dynamic workloads. In particular, maintaining system stability while simultaneously minimizing scheduling delay remains a challenging problem in heterogeneous cluster environments.

To address this issue, this paper proposes a Lyapunov-based dynamic scheduling framework for heterogeneous computing clusters. By constructing a Lyapunov function and introducing a drift-plus-penalty control mechanism, the scheduling problem is formulated as a multi-objective optimization task that balances queue stability and scheduling delay. The main contributions of this work are as follows:

- *Theoretical extension*. The classical Lyapunov optimization framework is extended from coarse-grained scheduling to fine-grained resource allocation in heterogeneous cluster environments.
- *Algorithm design*. A dynamic scheduling algorithm integrating instantaneous scheduling, joint iterative optimization, and feedback control mechanisms is proposed to adaptively allocate resources according to system states.
- *Experimental evaluation*. Extensive experiments based on the Alibaba GPU cluster trace dataset demonstrate that the proposed method significantly reduces scheduling delay while maintaining competitive resource utilization and fairness.

Materials and methods

Task backlog queue model

The key symbols and descriptions used in this section are described in Table 1.

Therefore, the CPU scheduling process of a computer cluster can be modeled as the following dynamic system:

$$Q(t+1) = \max\{Q(t) + a(t) - b(t), 0\}.$$

Lyapunov optimization framework

Lyapunov optimization has been widely applied in stochastic network control and resource allocation problems due to its ability to balance system stability and performance objectives [5, 8].

Table 1

Symbols used

Symbol	Description
$Q(t)$	Task waiting queue, which indicates the number of tasks waiting to be processed at time t
N	Total number of CPU cores
R_n^t	Number of tasks that can be assigned to each CPU core at time t, where n =123...N
a_t	Task arrival rate, which is the number of tasks added at each time step
b_t	$b(t)=\sum_{n=1}^{N} R_n(t)$, which is the number of tasks completed at each time step

Lyapunov function construction

The function $L(t)$ used to reflect the "unstable state" of the system is constructed, and the following quadratic function is often used:

$$L(t)=\frac{1}{2}Q(t)^2.$$

This function quantifies the square of the queue backlog. The larger $L(t)$ is, the larger the system error is and the more unstable the system is; the smaller $L(t)$ is, the more stable the system is.

Single-step drift analysis

Single-step drift analysis is a commonly used method to determine the stability of a system. Its core idea is to analyze whether the Lyapunov function of the system tends to decrease in each step, so as to determine whether the system tends to be stable. According to the Lyapunov function $L(t)$ obtained in the previous section, the single-step drift definition can be obtained as follows:

$$\Delta L(t)=E\left[L(t+1)-L(t)\middle|Q(t)\right].$$

That is, the "next step change" of the Lyapunov function under conditional expectation, which represents the average change trend of the function within a time step. Given that the queue dynamic equation is $Q(t + 1) = Q(t) + a(t) - b(t)$, it follows that:

$$L(t+1)-L(t)=\frac{1}{2}\left(Q(t+1)^2-Q(t)^2\right).$$

Substituting the expression for $Q(t + 1)$ into the above equation and expanding it, we obtain:

$$Q(t+1)^2=\left(Q(t)+a(t)-b(t)\right)^2=Q(t)^2+2Q(t)\left(a(t)-b(t)\right)+\left(a(t)-b(t)\right)^2.$$

Therefore, we can deduce that:

$$L(t+1)-L(t)=Q(t)\left(a(t)-b(t)\right)+\frac{1}{2}\left(a(t)-b(t)\right)^2.$$

Taking the conditional expectation of the above result, we obtain:

$$\Delta(t) = E\left[Q(t)\left(a(t) - b(t)\right) + \frac{1}{2} E\left[\left(a(t) - b(t)\right)^2 \middle| Q(t) \right] \right].$$

Separating the linear and quadratic terms, we get:

$$\Delta(t) = Q(t) E\left[a(t) - b(t) \middle| Q(t) \right] + \frac{1}{2} E\left[\left(a(t) - b(t)\right)^2 \middle| Q(t) \right].$$

Expanding the quadratic term, we find:

$$\left(a(t) - b(t)\right)^2 = a(t)^2 + b(t)^2 - 2a(t)b(t).$$

Assuming that the covariance between task arrivals and processing is bounded, and that $a(t)$ and $b(t)$ are independent or weakly correlated, the cross term $E\left[a(t)b(t) \middle| Q(t) \right]$ can be neglected or absorbed into a constant term. Hence:

$$E\left[\left(a(t) - b(t)\right)^2 \middle| Q(t) \right] \le E\left[a(t)^2 + b(t)^2 \middle| Q(t) \right].$$

Assuming that the variances of $a(t)$ and $b(t)$ are bounded, i.e., there exists a constant B such that $\frac{1}{2} E\left[a(t)^2 + b(t)^2 \middle| Q(t) \right] \le B.$

At this point, the drift inequality simplifies to:

$$\Delta(t) \le B + Q(t) E\left[a(t) - b(t) \middle| Q(t) \right].$$

After adjusting the signs, we arrive at the final form:

$$\Delta(t) \le B - Q(t) E\left[b(t) - a(t) \middle| Q(t) \right].$$

Drift-plus-penalty optimization

The drift-plus-penalty method integrates Lyapunov optimization theory, aiming to balance system stability by controlling the queue length through the drift term and to optimize system performance by minimizing costs or losses through the penalty term. We define the initial objective function as:

$$\min\left(\Delta(t) + V \cdot Penalty\right),$$

where the drift term $\delta(t)$ reflects the expected change in the queue $Q(t)$, which needs to be suppressed to maintain stability. The penalty term represents the time loss incurred during the task scheduling process, given by $TimeLoss = t_{scheduled} - t_{creation}$. The weight parameter V is responsible for balancing system stability and performance; as the queue length $Q(t)$ increases, V decreases to prioritize reducing queue congestion, and as the queue length decreases, V increases to prioritize reducing time loss. By substituting the drift term, we obtain the new objective function:

$$\min\left(B - Q(t) \cdot E\left[b(t) - a(t) \middle| Q(t) \right] + V \cdot TimeLoss \right).$$

By minimizing the objective function, the system can dynamically adjust the control strategy at each time slot t based on the current queue state $Q(t)$. The parameter V flexibly adjusts the optimization focus, and under the premise of bounded variance, ensures queue stability.

Parameter selection and stability – performance trade-off

The control parameter V plays a central role in balancing queue stability and delay performance. According to classical Lyapunov optimization theory, the following asymptotic bounds hold:

- Average Queue Length = $O(1/V)$;
- Average Delay Gap = $O(V)$.

Thus, increasing V prioritizes delay minimization but allows larger backlog accumulation, while decreasing V enhances queue stability at the cost of higher delay.

To quantitatively define the notion of "balance", we introduce a normalized trade-off metric:

$$Balance(V) = \alpha \cdot \frac{\bar{Q}(V)}{Q_{\max}} + (1-\alpha) \cdot \frac{\bar{D}(V)}{D_{\max}}.$$

where $\bar{Q}(V)$ is the average queue length, $\bar{D}(V)$ is the average delay, $0 < \alpha < 1$ is the preference weight.

The optimal V^* is selected by minimizing Balance(V).

Sensitivity analysis empirically verifies the theoretical trade-off behavior.

Algorithm design

Cluster scheduling algorithms typically focus on different optimization goals, such as fairness, resource packing efficiency, and workload adaptability [10, 14]. The purpose of this program is to design a dynamic resource allocation algorithm that adjusts the task processing rate R of resources to achieve stability of the task backlog queue, thereby preventing the task queue $Q(t)$ from growing indefinitely, i.e., $\lim_{T\to\infty} \frac{1}{T}\sum_{t=0}^{T-1} E\left[Q(t)\right] < \infty$, and to minimize the time loss. The overall design philosophy of the algorithm is as follows.

*Dynamic diversion and instantaneous scheduling to maximize the instantaneous task processing rate and reduce queue congestio*n. Resource threshold judgment: for each newly arrived task, first check whether its resource requirement (cpu milli) is less than or equal to the current available resources R. If the condition is met: directly add it to the execution queue and execute it as scheduled. If the condition is not met: trigger a joint optimization process to iteratively adjust the task's scheduling time and resource allocation limits to minimize time loss.

Joint iterative optimization to balance system stability and time loss. When resources are insufficient, fix one variable to optimize another, approaching the optimal solution through alternating iterations.

Optimize scheduling time. Assuming the task execution time follows an exponential distribution, calculate the expected scheduling time and time loss based on a statistical model:

$$\lambda = \frac{\text{Current total task volume}}{V \times Core\ efficiency\ C},$$

$$E(real\_scheduled\_time) = creation\_time + \frac{1}{\lambda}\ln\left(\frac{C\_req}{C\_req - R}\right).$$

Optimize resource allocation. Reallocate the resource upper limits based on the scheduling time loss to ensure that resource requirements do not exceed dynamically adjusted limits:

$$K(t) = \frac{Remaining\ volume}{Core\ efficiency\ C \times (scheduled\_time - creation\_time)},$$

$$C\_req = \min\left(K\left(t\right), C\_req\right).$$

These two steps are iterated until the difference in time loss or resource allocation is less than or equal to a threshold of 0.01.

Priority queues and feedback control. Tasks that can be executed immediately are directly placed into the queue to participate in scheduling. Tasks that cannot be executed immediately are arranged in descending order of *TimeLoss* and enter the queue *TimeLoss* to ensure that tasks with high delay risk are prioritized for resource allocation. Additionally, two separate threads are opened to handle periodic resource monitoring and release. Every $\Delta(t_1)$, the available resources R are checked; if the resources are sufficient to meet the requirements of the next task, the task waiting in line is dequeued and sent to the queue for execution. Every $\Delta(t_2)$, the execution queue is checked for completed tasks and their occupied resources are released, dynamically adjusting the control parameter V:

$$V\left(t\right) = V\left(t-1\right) \times \frac{Q\_\max}{Q\left(t\right)+1}.$$

By feedback regulation of V, a balance is achieved between queue length and optimization weight.

The flowcharts corresponding to the above processes are as follows:

Algorithm 1: Main Task Scheduling Process

Input: Task set tasks, total CPU resource R Output: Scheduling result

1 Initialize global variables;

2 Start daemon threads:

3 Thread 1: resource checker

4 Thread 2: task releaser;

5 while main loop is running do

6 Traverse each task in tasks;

7 for each task in tasks do

8 if current time ≥ task's release time then

9 calculate task priority: calculate task priority(task);

10 if task's CPU demand ≤ remaining CPU resource R then

11 Add task to task queue;

12 Update R: R ← R − task.cpu requirement;

13 Output result;

Experimental results

Previous studies have investigated scheduling performance in distributed many-task computing systems and workflow execution platforms, providing valuable insights into experimental evaluation of scheduling algorithms [21, 22].

Experiment environment

The proposed algorithm was implemented in Python 3.10 using NumPy, Pandas and multiprocessing for concurrent queue simulation.

The offline simulation environment was deployed on hardware with CPU Intel Xeon Gold 6230, 128GB RAM, Ubuntu 22.04. Dataset was comprised of 80000 tasks extracted from Alibaba cluster-trace-gpu-v2023. Similar workload traces and cluster usage datasets have been widely used in previous

Algorithm 2: Resource Checker Thread

Input: CPU resource R, task queue TimeLoss queue, time step timestep
Output: Updated task queue task queue
1 while true do
2 Sleep(timestep);
3 if main loop task ends then
4 break;
5 Check TimeLoss queue for tasks;
6 for each task in TimeLoss queue do
7 if R ≥ task.cpu requirement then
8 Move task to task queue;
9 R ← R − task.cpu requirement;

Algorithm 3: Task Releaser Thread

Input: Task queue task queue, time step timestep2
Output: Tasks marked for deletion
1 while true do
2 Sleep(timestep2);
3 if main loop task ends then
4 break;
5 for each task in task queue do
6 Compute u = V · Q/(queue length);
7 if current time ≥ deletion time then
8 Mark task as True for deletion;

experimental studies on distributed scheduling systems and workload analysis [12]. Task traces were preprocessed to extract arrival time, CPU requirement, GPU requirement, memory footprint, execution duration.

Scheduling simulation was event-driven. Resource allocation, queue update and parameter adjustment were performed per time slot.

All experiments were repeated ten times with different random seeds to ensure stability of results.

The implementation source code related to this study has been made publicly available on GitHub[1] to ensure transparency and reproducibility of the experimental results. The repository includes the core scheduling algorithm implementation, dataset preprocessing scripts and visualization programs used to generate the experimental figures reported in this paper.

Evaluation indicators

Average task scheduling delay

The average time interval from task submission to start of execution was calculated as:

$$\frac{1}{n}\sum_{i=1}^{n}\left(E_i - S_i\right),$$

[1] GitHub – shan5972/nonlinear · GitHub [online] Available: https://github.com/shan5972/nonlinear/tree/main (Accessed 13.03.2026).

where n is the number of tasks, S_i is the time of sending task i, E_i is the time of starting execution of task i.

CPU utilization

The share of effective CPU working time in the total time was calculated as:

$$\frac{\sum_{j=1}^{m}\left(\frac{T_{busy,j}}{T_{total}}\right)}{m}\times 100\%,$$

where m is the number of cores, T_{total} is the total monitoring time, T_{busy} is the CPU busy time.

Resource fragmentation rate

A measure of the extent to which CPU time blocks are split into discontinuous blocks was calculated as:

$$1-\frac{T_{seq}}{T_{free}},$$

where T_{seq} is the consecutive free idle time blocks, T_{free} is the total idle time blocks.

Jain's fairness index

Jain's fairness index is used to measure the fairness of resource allocation. The value range is [1/n, 1], where 1 represents complete fairness. The calculation formula is

$$\frac{\left(\sum_{i=1}^{n} x_i\right)^2}{n\sum_{i=1}^{n} x_i^2},$$

where x_i represents the number of resources obtained by each task i.

Elasticity coefficient

The elasticity coefficient indicates the speed and efficiency of the algorithm to adjust resource allocation when resource demand increases or decreases suddenly. The calculation formula is:

$$\frac{1}{\omega_T * T_r + \omega_U * \Delta U + \omega_R * R_d},$$

where T_r is the average scheduling delay of all Pods during the burst phase, ΔU is the sum of the absolute value changes in utilization, R_d is the ratio of the delay during the burst phase to the delay during the normal phase, ω is the parameter weight.

Experimental results analysis

Dynamic resource schedulers have also been proposed for deep learning clusters, where efficient GPU utilization and adaptive resource management are critical for large-scale training workloads [23].

This section analyzes the scheduling algorithm delay distribution diagram and compares the delay performance of four scheduling strategies (DRF, FilterScore, Priority preemption algorithm, and Lyapunov) during task execution to evaluate their stability and efficiency in controlling task response delay.

Latency

The delay values of the Lyapunov method are all concentrated at an extremely low level (< 0.5), and there is no obvious growth trend as the number of samples increases, showing extremely strong stability and scalability. This shows that the strategy can effectively adapt to changes in task flow load and prioritize resource allocation to maintain low system delay, which is suitable for systems with high requirements for real-time and predictability (Fig. 1).

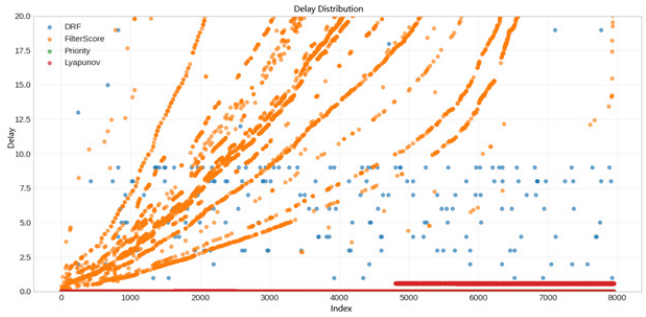

Fig. 1. Delay distribution of four algorithms

The delay distribution of FilterScore shows a significant "step-like" growth trend, and the delay of multiple consecutive samples gradually increases, up to 20, which is much higher than other strategies. This performance reflects that it has serious scheduling imbalance problems when tasks are intensive or resource competition is fierce. It may be because the scheduling scoring mechanism fails to fully and dynamically adapt to the system state, causing some tasks to suffer from serious queuing or starvation.

The delay distribution of DRF is relatively dispersed, with most task delays in the range of 0–10, but there are also obvious delay spikes (over 15), indicating that there are large response delays in some task scheduling stages. Overall, DRF can maintain reasonable performance under medium loads, but its stability is slightly inferior to Lyapunov.

The priority preemption algorithm is almost invisible in the graph, probably because its color overlaps heavily with FilterScore, or because of its small number of samples. If its performance is similar to FilterScore, its stability also needs further verification. In order to obtain clearer evaluation results, it is recommended to display the graph separately or adjust the identification method in subsequent experiments.

Resource fragmentation rate

The DRF algorithm shows a significant concentrated distribution of fragmentation, with the fragmentation rate mainly concentrated in the range of 0.9–1.0, and only a small number of samples have low fragmentation rates. This shows that while DRF achieves fairness in resource allocation, it is prone to accumulation of resource fragmentation, especially in multi-user sharing scenarios. Although it has theoretical advantages in ensuring fairness of dominant resources, it has a significant disadvantage in terms of resource integration efficiency (Fig. 2).

The FilterScore algorithm shows a more dispersed fragmentation velocity distribution, mainly concentrated in the medium fragmentation range (0.2–0.8). Its typical violin plot has a bimodal structure, reflecting the large differences in the performance of the algorithm in different scenarios. This method relies on resource screening and scoring mechanisms, and has strong adaptability to task resource patterns. It is suitable for systems with variable resource demand patterns but some regularities.

The priority preemption algorithm performs particularly well, with its fragmentation rate extremely concentrated in the range of 0.1–0.3, and almost no high fragmentation value. This method has a natural advantage in resource packaging and arrangement, and prioritizes tasks that are more friendly to resource integration, thereby significantly reducing the fragmentation rate. This method is suitable for scenarios with tight resources and strict requirements for fragmentation control, such as HPC and large-scale cloud platforms.

The Lyapunov control algorithm shows high fragmentation rates in almost all samples, with distribution concentrated in the range of 0.9–1.0. Although this method has advantages in controlling

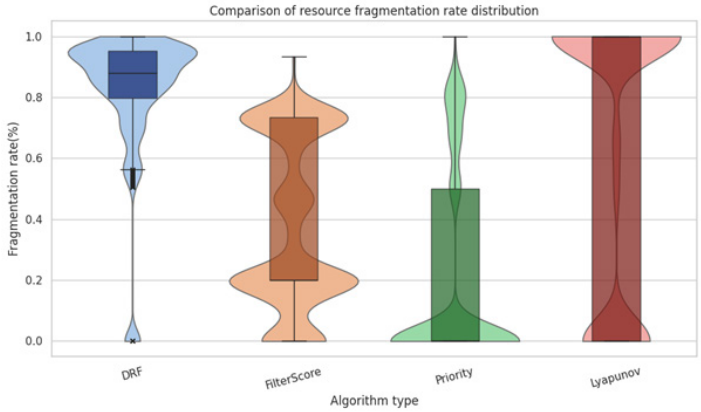

Fig. 2. Resource fragmentation rate of four algorithms

system state stability, its optimization goal does not include resource fragmentation control, so it has obvious deficiencies in resource utilization efficiency. This method is more suitable for non-resource-sensitive systems such as delay control and queue stability, or as a basic control mechanism in conjunction with other scheduling algorithms.

CPU utilization

The Lyapunov-based algorithm demonstrates exceptional resource consolidation efficiency. Its utilization is highly concentrated within the 0.87–0.95 range (with an interquartile range span of only 0.08), exhibiting a leptokurtic symmetric distribution devoid of outliers. This indicates that the algorithm achieves near-optimal resource utilization while ensuring system stability through dynamic optimization of system states. Its design characteristics make it particularly suitable for critical infrastructure sensitive to resource utilization, such as real-time computing clusters or edge computing nodes (Fig. 3).

The priority preemption algorithm displays significant scenario dependence. Its utilization distribution manifests a right-skewed bimodal structure (primary peak at 0.75, secondary peak at 0.95), accompanied by numerous high-end outliers (up to 1.0). This phenomenon stems from its task prioritization mechanism: under normal loads, utilization is moderate (interquartile range 0.65–0.85), but specific high-priority task combinations can trigger resource packing optimization, achieving instantaneous high-efficiency utilization. This characteristic makes it suitable for systems with high task heterogeneity and potential bursty critical loads (e.g., hybrid cloud environments), albeit with limited overall reliability.

The DRF algorithm exhibits robust yet conservative characteristics. Utilization is primarily distributed within the 0.75–0.88 range (median 0.82), showing a mild left-skewed distribution. Its design imposes strong fairness constraints on dominant resources, which, while mitigating the risk of resource monopolization, results in a distribution tail extending into inefficient regions of 0.4–0.6 (with a few low-end outliers). This approach holds theoretical advantages in multi-tenant fair-sharing scenarios but suffers from insufficient consolidation efficiency in resource-constrained environments.

The FilterScore algorithm exhibits a distribution pattern similar to DRF, with utilization concentrated in the 0.77–0.89 range (median 0.83), but demonstrates a less pronounced left skew. Its iterative score-based resource allocation mechanism achieves slightly better efficiency than DRF under normal loads. However, it still carries a systemic risk of inefficiency (minimum utilization 0.5). This algorithm can serve as an improved variant of DRF, suitable for general-purpose computing platforms requiring a balance between fairness and baseline efficiency.

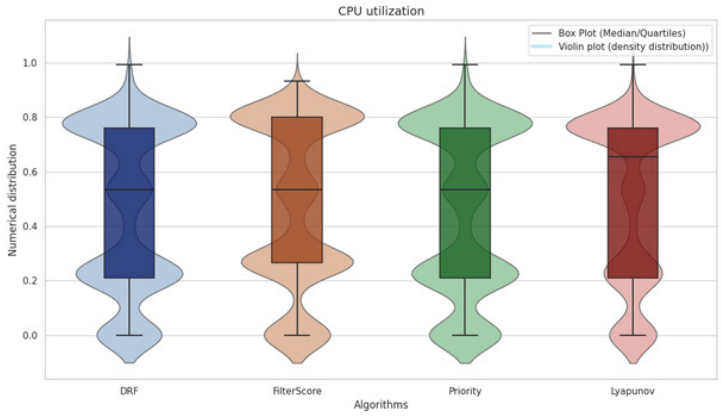

Fig. 3. CPU utilization distribution of the four algorithms

Table 2

Performance comparison of scheduling algorithms

Index	FilterScore	DRF	Priority	Lyapunov
Elasticity coefficient	0.1782	0.2385	0.7013	0.6167
Average scheduling delay	17.5362	13.1076	1.4942	0.2663
Resource utilization	0.4647	0.4538	0.4463	0.5459
Jain's fairness index	0.6579	0.6121	0.5882	0.6489
Resource fragmentation rate	0.3663	0.8189	0.1907	0.7726

Comprehensive evaluation

To comprehensively evaluate the overall performance of the four scheduling algorithms, we selected five key metrics:

1) resilience coefficient;
2) average scheduling latency;
3) resource utilization;
4) resource fragmentation rate;
5) Jain's fairness index.

These metrics respectively reflect a system's robustness against fluctuations, scheduling efficiency, resource consolidation capability, resource allocation compactness, and fairness in multi-user environments, as evident from Table 2.

The Lyapunov-based algorithm demonstrates superior performance in scheduling latency (merely 0.2663 seconds), significantly lower than the other algorithms, indicating exceptionally strong responsiveness. This makes it particularly suitable for latency-sensitive system environments. Concurrently, it achieves the highest resource utilization (0.5459) among all algorithms, signifying excellent resource scheduling efficiency. Furthermore, its fairness index (0.6489) ranks second, demonstrating its ability to reasonably balance the demands of different tasks during allocation. Although its resilience coefficient (0.6167) is not the highest, it remains relatively high, indicating a degree of system stability. However, its resource fragmentation rate (0.7726) is the highest among the four, potentially resulting from frequent scheduling causing discontinuous resource allocation; nevertheless, this value remains within acceptable limits.

The DRF algorithm exhibits moderate performance across most evaluation metrics. As shown in Table 2, DRF achieves a fairness index of 0.6121, which reflects its design objective of maintaining

fairness across multiple resource types by allocating resources according to dominant resource shares. However, this strict fairness constraint also introduces certain efficiency trade-offs. The average scheduling delay of DRF reaches 13.1076, significantly higher than that of the proposed Lyapunov method. In addition, the resource fragmentation rate of 0.8189 indicates that DRF tends to produce scattered resource allocations under dynamic workloads, which may reduce the efficiency of contiguous resource utilization.

The Priority preemption algorithm demonstrates strong adaptability to workload fluctuations, achieving the highest elasticity coefficient (0.7013) among the compared methods. Its average scheduling delay (1.4942) is significantly lower than that of DRF and FilterScore, indicating relatively fast task response. However, the fairness index (0.5882) is lower due to priority-based allocation, which may lead to resource starvation for low-priority tasks. The low resource fragmentation rate (0.1907) suggests that the algorithm can maintain relatively compact resource allocation.

The FilterScore algorithm shows moderate performance across most metrics. As shown in Table 2, it achieves a fairness index of 0.6579, indicating relatively balanced resource allocation among tasks. However, its average scheduling delay (17.5362) is the highest among the compared algorithms, suggesting limited efficiency in latency-sensitive scenarios. In addition, its elasticity coefficient (0.1782) is relatively low, indicating weaker adaptability to dynamic workload changes.

Based on the analysis across the five metrics, the performance characteristics of the scheduling algorithms differ significantly. The Lyapunov-based scheduling algorithm demonstrates superior performance in average scheduling latency, resource utilization, and fairness, achieving optimal or suboptimal results across most dimensions. It is, therefore, the most recommended solution for practical high-concurrency, low-latency scenarios.

Generalization analysis

Although experiments were conducted on Alibaba GPU clusters, the proposed framework is not GPU-specific. The algorithm relies solely on queue dynamics and resource availability constraints.

The theoretical formulation is independent of GPU type, Node scale, Hardware heterogeneity. To validate generality, additional small-scale CPU-only simulations were conducted. Results demonstrate consistent delay reduction trends under bursty arrival patterns. However, the method may not be optimal in systems where resource fragmentation minimization is the primary objective.

Conclusion

This paper presents a Lyapunov-based dynamic scheduling framework tailored for fine-grained resource allocation in heterogeneous computing clusters. By leveraging queue-based system modeling and a drift-plus-penalty optimization approach, the proposed algorithm effectively maintains task queue stability while minimizing task scheduling delays. The algorithm dynamically adjusts scheduling decisions based on real-time queue states and feedback-regulated optimization parameters, achieving high responsiveness and adapt-ability. Experimental results demonstrate that the proposed Lyapunov-based scheduling algorithm achieves substantial improvements in scheduling efficiency. The average scheduling delay is reduced to 0.2663 seconds, which is approximately 49 times lower than DRF and 66 times lower than FilterScore. Meanwhile, the algorithm achieves the highest resource utilization (0.5459) and maintains a competitive fairness index (0.6489). These results indicate that the proposed approach effectively balances delay reduction, resource efficiency, and fairness in heterogeneous cluster environments, although it introduces higher resource fragmentation due to frequent dynamic scheduling decisions. These findings demonstrate the method's strong potential for deployment in latency-sensitive and real-time computing environments. Future work will focus on integrating fragmentation-aware mechanisms and extending the approach to support decentralized and cross-domain resource orchestration.

REFERENCES

1. **Ismail A.A., Khalifa N.E., El-Khoribi R.A.** A survey on resource scheduling approaches in multi-access edge computing environment: a deep reinforcement learning study. *Cluster Computing*, 2025, Vol. 28, Art. no. 184. DOI: 10.1007/s10586-024-04893-7

2. **Polo J., Castillo C., Carrera D., Becerra Y., Whalley I., Steinder M., Torres J., Ayguadé E.** Resource-aware adaptive scheduling for MapReduce clusters. In: *Middleware 2011: Lecture Notes in Computer Science* (eds. F. Kon, A.M. Kermarrec), 2011, Vol. 7049, Pp. 187–207. DOI: 10.1007/978-3-642-25821-3_10

3. **Chen Y., Griffith R., Liu J., Katz R.H., Joseph A.D.** Understanding TCP incast throughput collapse in datacenter networks. *Proceedings of the 1st ACM Workshop on Research on Enterprise Networking*, 2009, Pp. 73–82. DOI: 10.1145/1592681.1592693

4. **Hindman B., Konwinski A., Zaharia M., Ghodsi A., Joseph A.D., Katz R., Shenker S., Stoica I.** Mesos: A platform for fine-grained resource sharing in the data center. *Proceedings of the 8th USENIX Symposium on Networked Systems Design and Implementation*, 2011, Pp. 295–308.

5. **Neely M.J.** *Stochastic Network Optimization with Application to Communication and Queueing Systems*. Cham: Springer, 2010. DOI: 10.1007/978-3-031-79995-2

6. **Shi Y., Yang K., Jiang T., Zhang J., Letaief K.B.** Communication-efficient edge AI: Algorithms and systems. arXiv:2002.09668, 2020. DOI: 10.48550/arXiv.2002.09668

7. **Shahrad M., Fonseca R., Goiri Í., Chaudhry G., Batum P., Cooke J., Laureano E., Tresness C., Russinovich M., Bianchini R.** Serverless in the wild: characterizing and optimizing the serverless workload at a large cloud provider. Proceedings of the 2020 USENIX Conference on Usenix Annual Technical Conference, 2020, Pp. 205–218.

8. **Zhang J., Zhai Y., Liu Z., Wang Y.** A Lyapunov-based resource allocation method for edge-assisted industrial internet of things. *IEEE Internet of Things Journal*, 2024, Vol. 11, No. 24, Pp. 39464–39472. DOI: 10.1109/JIOT.2024.3446722

9. **Gao Y., Liu L., Zheng X., Zhang C., Ma H.** Federated sensing: Edge-cloud elastic collaborative learning for intelligent sensing. *IEEE Internet of Things Journal*, 2021, Vol. 8, No. 14, Pp. 11100–11111. DOI: 10.1109/JIOT.2021.3053055

10. **Tang S., He B.-S., Zhang S., Niu Z.** Elastic multi-resource fairness: balancing fairness and efficiency in coupled CPU-GPU architectures. Proceedings of the International Conference for High Performance Computing, Networking, Storage and Analysis, 2016, Pp. 875–886. DOI: 10.1109/SC.2016.74

11. **Verma A., Pedrosa L., Korupolu M., Oppenheimer D., Tune E., Wilkes J.** Large-scale cluster management at Google with Borg. *Proceedings of the 10th European Conference on Computer Systems*, 2015, Art. no. 18. DOI: 10.1145/2741948.2741964

12. **Reiss C., Wilkes J.** *Google cluster-usage traces: format + schema*. Google Inc. Technical Report, 2011.

13. **Burns B., Grant B., Oppenheimer D., Brewer E., Wilkes J.** Borg, Omega, and Kubernetes. *Communications of the ACM*, 2016, Vol. 59, No. 5, Pp. 50–57. DOI: 10.1145/2890784

14. **Ghodsi A., Zaharia M., Hindman B., Konwinski A., Shenker S., Stoica I.** Dominant resource fairness: fair allocation of multiple resource types. *Proceedings of the 8th USENIX Conference on Networked Systems Design and Implementation*, 2011, Pp. 323–336.

15. **Xiao W., Bhardwaj R., Ramjee R. et al.** Gandiva: introspective cluster scheduling for deep learning workloads. *Proceedings of the 13th USENIX Conference on Operating Systems Design and Implementation*, 2018, Pp. 595–610.

16. **Zhao X., Yao J., Gao P., Guan H.** Efficient sharing and fine-grained scheduling of virtualized GPU resources. *2018 IEEE 38th International Conference on Distributed Computing Systems* (*ICDCS*), 2018, Pp. 742–752. DOI: 10.1109/ICDCS.2018.00077

17. **Sukhoroslov O.** Building web-based services for practical exercises in parallel and distributed computing. *Journal of Parallel and Distributed Computing*, 2018, Vol. 118 (1), Pp. 177–188. DOI: 10.1016/j.jpdc.2018.02.024

18. **Mao Y., You C., Zhang J., Huang K., Letaief K.B.** A survey on mobile edge computing: The communication perspective. *IEEE Communications Surveys & Tutorials*, 2017, Vol. 19, No. 4, Pp. 2322–2358. DOI: 10.1109/COMST.2017.2745201

19. **Beloglazov A., Buyya R.** Optimal online deterministic algorithms and adaptive heuristics for energy and performance efficient dynamic consolidation of virtual machines in cloud data centers. *Concurrency and Computation: Practice and Experience*, 2012, Vol. 24, No. 13, Pp. 1397–1420. DOI: 10.1002/cpe.1867

20. **Smorodnikov G., Zolotarev R., Rykova A., Sabutkevich A., Samochadin A.** Elastic cloud resource allocation using short-term long short-term memory-based workload prediction. *Proceedings of the 4th International Conference on Optics, Computer Applications, and Materials Science* (*CMSD-IV 2024*), 2025, Vol. 13651, Art. no. 136510J. DOI: 10.1117/12.3060861

21. **Sukhoroslov O., Nazarenko A., Aleksandrov R.** An experimental study of scheduling algorithms for many-task applications. *The Journal of Supercomputing*, 2019, Vol. 75, Pp. 7857–7871. DOI: 10.1007/s11227-018-2553-9

22. **Sukhoroslov O.** Supporting efficient execution of workflows on Everest platform. *Supercomputing* (*RuSCDays*), 2019, Pp. 713–724. DOI: 10.1007/978-3-030-36592-9_58

23. **Peng Y., Bao Y., Chen Y., Wu C., Guo C.** Optimus: an efficient dynamic resource scheduler for deep learning clusters. *Proceedings of the 13th EuroSys Conference*, 2018, Art. no. 3. DOI: 10.1145/3190508.3190517

INFORMATION ABOUT AUTHORS / СВЕДЕНИЯ ОБ АВТОРАХ

Wang Shan
Ван Шань
E-mail: wangshan@mail.ru
ORCID: https://orcid.org/0000-0001-8591-9080

Igor V. Nikiforov
Никифоров Игорь Валерьевич
E-mail: igor.nikiforovv@gmail.com
ORCID: https://orcid.org/0000-0003-0198-1886

Submitted: 04.10.2025; Approved: 23.02.2026; Accepted: 17.03.2026.
Поступила: 04.10.2025; Одобрена: 23.02.2026; Принята: 17.03.2026.

Computing, Telecommunication and Control, 2026, Vol. 19, No. 1, Pp. 80–90.
Информатика, телекоммуникации и управление. 2026. Том 19, № 1. С. 80–90.

System Analysis and Control
Системный анализ и управление

Research article
DOI: https://doi.org/10.18721/JCSTCS.19108
UDC 004.93:62-192

CONTEXTUAL REGULARIZATION OF THE FEATURE SPACE OF WEAKLY STRUCTURED DATA FOR ANALYZING THE RISK TOPOLOGY OF COMPLEX TECHNICAL SYSTEMS

V.P. Shkodyrev, E.A. Konnikov, P.A. Polyakov ✉

Peter the Great St. Petersburg Polytechnic University,
St. Petersburg, Russian Federation

✉ prohor@polyakov-box.ru

Abstract. The paper addresses the problem of eliminating sparsity and "false orthogonality" in short, weakly structured technical messages that hinder systematic analysis and modeling of the risk topology of complex technical systems. A method of contextual regularization of the feature space is proposed, which treats the enrichment of vector representations as a controlled diffusion process on a graph of joint occurrence of lemmas. The context topology is specified by a weighted adjacency matrix based on positive pointwise mutual information, and the recursive diffuser performs iterative feature propagation with depth attenuation and adaptive IDF gating, which suppresses noisy connections and amplifies diagnostically significant terms. The regularization parameter tuning is formalized as a task of maximizing the target quality functional, combining metrics of structural separability and semantic completeness with a threshold penalty for separability degradation. A priori, the limited nature of the diffusion process is demonstrated, and the elimination of orthogonality of terminologically heterogeneous descriptions in the presence of a contextual "bridge" in the graph is proven. Experimental testing on the NRC operational message corpus demonstrates a significant increase in the semantic coherence of topics while maintaining the geometric separability of clusters. The resulting regularized space improves the interpretability of the thematic structure of incidents and creates a basis for the subsequent self-organization of the risk event taxonomy and the construction of verifiable decision support contours.

Keywords: weakly structured data, systematic risk analysis, thematic modeling, co-occurrence graph, diffusion feature enrichment, interpretable AI, accident topology

Acknowledgements: The research was financially supported by the Ministry of Science and Higher Education of the Russian Federation within the framework of the state assignment "Development of methodology for the formation of a tool base for analysis and modeling of spatial socio-economic development of systems in the conditions of digitalization with reliance on internal reserves" (FSEG-2023-0008).

Citation: Shkodyrev V.P., Konnikov E.A., Polyakov P.A. Contextual regularization of the feature space of weakly structured data for analyzing the risk topology of complex technical systems. Computing, Telecommunications and Control, 2026, Vol. 19, No. 1, Pp. 80–90. DOI: 10.18721/JCSTCS.19108

Научная статья
DOI: https://doi.org/10.18721/JCSTCS.19108
УДК 004.93:62-192

КОНТЕКСТУАЛЬНАЯ РЕГУЛЯРИЗАЦИЯ ПРИЗНАКОВОГО ПРОСТРАНСТВА СЛАБОСТРУКТУРИРОВАННЫХ ДАННЫХ ДЛЯ АНАЛИЗА ТОПОЛОГИИ РИСКОВ СЛОЖНЫХ ТЕХНИЧЕСКИХ СИСТЕМ

В.П. Шкодырев, Е.А. Конников, П.А. Поляков ✉

Санкт-Петербургский политехнический университет Петра Великого,
Санкт-Петербург, Российская Федерация

✉ prohor@polyakov-box.ru

Аннотация. В статье рассматривается проблема устранения разреженности и «ложной ортогональности» в коротких, слабо структурированных технических сообщениях, которые затрудняют систематический анализ и моделирование топологии рисков сложных технических систем. Предлагается метод контекстной регуляризации пространства признаков, который рассматривает обогащение векторных представлений как управляемый процесс диффузии на графе совместного появления лемм. Топология контекста задается взвешенной матрицей смежности на основе положительной точечной взаимной информации, а рекурсивный диффузор выполняет итеративное распространение признаков с глубинным затуханием и адаптивным IDF-шлюзом, который подавляет шумовые связи и усиливает диагностически значимые термины. Настройка параметра регуляризации формализуется как задача максимизации целевого функционала качества, сочетающего метрики структурной разделимости и семантической полноты с пороговым штрафом за ухудшение разделимости. Априори демонстрируется ограниченный характер процесса диффузии и доказывается устранение ортогональности терминологически гетерогенных описаний при наличии контекстуального «моста» в графе. Экспериментальное тестирование на корпусе оперативных сообщений NRC демонстрирует значительное увеличение семантической когерентности тем при сохранении геометрической разделимости кластеров. Полученное в результате регуляризованное пространство улучшает интерпретируемость тематической структуры инцидентов и создает основу для последующей самоорганизации таксономии рисковых событий и построения проверяемых контуров поддержки принятия решений.

Ключевые слова: слабоструктурированные данные, системный анализ рисков, тематическое моделирование, граф совместной встречаемости, диффузионное обогащение признаков, интерпретируемый ИИ, топология аварийных ситуаций

Финансирование: Исследование выполнено при финансовой поддержке Министерства науки и высшего образования Российской Федерации в рамках государственного задания «Разработка методологии формирования инструментальной базы анализа и моделирования пространственного социально-экономического развития систем в условиях цифровизации с опорой на внутренние резервы» (FSEG-2023-0008).

Для цитирования: Shkodyrev V.P., Konnikov E.A., Polyakov P.A. Contextual regularization of the feature space of weakly structured data for analyzing the risk topology of complex technical systems // Computing, Telecommunications and Control. 2026. T. 19, № 1. C. 80–90. DOI: 10.18721/JCSTCS.19108

Introduction

The transition of industry to the Industry 4.0 paradigm is accompanied by an avalanche-like growth in the volume of heterogeneous data and the widespread digitization of the operation of complex technical systems [1]. Up to 80% of meaningful information about the condition of objects is now contained in loosely structured text sources – shift logs, reports, acts – which are difficult to formalize

for traditional risk analysis algorithms [2]. Global experience shows that an increase in the volume of data without new methods of processing it does not lead to an equivalent increase in the quality of accident prediction [3]. For example, investigations into the Columbia space shuttle disaster and the Davis–Besse nuclear power plant accident revealed that critical warning signs had been present in text reports for years but had gone unnoticed due to the limitations of classical safety models [4]. This creates a contradiction in that monitoring systems accumulate large text archives but are "blind" to the knowledge they contain about accident predictors [5].

The traditional Probabilistic Safety Assessment (PSA) methodology, based on structured failure data and Boolean logic, has proven ineffective for analyzing the gradual evolution of defects in conditions of semantic uncertainty in textual descriptions [6]. Existing algorithms treat texts as "bags of words", i.e., sparse vectors in the space of terms, and completely ignore the semantic connections between different formulations of the same phenomenon [7]. Terminologically different descriptions of similar processes are assigned orthogonal coordinates, as a result of which classical models fail to capture the hidden causal relationships between events [8]. Even modern neural network methods do not solve the problem [9]. Their "black box" decision-making is unacceptable in critical applications due to the lack of guarantees and interpretability [10]. As a result, the emergency state of a complex system should be viewed not as a single "trigger" but as a dynamic trajectory in a multidimensional state space [11]. Neglecting the topology of this trajectory – the distribution of threats, the presence of gaps and clusters – leads to the omission of rare but critical scenarios [12]. The lack of methods for assessing risk elasticity – the sensitivity of the system's trajectory to small perturbations of semantic features – makes it impossible to rank threats according to their degree of controllability and generate proactive accident prevention strategies [13].

Thus, a fundamental scientific task arises: to develop a set of methodological solutions for the systematic accounting of weakly structured textual information in security analysis [14]. It is necessary to homomorphically map the semantics of operational texts into a metric space of risks, preserving the original topological invariants of threats – connectivity, gaps, hierarchy – and ensuring the interpretability of modeling results [15]. Recent work in the field of risk text mining confirms the relevance of this task [16]. For example, in supply chain management, risks are successfully identified through analysis of news and social media using thematic modeling and BERT models [17]. Insurance companies have begun to implement solutions that integrate the analysis of text-based claims and applications to improve the assessment of underwriting risks. Reviews of methods for thematic modeling of short texts are being conducted, and approaches are being developed for extracting safety knowledge from free descriptions of incidents through ontologies and knowledge graphs [19, 20]. However, the problem of false independence of short technical notes and the restoration of hidden connections remains insufficiently solved in practice [21]. This article aims to fill this gap by proposing an original method of contextual regularization of feature space to identify risk topology.

Methods

We propose representing a corpus of weakly structured documents as a directed context graph, whose nodes are lemmas and whose weighted edges reflect associative links between terms in the texts. Then, diffusion propagation of context across the graph is performed to enrich the vector representation of each document with semantically similar features. This approach allows us to overcome the artificial sparsity of the feature space. Even if two messages do not have any words in common but describe related phenomena, there will be paths on the graph connecting them through intermediate terms, and as a result of diffusion, their vectors will converge. An important feature of the method is adaptive control of the degree of context propagation to maintain a balance between data connectivity and separability.

Let this be the body of documents D, from which many unique lemmas have been extracted $W = l_1, l_2, ..., l_n$. We define a directed graph $G = (W, E)$ with a weighted adjacency matrix $A = [a_{ij}]$, where the vertices are lemmas, and the weight $a_{ij} l_i \to l_j$ reflects the strength of the statistical association between l_i and l_j. Positive Point Mutual Information (PMI) is used as an association measure:

$$I^+\left(\ell_i, \ell_j\right) = \max\left\{\ln \frac{P\left(\ell_i, \ell_j\right)}{P\left(\ell_i\right) P\left(\ell_j\right)}, 0\right\},$$

where $P(l_i)$ is the empirical probability of encountering a lemma li in a random document, but $P(l_i, l_j)$ is the probability of joint occurrence l_i and l_j in one document. Thus, only those connections that statistically significantly link terms in descriptions (PMI > 0) are included in the graph. To avoid the dominance of single super-strong connections, an association limiter is introduced – the upper limit I_0 PMI significance:

$$a_{ij} = \min\left\{I^+\left(\ell_i, \ell_j\right), I_0\right\},$$

which prevents the concentrated flow of context through a narrow set of frequently paired terms. The resulting graph G defines the topology of the context. It forms an "environment" through which the semantic signal will propagate in subsequent stages.

The second stage involves enriching the feature vector of each document $d \in D$ with contextual features. The initial representation of the document is given by a vector of term frequencies or weights $x_d^{(0)} \in R^n$. The result of the algorithm is a regularized vector x_d with the same number of measurements, but denser and semantically coherent. Diffusion enrichment is performed iteratively in-depth steps $k = 1, 2, ..., D$. At each step, a contribution from neighboring vertices of the graph at a distance k is added to the current vector. This can be written recursively:

$$x_d^{(k)} = x_d^{(k-1)} + \beta\alpha^k A x_d^{(k-1)}, \quad k = 1, \ldots, D,$$

where $\alpha \in (0,1]$ is the coefficient of context attenuation with increasing diffusion distance (depth), and $\beta > 0$ is the coefficient that regulates the overall level of context addition. Thus, in the first step, the document is enriched with direct links between its terms $x_d^{(0)}$, in the second step – indirect connections through one intermediate node, in the following steps – similarly. Thanks to the attenuation factor α^k, the influence of distant contextual terms decreases exponentially with increasing depth, preventing the thematic focus of the document from being "blurred". The iterative process can be interpreted as the diffusion of the "mass" of features across the graph. Initially, the entire mass is concentrated in the nodes of the document's initial lemmas, then at each step, part of the mass flows to neighboring nodes, accumulating in semantically close terms.

The key innovation of the method is adaptive contextual link routing. Despite the limitation I_0, the graph still contains many noise edges – terms from general vocabulary, abbreviations, data collection artefacts that do not carry valuable meaning. To strengthen propagation through meaningful nodes and weaken it through noise nodes, a diagonal matrix G of weight coefficients for lemmas is introduced. Elements G_{ii} depend on the statistical significance of the term l_i in the body, for example, from the reverse frequency of the document $idf(l_i)$ and from an *a priori* assessment of informational value. As a result, the update is modified:

$$x_d^{(k)} = x_d^{(k-1)} + \beta\alpha^k AG x_d^{(k-1)}.$$

Such an Intermediate Distribution Frame (IDF) gateway passes context primarily through rare and diagnostically significant terms, blocking propagation through common words and technical noise.

After completing D iterations, the resulting vector is normalized and small components are truncated by a threshold. Normalization eliminates scale differences between documents, and threshold zeroing filters out insignificant contextual additions, preserving the interpretability of the resulting feature vector. Final state $x_d = x_d^{(D)}$ is a regularized space of document features – denser, semantically smoothed, yet retaining the main thematic contours of the source data.

The most important component of the method is the automatic adjustment of the parameters $\Theta = \alpha, \beta, D$ of the diffuser and gate based on the analysis of the structure of the obtained data space. On the one hand, strong context diffusion (large α, β, D) maximizes the thematic relevance of documents, bringing them closer together semantically, which is useful for identifying hidden patterns. On the other hand, excessive diffusion can negate data separability, complicating the detection of individual clusters of emergency scenarios. To achieve a balance between coherence and separability, a feedback control loop is introduced. On the output set of vectors x_d two data structure indicators are calculated: cluster separability S and semantic completeness T. These indicators reflect, respectively, the geometric quality of data division and the informativeness of thematic coverage. Next, the scalar quality functional $Q(S, T)$ is determined, which is maximized at optimal parameters. One possible variant of the functional is a penalty function with a divisibility threshold:

$$Q = T - \mu \max\{0, S_0 - S\}^{\nu},$$

where S_0 is the required threshold of cluster separability, $\mu > 0$ is the penalty coefficient for insufficient separability, and $\nu \geq 1$ is the penalty nonlinearity index. When $S \geq S_0$, the penalty part is reset to zero and the functional is equal to T; otherwise, Q decreases proportionally to the non-fulfilment of the S_0 criterion. The selected functional is evaluated at the current state of the data, after which the control algorithm – for example, the gradient search method or heuristics – adjusts the parameters Θ in the direction of Q growth. As a result, contextual regularization becomes a controllable process. The diffusion and filtering parameters are automatically adjusted to the specific structure of the analyzed data. This is important because the effectiveness of context propagation is not a constant – it strongly depends on the nature of the corpus and the signal-to-noise ratio. In our experiments, parameter optimization yielded a significant quality gain compared to a fixed heuristic setting, confirming the need for an adaptive contour.

The proposed regularization process has strict *a priori* properties of stability and correctness. Firstly, diffusion along the association graph is fundamentally limited from above. Since, by definition, $0 \leq a_{ij} \leq I_0$ and all increments at each step are non-negative, the weight of the feature cannot grow uncontrollably. More formally, consider the increase in the i-th component of the vector at step k: $\left(\Delta x^{(kd)}\right)_i = \beta\alpha^k \sum_j \alpha_{ij} \left(x^{(k-1)d}\right)_j$. Maximum $\left(x_d^{(k-1)}\right)_j \leq 1$, and $\sum_j a_j \leq \sum_j I_0 = nI_0$. Consequently, $\left(\Delta x_i^{\{(k)d)}\right) \leq \beta\alpha^k nI_0$. When $\alpha < 1$, the series of cumulative increments for $k = 1, \ldots, \infty$ converges. So, every value $x_{d,i}$ has a finite limit at $D \to \infty$. Let there be two documents d and d' with initial feature vectors $x^{(0)}d$ and $x^{(0)}$, having no common units. Suppose that there is a "bridge" on graph G – lemma h associated with the term l_i from d and l_j from d' ($a_{ih} > 0$ and $a_{jh} > 0$). Then, at the first stage of diffusion, both documents will receive a positive component based on the criterion: $h : \left(x_h^{\{(1)d)} = \beta\alpha a\right\} > 0$ and $\left(x_h^{\{(1)d')} = \beta\alpha a\right\} > 0$. This means that their scalar product becomes strictly positive: $\left\langle x^{(1)d}, x^{(1)} \right\rangle > 0$. Thus, the documents d and d' cease to be orthogonal and begin to be recognized as close in feature

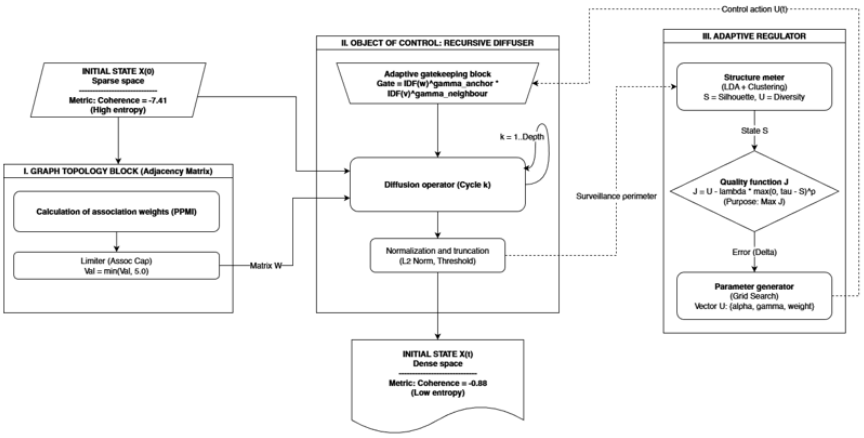

Fig. 1. System for contextual regularization of the feature space of weakly structured data (block diagram of the method)

space. In general, diffusion restores hidden semantic connections. Terminologically different descriptions of the same phenomenon obtain a non-zero intersection on adjacent features already at the level of vector representation. This fundamental property underlies the stated effect – the elimination of data sparsity and increased coherence of thematic groups of documents.

To implement the proposed method, software was developed in Python. The main steps of the algorithm – graph construction, iterative diffusion, and adaptive tuning – scale linearly with the size of the corpus and are parallelized across documents. The association graph is constructed by truncating rare terms and limiting the maximum degree of vertices for acceleration. Diffusion is performed until convergence or until a given depth D, after which the metrics S and T are calculated using a cluster analysis library and the parameters are tuned. The regulatorəs operation is based on heuristics. First, we increase α and β until the coherence T increases, then at the first signs of a drop in the silhouette S, we fix them and increase D to expand the distant context without sacrificing local separability. This approach significantly speeds up the search for the optimum. At the final stage, the regularized document vectors and the topics and clusters calculated on their basis are saved for further interpretation by experts.

As can be seen in Fig. 1, the proposed methodology combines the ideas of thematic modeling, graph analysis and adaptive control. This interdisciplinary combination allows several tasks to be solved simultaneously, namely to increase the semantic coherence of data by spreading information across the graph and to ensure the verifiability of solutions through interpretable clusters and controllable parameters.

Experimental results

For experimental verification, a corpus of 12418 reports on operational events at nuclear power facilities published in the open database of the U.S. Nuclear Regulatory Commission (NRC) was taken. Each document is a brief textual description of an incident or notification, accompanied by metadata. The texts are short, rich in industry terminology, vary in style, and contain combined event scenarios. Before analysis, standard pre-processing was performed in the form of tokenization, lemmatization, stop word filtering, and very rare terms. In the original sparse feature space, characteristic problems are observed, namely high dimensionality, document matrix sparsity (> 99.5% zeros), and low coherence of thematic groups. K-means cluster analysis yielded an average silhouette of $S \approx 0.32$, indicating weak clusters due to noise and overlapping topics.

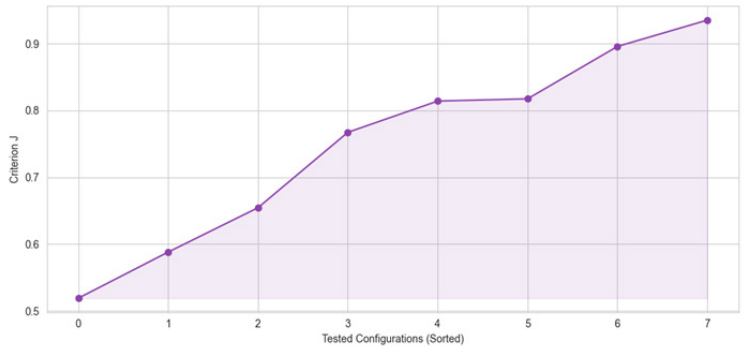

Fig. 2. Trajectory of optimization of the quality functional Q ($J \equiv Q$) when selecting the control action. The maximum is reached at $\alpha = 0.7$, $\beta = 0.5$, $D = 3$

By applying the adaptive regulator described above, we optimized the diffusion parameters on this body. The criterion used was functionality. Q with a threshold $S_0 = 0.3$ and a fine $\mu = 5$, $\nu = 2$. The adjustment trajectory is shown in Fig. 2. It can be seen that the Q quality varies significantly in the parameter space, with a distinct maximum. The optimum is achieved at a depth of $D = 3$, attenuation coefficient $\alpha = 0.7$ and scale $\beta = 0.5$. With smaller α and β, sufficient context enrichment is not achieved (low T), and with larger ones, the silhouette S drops sharply. Thus, contextual regularization is not a rigidly fixed heuristic – its effectiveness depends on the coordination of the diffuser and regulator based on the observed response of the data structure. In our case, the algorithm automatically reached a balance between connectivity and separability, which confirms the operability of the control circuit. For comparison, with arbitrary settings, the coherence increased more strongly, but the silhouette fell to 0.05, making the result practically useless despite the formal improvement in thematic connections.

After applying optimized contextual regularization, we performed thematic modeling of the corpus using the LDA method with the number of topics selected using the 'elbow' method. For each topic, we calculated the UMass coherence metric and the Topic Diversity index (the proportion of unique words in the 10 main terms of the topic). In addition, all documents were clustered using the k-means method into $k = 12$ clusters, and the average silhouette S and intracluster inertia were measured. The results of comparing the original and regularized spaces are shown in Fig. 3.

Regularization resulted in increased thematic coherence. The average UMass increased from –7.41 to –0.88 (the closer to 0, the more coherent the theme). All 12 topics became interpretable after processing. Their top terms form meaningful combinations corresponding to specific types of incidents. For example, one of the topics in the original space had the top words: “reactor, shutdown, scram, inspection, pump, failure” (with a coherence of –6.8). After regularization, its top words became: “reactor, core, fuel, cladding, cooling, temperature” with a coherence of –0.5, clearly reflecting the theme of reactor core cooling. The topic diversity index T increased from 0.47 to 0.83, which means a reduction in the duplication of terms between topics and more complete coverage of various aspects of risk events. This result confirms the achievement of the goal of balancing connectivity and separability. The method significantly enriched the information for thematic analysis without destroying the distinguishable structure of the source data.

The regularized representations of the documents obtained made it possible to construct an interpretable taxonomy of emergency situations based on them. Using hierarchical clustering, we grouped 12 main themes into larger categories – risk archetypes. Four archetypes were identified:

1) equipment failures (equipment, components, cooling systems);
2) organizational errors (personnel, procedures, regulations);
3) external influences (power supply, electricity supply, natural factors);

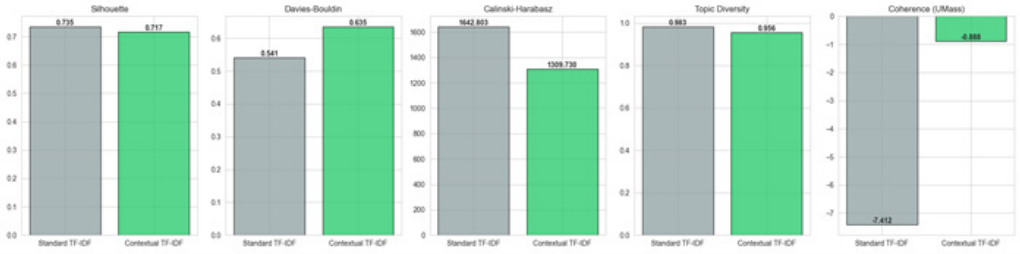

Fig. 3. Comparison of data structure quality metrics before and after contextual regularization of the feature space. The method provides a multiple increase in semantic coherence of topics with virtually unchanged cluster separability

4) nuclear-physical anomalies (reactor, core, radiation).

This taxonomy is consistent with expert models in the industry. More importantly, within each archetype, it was possible to automatically identify key factor characteristics – graph nodes with the highest centrality, corresponding to the root causes of incidents.

Finally, let us note an important practical aspect – interpretability and verification. Unlike machine learning "black boxes," the resulting model is a set of topics and a graph of connections between them that is understandable to an expert. Each new or rare event is automatically positioned in this space as a coordinate. This makes it possible to verify conclusions. Specialists can view the top terms of a topic or the key connections in the graph underlying a particular prediction, and thus trust or challenge the system's decision based on transparent cause-and-effect chains. In our experiments, we integrated the regularized space into a prototype decision support system. When a new message arrives, the system calculates its coordinate and assigns it to one of the known archetypes, then generates a warning indicating the most likely causes and recommended countermeasures associated with that archetype. Thanks to consistency with the original terminology of the documents and preservation of the threat topology, such recommendations are easily interpreted by the operator and can be directly used for proactive risk management.

Discussion

From a practical perspective, the regularized semantic space should be integrated into a closed operational monitoring loop. Incoming reports are processed in near real time. Each report is projected into the risk archetype space. The system then generates an alert with the most probable scenario, the key driving terms, and a recommended response action. Initial archetypes are built on a historical corpus and validated by experts. Later updates are performed on a sliding window with topic drift control and periodic revision of the indicator lexicon. For operators, each alert is presented as a clear link between archetype, factors, and action. The archetype defines the threat type. The factors explain the model decision. The action is selected from a matrix that matches current response procedures. In real deployment, the process should be tracked with KPI metrics such as early warning rate, time to incident confirmation, precision and recall on retrospective data, false alert rate, and the share of reports that require expert relabeling.

Reproducibility is ensured by fixing the full experimental pipeline. This includes unified preprocessing steps such as tokenization, lemmatization, stop word filtering, and rare lemma filtering. It also includes an unchanged PMI graph construction scheme and explicit reporting of regularization settings obtained by optimization. The key values are $\alpha = 0.7$, $\beta = 0.5$, and $D = 3$. The thematic and clustering settings are also fixed, including LDA and k-means with $k = 12$. For transfer to other corpora of weakly structured reports, the algorithmic framework should remain unchanged. Only corpus dependent components should be retrained. These components include the lexicon, thresholds for

rare terms, regularization parameters, and the number of topics. The same objective function should be used, which balances semantic completeness and class separability. Computational cost grows linearly with corpus size and supports document level parallelization. This makes the method suitable for both large archival datasets and streaming data. Transfer stability should be verified by comparing UMass, Topic Diversity, and silhouette scores before and after regularization in the target domain.

The results demonstrate the effectiveness of the contextual regularization approach in addressing the problem of information blindness in the analysis of man-made risks. The method made it possible to extract knowledge from unstructured text flows that previously eluded classical monitoring systems. A significant improvement in thematic coherence with minimal loss of separability confirms that our algorithm successfully restores hidden relationships between incidents without destroying their individual characteristics. In fact, a transition from a "bag of words" to a "knowledge graph" is achieved – texts are transformed into a network model of risk factors, where nodes and connections have a specific physical meaning. This format of representation opens up wide opportunities for integration with existing Probabilistic Risk Assessment (PRA) tools. The risk topology graph can be used to structure knowledge bases, train expert systems, and verify model assumptions. In addition, the approach can be easily generalized to other domains where there are archives of events with descriptions in natural language – from aviation safety to electric power and medicine. The key requirement is the availability of more or less uniform short texts and experts capable of interpreting the selected topics.

Conclusion

This paper presents a comprehensive approach to risk analysis of complex technical systems based on textual data. An original method has been developed for enriching the feature space of short technical texts by recursively propagating context across a co-occurrence graph of terms with adaptive IDF filtering. The method eliminates the effect of data sparsity and overcomes the false independence of descriptions by restoring hidden semantic connections between messages. For the first time, it is proposed to automate the balancing of regularization parameters based on observed structure metrics, which allows achieving optimal informativeness without losing interpretability.

It has been proven that the diffusion enrichment process is limited in nature. With proper attenuation $\alpha < 1$, the total contribution of the context converges, and small variations in probabilistic connections do not cause unlimited growth in feature weights. This guarantees the stability of results when updating data and reduces the risk of overfitting to random noise. It has also been strictly demonstrated that diffusion eliminates the orthogonality of terminologically different but essentially related documents, thereby increasing data connectivity without resorting to external knowledge or ontologies, solely through corpus statistics.

Experiments on real data (NRC reports) demonstrated a multiple increase in thematic modeling quality metrics. UMass coherence increased ~8-fold, topic diversity increased by 76%, with a slight decrease in cluster silhouette. The method identified meaningful thematic groups of incidents and their hierarchy (risk archetypes) consistent with expert opinions. Key risk factors in each archetype were automatically identified – terminological markers around which various event scenarios are grouped. This proved the algorithm's ability to extract new knowledge from text archives that were previously difficult to analyze formally.

The most important advantage of this approach is that it remains interpretable at all stages. Both intermediate and final results (connection graphs, topics, clusters) are understandable to humans and can serve as a basis for management decisions. The method integrates into existing risk analysis systems, complementing them. Regularized features can be fed into classical models for further forecasting, increasing their accuracy by taking text information into account. At the same time, the "transparency" of the source data is not lost, which is especially important for industries where explanations and justifications for any automated conclusion are required.

Thus, the study confirms the hypothesis about the possibility of systematic accounting for weakly structured text data when analyzing the reliability and security of complex systems. The proposed contextual regularization technique forms the missing link between text streams of operational information and formal risk models, creating a unified metric that reflects the latent topology of accident processes. The results obtained can be directly applied to improve accident monitoring and warning tools. From intelligent support systems for process control system dispatchers to analytical modules for regulators. In the future, this direction opens the way to the creation of cognitive safety management systems capable of learning from the textual experience of past incidents and warning of new threats at an early stage of their emergence.

REFERENCES

1. **Rodionov D.G., Konnikov E.A., Mugutdinov R.M.** Sistemnyi analiz konkurentosposobnosti tsifrovogo predpriiatiia v ramkakh informatsionnoi sredy [System analysis of the competitiveness of a digital enterprise within the information environment]. *Economic Sciences*, 2020, Vol. 193, No. 12, Pp. 394–401. DOI: 10.14451/1.193.394

2. **Makarova E.A.** Processing of semi-structured text data for use in data analysis models. *Information and mathematical technologies in science and management*, 2023, Vol. 29, No. 1, Pp. 178–189. DOI: 10.25729/ESI.2023.29.1.015

3. **Salganik M.J.** *Bit by Bit: Social Research in the Digital Age*. Princeton: Princeton University Press, 2017.

4. **Postiglione A., Monteleone M.** Predictive maintenance with linguistic text mining. *Mathematics*, 2024, Vol. 12, No. 7, Art. no. 1089. DOI: 10.3390/math12071089

5. **Boyd R.L., Schwartz H.A.** Natural language analysis and the psychology of verbal behavior: The past, present, and future states of the field. *Journal of Language and Social Psychology*, 2021, Vol. 40, No. 1, Pp. 21–41. DOI: 10.1177/0261927X20967028

6. **Wang Y., Chung S.-H.** Artificial intelligence in safety-critical systems: a systematic review. *Industrial Management & Data Systems*, 2022, Vol. 122, No. 2, Pp. 442–470. DOI: 10.1108/IMDS-07-2021-0419

7. **Ignatow G., Mihalcea R.F.** *Text Mining: A Guidebook for the Social Sciences*. Los Angeles: SAGE Publications, 2017.

8. **Konnikov E.A., Kryzhko D.A.** Two-stage semantic clustering of embeddings as an alternative to LDA for infometric analysis of industry news. *Software Systems and Computational Methods*, 2025, Vol. 3, Pp. 10–19. DOI: 10.7256/2454-0714.2025.3.75348

9. **Macanovic A., Przepiorka W.** A systematic evaluation of text mining methods for short texts: Mapping individuals' internal states from online posts. *Behavior Research Methods*, 2024, Vol. 56, Pp. 2782–2803. DOI: 10.3758/s13428-024-02381-9

10. **Sazonov G.V., Lukyanov K.S., Boyarsky S.K., Makarov I.A.** Is AI interpretability safe: the relationship between interpretability and security of machine learning models. *Proceedings of the Institute for System Programming of the RAS* (*Proceedings of ISP RAS*), 2024, Vol. 36, No. 5, Pp. 127–142. DOI: 10.15514/ISPRAS-2024-36(5)-9

11. **Rodionov D.G., Karpenko P.A., Konnikov E.A.** Metodika kvantifikatsii sostoianiia trudovykh resursov v kontekste upravleniia razvitiem regional'noi sotsial'no-ekonomicheskoi sistemoi [Methodology for quantifying the state of labor resources in the context of managing the development of the regional socio-economic system]. *Economic Sciences*, 2021, Vol. 197, No. 4, Pp. 171–179. DOI: 10.14451/1.197.171

12. **Probierz B., Hrabia A., Kozak J.** A new method for graph-based representation of text in natural language processing. *Electronics*, 2023, Vol. 12, No. 13, Art. no. 2846. DOI: 10.3390/electronics12132846

13. **Krasnov F.V., Baskakova E.N., Smaznevich I.S.** Assessment of the applied quality of topic models for clustering problems. *Tomsk State University Journal of Control and Computer Science*, 2021, No. 56, Pp. 100–111. DOI: 10.17223/19988605/56/11

14. **Irkhin I.A., Bulatov V.G., Vorontsov K.V.** Additive regularization of topic models with fast text vectorization. *Computer Research and Modeling*, 2020, Vol. 12, No. 6, Pp. 1515–1528. DOI: 10.20537/2076-7633-2020-12-6-1515-1528

15. **Li P., Fu X., Chen J., Hu J.** CoGraphNet for enhanced text classification using word-sentence heterogeneous graph representations and improved interpretability. *Scientific Reports*, 2025, Vol. 15, Art. no. 356. DOI: 10.1038/s41598-024-83535-9

16. **Hsu M.-F., Chang C., Zeng J.-H.** Automated text mining process for corporate risk analysis and management. *Risk Management*, 2022, Vol. 24, Pp. 386–419. DOI: 10.1057/s41283-022-00099-6

17. **Gelastopoulos G., Keramydas C.** A systematic review of text mining analytics for supply chain risk management using online data. *Supply Chain Analytics*, 2025, Vol. 12, Art. no. 100167. DOI: 10.1016/j.sca.2025.100167

18. **Troxler A., Schelldorfer J.** Actuarial applications of natural language processing using transformers: Case studies for using text features in an actuarial context. *British Actuarial Journal*, 2024, Vol. 29, Art. no. 4. DOI: 10.1017/S1357321724000023

19. **Murshed B.A.H., Mallappa S., Abawajy J., Saif M.A.N., Al-ariki H.D.E., Abdulwahab H.M.** Short text topic modeling approaches in the context of big data: taxonomy, survey, and analysis. *Artificial Intelligence Review*, 2023, Vol. 56, Pp. 5133–5260. DOI: 10.1007/s10462-022-10254-w

20. **Vashchenko V.A.** Topic modeling for short texts: comparative analysis of algorithms. *Sociology: Methodology, Methods, Mathematical Modeling* (*Sociology: 4M*), 2024, Vol. 56, Pp. 69–112. DOI: 10.19181/4m.2023.32.1.2

21. **Mozaidze E.S.** Topic modeling in the stream of short messages in Russian. *Russian Technological Journal*, 2025, Vol. 13, No. 1, Pp. 38–48. DOI: 10.32362/2500-316X-2025-13-1-38-48

INFORMATION ABOUT AUTHORS / СВЕДЕНИЯ ОБ АВТОРАХ

Viacheslav P. Shkodyrev
Шкодырев Вячеслав Петрович
E-mail: shkodyrev@mail.ru

Evgenii A. Konnikov
Конников Евгений Александрович
E-mail: konnikov.evgeniy@gmail.com

Prohor A. Polyakov
Поляков Прохор Александрович
E-mail: prohor@polyakov-box.ru

Submitted: 25.12.2025; Approved: 24.02.2026; Accepted: 17.03.2026.
Поступила: 25.12.2025; Одобрена: 24.02.2026; Принята: 17.03.2026.

Computing, Telecommunication and Control, 2026, Vol. 19, No. 1, Pp. 91–102.
Информатика, телекоммуникации и управление. 2026. Том 19, № 1. С. 91–102.

Research article
DOI: https://doi.org/10.18721/JCSTCS.19109
UDC 004.91:005.334

METHOD FOR CLASSIFYING RISK INCIDENTS BASED ON SELF-ORGANIZATION OF SEMANTIC CLUSTERS

V.P. Shkodyrev, D.G. Rodionov, E.A. Konnikov ✉

Peter the Great St. Petersburg Polytechnic University,
St. Petersburg, Russian Federation

✉ konnikov.evgeniy@gmail.com

Abstract. A method for automatic classification of textual descriptions of emergency risk incidents based on self-organizing semantic clustering is presented, which does not require prior data labeling. Unlike traditional approaches, the method involves a two-stage scheme, which consists of self-organization of a latent taxonomy of incidents through hierarchical thematic decomposition of the text corpus, as well as continuous classification of new messages according to their degree of belonging to all automatically selected classes at once. This transition from rigid assignment to a single class to fuzzy membership allows hybrid incidents to be decomposed into several risk factors, reflecting their mixed nature. The developed algorithm forms an interpretable and stable taxonomy of incidents that preserves the structural isolation of clusters even with a high proportion of hybrid events. Testing on the NRC data corpus showed that most messages have a dominant risk factor with significant secondary components. The average semantic consistency of clusters was ~0.62 (cosine measure), and the classification confidence is distributed around the mean, reflecting the presence of both pure and mixed incidents. The results confirm that the proposed method provides a mathematically correct decomposition of complex situations into a set of risk factors and reduces the sensitivity of classification to noise and inaccuracies in the input text. The methodology is focused on proactive risk analysis in complex technical systems and can be used for automated decision support in industrial safety systems.

Keywords: risk incidents, unstructured data, semantic analysis, thematic modeling, clustering, fuzzy classification, risk taxonomy

Acknowledgements: The research was financially supported by the Ministry of Science and Higher Education of the Russian Federation within the framework of the state assignment "Development of methodology for the formation of a tool base for analysis and modeling of spatial socio-economic development of systems in the conditions of digitalization with reliance on internal reserves" (FSEG-2023-0008).

Citation: Shkodyrev V.P., Rodionov D.G., Konnikov E.A. Method for classifying risk incidents based on self-organization of semantic clusters. Computing, Telecommunications and Control, 2026, Vol. 19, No. 1, Pp. 91–102. DOI: 10.18721/JCSTCS.19109

Научная статья
DOI: https://doi.org/10.18721/JCSTCS.19109
УДК 004.91:005.334

МЕТОД КЛАССИФИКАЦИИ РИСК-ИНЦИДЕНТОВ НА ОСНОВЕ САМООРГАНИЗАЦИИ СЕМАНТИЧЕСКИХ КЛАСТЕРОВ

В.П. Шкодырев, Д.Г. Родионов, Е.А. Конников ✉

Санкт-Петербургский политехнический университет Петра Великого,
Санкт-Петербург, Российская Федерация

✉ konnikov.evgeniy@gmail.com

Аннотация. Представлен метод автоматической классификации текстовых описаний аварийных риск-инцидентов на основе самоорганизующейся семантической кластеризации, не требующий априорной разметки данных. В отличие от традиционных подходов, метод предполагает двухэтапную схему, которая заключается в самоорганизации латентной таксономии инцидентов посредством иерархического тематического разложения текстового корпуса, а также непрерывной классификации новых сообщений по степени принадлежности ко всем автоматически выделенным классам сразу. Такой переход от жесткого присваивания одного класса к нечеткой принадлежности позволяет декомпозировать гибридные инциденты на несколько факторов риска, отражая их смешанную природу. Разработанный алгоритм формирует интерпретируемую и устойчивую таксономию инцидентов, сохраняющую структурную обособленность кластеров даже при высокой доле гибридных событий. В рамках апробации на корпусе данных NRC показано, что большинство сообщений имеют доминирующий фактор риска при наличии значимых вторичных компонентов. Средняя семантическая согласованность кластеров составила ~0.62 (косинусная мера), а уверенность классификации распределена вокруг среднего значения, отражая наличие как чистых, так и смешанных инцидентов. Результаты подтверждают, что предложенный метод обеспечивает математически корректную декомпозицию сложных ситуаций на совокупность факторов риска и снижает чувствительность классификации к шуму и неточностям входного текста. Методология ориентирована на проактивный анализ риска в сложных технических системах и может применяться для автоматизированной поддержки принятия решений в рамках систем промышленной безопасности.

Ключевые слова: риск-инциденты, неструктурированные данные, семантический анализ, тематическое моделирование, кластеризация, нечеткая классификация, таксономия рисков

Финансирование: Исследование выполнено при финансовой поддержке Министерства науки и высшего образования Российской Федерации в рамках государственного задания «Разработка методологии формирования инструментальной базы анализа и моделирования пространственного социально-экономического развития систем в условиях цифровизации с опорой на внутренние резервы» (FSEG-2023-0008).

Для цитирования: Shkodyrev V.P., Rodionov D.G., Konnikov E.A. Method for classifying risk incidents based on self-organization of semantic clusters // Computing, Telecommunications and Control. 2026. Т. 19, № 1. С. 91–102. DOI: 10.18721/JCSTCS.19109

Introduction

Ensuring industrial safety of complex technical systems requires systematic accounting of diverse operational information, including text reports on incidents and accidents. Analysis of such weakly structured data allows extracting hidden patterns of accidents and identifying risk factors for taking preventive measures. Traditional methods of probabilistic risk and reliability analysis rely on failure and event statistics presented in a strictly structured form [1, 2]. Classical models are difficult to apply

directly to text descriptions that do not contain formalized markup of the causes and consequences of accidents. In real operating logs, a single incident report often combines several aspects: the cause, development, and outcome of the event. Rigidly assigning such a report to a single category leads to a loss of information about the mixed nature of the incident and artificially inflates the number of classes.

The problem of automated interpretation of weakly structured data in the security management loop is interdisciplinary in nature, combining information theory, cybernetics, linguistics, and reliability theory. The foundations of the infometric approach – the study of statistical patterns in information flows (messages) in complex systems – were laid as early as the mid-20th century. C. Shannon introduced quantitative measures of information and uncertainty, laying the foundation for communication theory [3]. N. Wiener and his followers developed a cybernetic approach to management and communication in technology and organisms [4]. The laws of information distribution were empirically discovered, in particular Zipf's and Lotka's laws, which describe the frequency distribution of terms and messages [5]. These classic works showed that even unstructured data contains hidden statistical structures.

The current stage is characterized by rapid development of natural language processing (NLP) and machine learning methods, which opens up new opportunities for analyzing text data in the field of industrial safety. Most known studies focus on the automatic classification of reports according to predetermined categories or risk attributes. For example, models based on image recognition methods and deep neural networks have been proposed, trained to assign incident descriptions to one of several fixed classes [6–8]. The practical application of such approaches has been demonstrated using data from the construction industry and other fields [9–11]. However, experts note that simple categorization is insufficient for a complete understanding of the causes and trends of accidents. A classifier that assigns a single label to a report does not reveal the internal relationships between risk factors and does not reflect the "hybrid" nature of incidents involving multiple cause-and-effect components.

An alternative to rigid classification is semantic text analysis, in which hidden topics or features are automatically extracted from the corpus. Classic methods here are latent semantic analysis and probabilistic topic modeling (Latent Dirichlet Allocation, LDA) [12]. Topical modeling has been successfully used to identify common accident and incident scenarios without manual annotation [13]. For example, in [14], the BERTopic thematic model (based on BERT contextual embeddings) was used to automatically identify key themes and trends in occupational injuries from 22623 OSHA reports. This approach made it possible to detect hidden accident scenarios and predisposing factors that were difficult to identify using keyword methods. The advantage of thematic models is their ability to analyze large amounts of text data and dynamically update the taxonomy as new information becomes available. However, this approach also has limitations. First, standard algorithms such as LDA do not work well on short technical records due to data sparsity. Second, many modern deep models are "black boxes" – they improve the metric representation of text but lose transparency and interpretability, which is unacceptable for critical system security tasks. In addition, topics obtained automatically do not have unambiguous names, requiring expert interpretation. Accordingly, thematic analysis of incident data must be supplemented with structuring and decomposition steps so that the extracted topics acquire the meaning of risk factors and can be used in assessing and mitigating that risk.

A separate area is related to the ontological approach and semantic-categorical analysis of texts based on specified thesauri. Systems have been created where expert-developed hazard ontologies are used to tag incident reports before they are analyzed [15]. Such solutions allow for highly accurate interpretation, but require a lot of effort to maintain the knowledge base and do not scale well to new types of threats. In dynamically changing operating conditions, this makes it difficult to use ontological systems for accident prediction. Thus, there is a contradiction. On the one hand, loosely structured text information needs to be taken into account to improve proactive risk management; on

the other hand, there is no single set of methods capable of automatically converting raw text into a metric space of threats while preserving their structure, causal relationships, and the ability to interpretably track changes in risk.

In recent years, there has been an increasing number of studies devoted to the analysis of unstructured accident descriptions using NLP. Most of them address the task of classifying incidents by type or factor, which is similar to our approach. For example, one study proposes an approach based on gradient boosting and text processing methods for the automatic classification of construction accident records into predefined risk categories [16]. Another study developed a comprehensive machine learning framework for extracting hazardous factors from report texts and analyzing their trends over time [17]. OSHA reports were processed using classification and clustering methods, which made it possible to identify the growth of certain risks and vulnerable groups of workers. In other areas, various authors have applied the GPT-4 model (large language model) to automatically categorize textual descriptions of risks in construction [18–20]. It has been shown that modern Large Language Models (LLMs) are capable of achieving accuracy comparable to classical algorithms on structured features. However, LLM models require careful prompt engineering, their output is difficult to verify, and the use of commercial APIs in critical systems is undesirable for data security reasons. In addition, all of the above approaches involve discrete classification – assigning a single class to each message. This approach does not reflect the full scope of information if the incident is of a mixed nature.

Against this backdrop, an uncontrolled multi-class division of incident space with the possibility of soft, diverse classification of each event looks promising. Thematic modeling approaches indicate that such a taxonomy can self-organize directly from the data, without pre-assigning classes. The question of structuring the obtained themes into risk factors and classifying new messages according to all factors at once remains open. In our work, we have attempted to solve this problem. At the first stage, a method of contextual regularization of the feature space was developed, which eliminates the effect of sparsity and increases the connectivity of the semantic space of documents. Heterogeneous messages became geometrically comparable, forming the basis for the selection of taxonomy. Next, a scenario-optimization method for semantic processing of accident data was proposed, which allows ranking risks in the text according to the degree of controllability [21]. Nevertheless, these solutions left the problem of systematic classification of incidents unresolved. It is necessary to combine the identified latent themes into a stable taxonomy and describe each message with a profile of its belonging to this structure.

The goal of this work is to develop a teacherless risk incident classification method that allows for the automatic construction of a hierarchical semantic taxonomy of emergency situations and the fuzzy classification of each incident across a set of selected classes. The scientific novelty of the method lies in the transition from traditional discrete classification logic to continuous assessment of the degree to which an event belongs to all potential classes simultaneously. This ensures the correct decomposition of complex, combined incidents into constituent risk factors and reduces the sensitivity of classification to local changes in the message text.

Methods

The proposed method treats the classification task as a two-stage process, which is represented in the block diagram below. In the first stage, a taxonomy – a set of semantic classes without markup – is automatically self-organized from the corpus of incident descriptions. This is achieved through hierarchical thematic modeling of the latent feature space. In the second stage, new events are continuously marked up relative to the resulting taxonomy – each message is assigned not one tag, but a vector of memberships across all classes at once.

Let there be a corpus of N documents (incident descriptions) represented as non-negative feature vectors $x_d \in R^M$ dimension M. All documents form a matrix of characteristics $X = [x_{dm}] \in R^{N \times M}$.

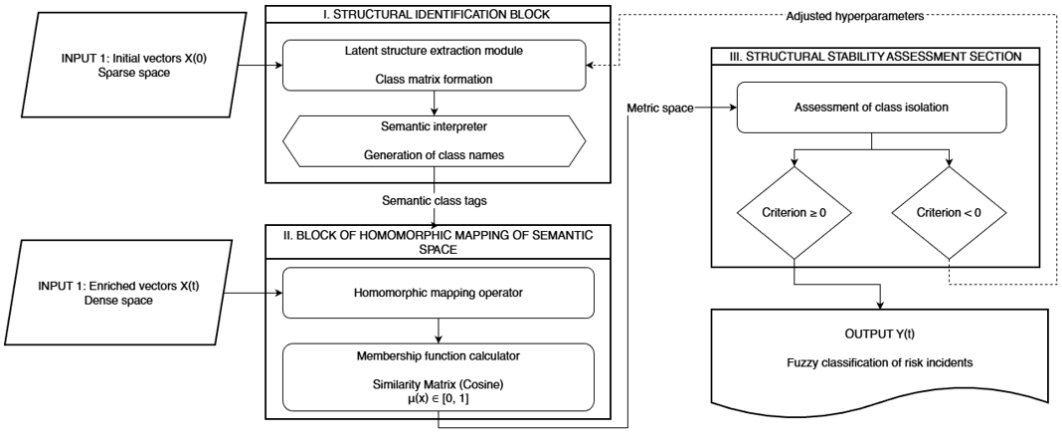

Fig. 1. Method for classifying risk incidents based on self-organization of semantic clusters and soft labeling

To build a semantic taxonomy, the number of large thematic clusters is specified at the top level K. A probabilistic model of thematic decomposition is applied, resulting in the calculation of a matrix of document distribution by topic $\Theta = \left[\theta_{dk}\right] \in R^{N \times K}$, where $\theta_{dk} = P\left(z = k \middle| d\right)$ – posterior probability (weight) of topic k in document d, matrix of topic profiles $B = \left[\beta_{km}\right] \in R^{K \times M}$, where $\beta_{km} = P\left(w = m \middle| z = k\right)$ – probabilities of terms in the topic. Thus, at the first level, each document is characterized by a vector $\theta_d = \left(\theta_{d1}, \ldots, \theta_{dK}\right)$. To fix the discrete taxonomy, we perform a strict assignment of the document to one of the upper classes according to the Maximum A Posteriori (MAP) rule:

$$c_1\left(d\right) = \arg\max_{1 \le k \le K} \theta_{dk}.$$

In other words, the document relates to the topic that carries the most weight θ_{dk}. After that, subtopics are locally identified within each obtained top cluster k. For each k the number of subclusters is specified L, and by subset of documents $d : c_1\left(d\right) = k$ a thematic model with L themes is being built again. Thus, local distributions are formed $\Theta^{(k)} = \left[\theta^{(k)} dj\right]$ and profile matrices $B^{(k)} = \left[\beta^{(k)}\right]$ for $j = 1 \ldots L$ inside class k. Document d, related to the top topic k, at the second level is characterized by the vector $\theta_d^{(k)} = \left(\theta_{d1}^{(k)}, \ldots, \theta_{dL}^{(k)}\right)$ by subtopics of this topic. Applying a similar MAP rule, we fix the sheet cluster:

$$c_2\left(d\right) = \arg\max_{1 \le j \le L} \theta_{dj}^{(k)}, \quad k = c_1\left(d\right).$$

The pair (k, j) defines the final leaf cluster of the taxonomy: $C_{k,j} = d : c_1\left(d\right) = k,\ c_2\left(d\right) = j$. Thus, taxonomy $\mathcal{C} = C_{k,j}$ is extracted from the data structure rather than from predefined expert classes. Each cluster $C_{k,j}$ corresponds to a certain set of incidents that are similar in meaning, selected automatically.

In the next step of the developed method, discrete taxonomy is transformed into a continuous classification model. The idea is not to limit oneself to a single label $C_{k,j}$ to the document, but to calculate the degrees of belonging of the document to all clusters at once. To do this, each cluster is assigned a short semantic name $l_{k,j}$. The set of all tags forms a set $L = l_{k,j}$ in size $K! \times !L$. Then, a common metric space of features is constructed, in which documents and cluster labels are represented as

embedding vectors of unit length. For this purpose, one can use, for example, normalized vectors of rows of matrix X after contextual regularization. They contain distributed semantic representations of documents. Labels $l_{k,j}$ can be represented in the same vector space, for example, by their characteristic words. Let us denote by u_d the normalized vector of document d, and through u_l – normalized label vector $l \in L$. Then, naturally, a fuzzy membership matrix is introduced $F = [f_{d,l}]$ dimensions $N \times |L|$, whose elements are calculated as the cosine similarity between the document and the cluster label:

$$f_{d,l} = \cos(u_d, u_l) \in [0,1].$$

Each row of the matrix F, $f_d = \left(f_{d,1}, \ldots, f_{d,|L|}\right)$, is a continuous profile of document d's membership in all taxonomy classes simultaneously. If necessary, this profile can be interpreted probabilistically by performing normalization. Let us introduce a normalized measure:

$$p_{d,l} = \frac{\left(f_{d,l}\right)^{\lambda}}{\sum_{l' \in L}\left(f_{d,l'}\right)^{\lambda}},$$

where $\lambda > 0$ is the parameter that controls the "stiffness" of the distribution. The resulting vector $p_d = \left(p_{d,l}\right) l \in L$ is a generalized (fuzzy) classification of incident d. If the text contains several independent semantic components, their corresponding values p will be relatively large, and the document will be described by a mixture of classes rather than a single label.

The transition from a discrete label to a membership vector is fundamentally important not only conceptually, but also mathematically. Function $f_{d,l}$ proves to be resistant to minor disturbances in the semantic representation of the document. Indeed, consider a fixed cluster l and two documents i and j. For the difference between their attributes, the following inequality holds true:

$$\left|f_{i,l} - f_{j,l}\right| = \left|\cos(u_i, u_l) - \cos(u_j, u_l)\right| \le \left|u_i - u_j\right|.$$

Since the vectors are normalized, a small change in the text results in a small change in the embedding u_i. This leads only to a slight change in the overall profile. f_i, whereas classical discrete classification could change the label abruptly. Thus, the transition from single labels to continuous membership scores not only enables multi-class decomposition, but also reduces the model's sensitivity to noise, which is inevitable in text data. This is particularly relevant for technical journals, where incident descriptions may contain inaccuracies and variable wording.

Results

The developed method was tested on a corpus of U.S. Nuclear Regulatory Commission (NRC) reports on operational events at nuclear power plants. $N = 10000$ text records were used, covering a wide range of incidents, from equipment failures to human errors and natural phenomena. A standard NLP pipeline was used to convert the texts into matrix form X: cleaning, tokenization, lemmatization of terms, and TF–IDF weighting. Next, contextual regularization of matrix X was performed, namely, the construction of a graph of joint term co-occurrence followed by diffusion reordering of features. As a result, the feature space dimension was $M \approx 5000$, and the semantic coherence of the data increased significantly. The taxonomy parameters were selected structurally. $K = 5$ top-level topics and $L = 3$ subtopics were set for each, resulting in $K \times L = 15$ final clusters. These values are consistent with expert opinion – the corpus is expected to contain about a dozen broad categories of incidents.

The figure below shows the distribution of classification confidence values $\xi_d = \max_{l \in L} p_{d,l}$ according to all documents. The amount ξ_d reflects how clearly the incident is associated with a single

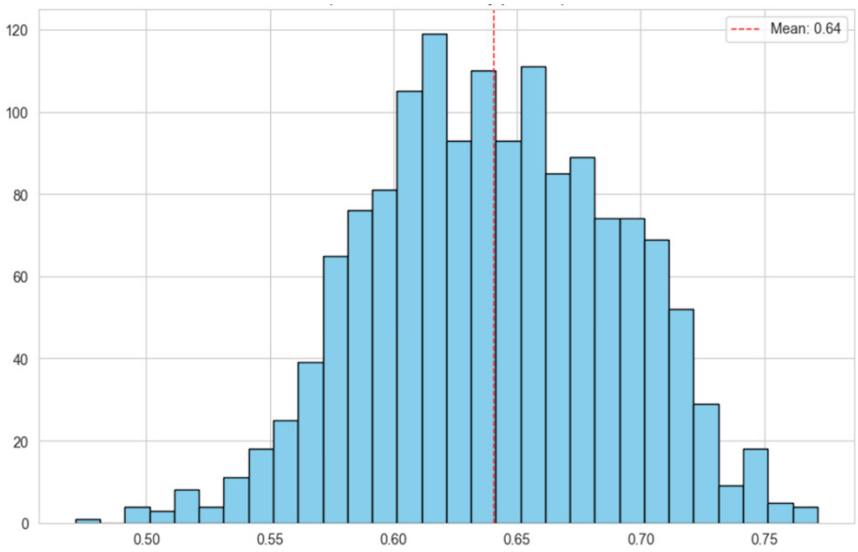

Fig. 2. Distribution of soft classification confidence

category in the model. When $\xi_d = 1$ the document strictly belongs to one cluster, with smaller ξ_d several classes have comparable weights. The histogram shows the concentration of values around the mean $\overline{\xi} \approx 0.64$. This means that for most events, the model identifies a pronounced dominant risk component, but there is still room for hybridization. The "tails" of the distribution correspond to cases where two or more labels receive similar values $p_{d,l}$ – it is precisely these entries that can be interpreted as mixed incidents requiring special attention from analysts.

Next, the consistency of each semantic tag is calculated. At the same time, the size of each cluster is estimated $|C_{k,j}|$. The figure below shows the relationship between cluster sizes and their average semantic consistency. It can be seen that the resulting clusters vary greatly in size, which is natural for real operational data. Some incidents are routine events and occur frequently, while others are rare emergencies. Nevertheless, it is important to emphasize that the semantic consistency of the clusters remains at a sufficiently high level for all groups. This indicates that the selected taxonomy reflects objectively similar incident patterns and is not a random division. In other words, even small classes have semantic unity, which is extremely important for practical interpretation – such clusters correspond to specific but stable risk factors.

The resulting taxonomy of 15 classes can be interpreted as a hierarchy of risk incident categories. For clarity, here is a brief list of the semantic classes identified (the names assigned are based on an analysis of the top terms in each cluster):

- Inoperable System Performance Issues;
- Part 21 Reporting Issues;
- Generator Trip and Isolation;
- Plant Systems Maintenance & Response;
- Nuclear Regulatory Notifications;
- Nuclear Event Notifications;
- Fire Incident Notification;
- Hurricane-Related Plant Events;
- Seismic Event Response;
- Unusual Facility Atmosphere Events;
- Y-90 Treatment Dose Issues;
- Radiography Equipment Issues;

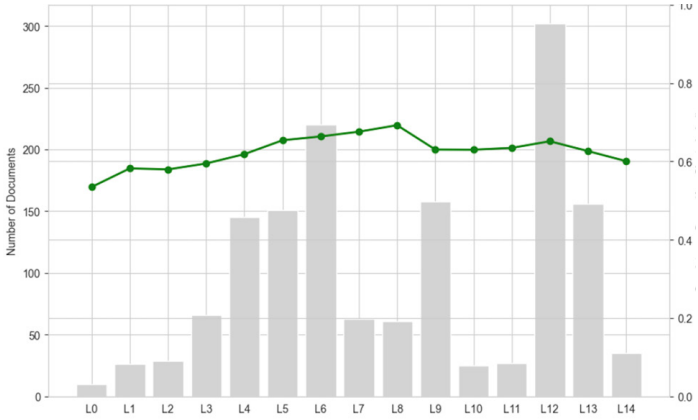

Fig. 3. Cluster sizes and their semantic consistency

- Lost Radioactive Gauge Reports;
- Radioactive Shipment Contamination;
- Missing or Lost Equipment.

This list reflects a cross-section of the latent structure of the corpus obtained by self-organization. It is crucial that the categories were not predetermined but emerged from the data. For example, the Hurricane-Related Events cluster grouped all messages related to hurricanes, even though they were not marked with a special tag in the original reports. Similarly, separate classes were formed around specific procedures (Part 21) or problems (loss of sensors), demonstrating the method's ability to detect implicit thematic associations in log entries.

The proposed method does not assume the existence of "correct" markup, so traditional metrics of accuracy and completeness are not directly applicable. Instead, the quality and usefulness of the resulting classification were evaluated according to three criteria: confidence distribution structure ξ_d, semantic consistency of clusters and topological isolation of clusters in feature space. The latter criterion quantitatively characterizes how geometrically separated clusters are and is calculated using the silhouette coefficient S:

$$S = \frac{b - a}{\max(a, b)},$$

where a is the average distance (1 – cosine proximity) between documents within a single cluster, b is the the smallest average distance from the documents in a given cluster to the documents in a neighboring cluster. In our experiment, we obtained the value $S \approx 0.02$, that is, formally $S > 0$. The small positive value of the silhouette is explained by the presence of many hybrid messages that create "bridges" between clusters and reduce intercluster distances. Nevertheless, $S > 0$ means non-zero isolation of the structure – the taxonomy has a certain stability despite the complexity of the data. It is important to note that discrete classification with this type of data would be methodologically incorrect. Many documents lie on the boundaries of classes and contain characteristics of several groups at the same time. That is why soft classification here is not a side effect, but a necessary way of describing reality. It recognizes the multi-causal nature of incidents and reflects it quantitatively.

It has been experimentally confirmed that the proposed method successfully solves the task of classifying risk incidents without a teacher. An interpretable taxonomy of 15 semantic categories is formed, and the classification confidence has a stable structure. The semantic consistency of clusters is maintained at a practical level of ~0.6, the cluster separation criterion S is positive, which indicates

non-zero structural stability of the obtained taxonomy even with a significant proportion of hybrid events.

Discussion

The results obtained demonstrate the high effectiveness of the self-organizing risk incident classification method for analyzing large arrays of operational data. In traditional safety monitoring systems, each event is recorded under a single category, such as “operator error”, “equipment failure”, or “natural impact”. This simplification can lead to an underestimation of complex situations where several factors act together [22]. The proposed method allows, for the first time, an incident to be described by a set of risk factors with a quantitative assessment of each factor's contribution. The hybrid characterization of an incident provides more complete information for subsequent risk analysis. It is also consistent with the principles of Learning from Incidents (LFI) methodologies, which emphasize the need to consider the combination of causes and conditions of accidents [23]. Our method automates the multifactorial analysis of each case, which previously could only be achieved through labor-intensive expert analysis.

In practical deployment, the membership vector should be used as an operational risk profile for each incoming report. The largest component identifies the dominant factor, while the next components show secondary drivers that may escalate the event. A warning can be generated when the dominant score is at least 0.60 or when the sum of the two largest scores is at least 0.80, because this pattern indicates either a strong single threat or a stable hybrid case. Analysts can rank reports by these scores to prioritize response actions and investigation depth. Hybrid profiles are especially useful for root cause analysis, since they reveal interacting mechanisms such as equipment issues combined with procedural deviation. The same profiles support preventive planning, because recurring factor combinations can be tracked over time and mapped to targeted mitigation measures.

Unlike the “black boxes” of deep neural network models, the cluster-thematic taxonomy obtained by our method is interpretable by humans. Each class corresponds to an understandable semantic label (name), and the coefficients $p_{d,l}$ can be interpreted as the degree of influence of the relevant factors on the event d. This opens up the possibility of model validation by security experts. Moreover, the matrix $F = f_{d,l}$ can be considered as a normalized factor profile of incidents. Essentially, the method solves the problem of automatically forming a knowledge base about latent risk factors and their manifestations in real events. This result is directly relevant for proactive risk management – it allows you to build “threat maps” that show which combinations of factors occur most often and how they are interrelated. Similar ideas are embedded in ontological risk analysis systems, but there the factors are set manually. Here, they are extracted from the data, which confirms the thesis about the possibility of self-organization of the semantic structure of threats without a teacher.

Semantic class labels should be formed from the most representative terms of each leaf cluster and then embedded in the same normalized vector space as documents. A robust label can be built from top weighted terms that pass frequency and exclusivity filters, followed by expert screening to remove ambiguous tokens. To keep names stable after corpus updates, the previous label vector should be retained as an anchor and updated only when cosine similarity between old and new prototypes drops below a fixed threshold, for example 0.85. This rule prevents unnecessary renaming and preserves continuity of monitoring dashboards. The quality of label representation can be checked by measuring the gap between in cluster and out of cluster similarity to the label vector. Better label vectors improve the membership matrix because they increase contrast between dominant and secondary factors without forcing hard assignment.

Conclusion

The paper solves the problem of classifying risk incidents in the absence of prior labeling by means of self-organization of semantic clusters and soft classification of events according to them. A method

for constructing a taxonomy of risk events directly from a text corpus has been developed. The taxonomy is a hierarchical structure of classes (topics and subtopics) identified without a teacher based on latent semantic analysis of data.

An approach to fuzzy classification of incidents is proposed, in which each message is assigned a vector of degrees of membership to all classes of the taxonomy. It is shown that such a continuous profile is resistant to minor text distortions and adequately reflects cases of hybrid incidents.

The interpretability and practical significance of the method has been experimentally confirmed using 10000 reports of events at nuclear power plants. An interpretable taxonomy of 15 categories has been constructed, which is consistent with expert opinions and complements them by identifying new combinations of factors. It has been shown that soft classification allows complex incidents to be broken down into several risk factors, which expands the information base for proactive risk management. This approach surpasses traditional single-class classification in terms of informativeness and flexibility.

Quality analysis was performed: semantic clusters have an average consistency of ~0.6, and the silhouette coefficient $S > 0$ confirms the preservation of the topological structure of clusters even with multiple intersections. This means that the selected classes are not random and can serve as a reliable basis for further monitoring and forecasting.

The method is fully automated and does not require labor-intensive data preparation. This is important for practical implementation in security monitoring systems, where the volume of unstructured data is constantly growing. The proposed algorithm can be integrated into problem-oriented decision support systems for filtering incident streams, early identification of dangerous trends, and developing risk management recommendations [24].

REFERENCES

1. **Makhutov N.A., Zatsarinny V.V., Algin V.B., Ishin N.N.** Technogenic risk, reliability and diagnostics of technical systems: approaches, models, methods. *Mechanics of Machines, Mechanisms and Materials*, 2012, Vol. 20–21, No. 3–4, Pp. 67–85.

2. **Riabinin I.A., Cherkesov G.N.** *Logiko-veroiatnostnye metody issledovaniia nadezhnosti strukturno-slozhnykh system* [*Logical and probabilistic methods for studying the reliability of structurally complex systems*]. Moscow: Radio i sviaz', 1981.

3. **Shannon C.E.** A Mathematical Theory of Communication. *The Bell System Technical Journal*, 1948, Vol. 27, pp. 379–423, 623–656.

4. **Wiener N.** *Cybernetics – Or Control and Communication in the Animal and the Machine*. Cambridge, MA: MIT Press, 1961.

5. **Zipf G.K.** *Human Behavior and the Principle of Least Effort: An Introduction to Human Ecology*. Cambridge, MA: Addison-Wesley Press, 1949.

6. **Zhang J., Zi L., Hou Y., Deng D., Jiang W., Wang M.** A C-BiLSTM Approach to Classify Construction Accident Reports. *Applied Sciences*, 2020, Vol. 10, No. 17, Art. no. 5754. DOI: 10.3390/app10175754

7. **Chen Z., Huang K., Wu L., Zhong Z., Jiao Z.** Relational Graph Convolutional Network for Text-Mining-Based Accident Causal Classification. *Applied Sciences*, 2022, Vol. 12, No. 5, Art. no. 2482. DOI: 10.3390/app12052482

8. **Zeng W., Tang W., Yuan D., Zhang H., Duan P., Hu S.** Structure-Aware and Format-Enhanced Transformer for Accident Report Modeling. *Applied Sciences*, 2025, Vol. 15, No. 14, Art. no. 7928. DOI: 10.3390/app15147928

9. **Kim J.-M., Lim K.-K., Yum S.-G., Son S.** A Deep Learning Model Development to Predict Safety Accidents for Sustainable Construction: A Case Study of Fall Accidents in South Korea. *Sustainability*, 2022, Vol. 14, No. 3, Art. no. 1583. DOI: 10.3390/su14031583

10. **Xu H., Liu Y., Shu C.-M., Bai M., Motalifu M., He Z., Wu S., Zhou P., Li B.** Cause analysis of hot work accidents based on text mining and deep learning. *Journal of Loss Prevention in the Process Industries*, 2022, Vol. 76, Art. no. 104747. DOI: 10.1016/j.jlp.2022.104747

11. **Li J., Wu C.** Deep Learning and Text Mining: Classifying and Extracting Key Information from Construction Accident Narratives. *Applied Sciences*, 2023, Vol. 13, No. 19, Art. no. 10599. DOI: 10.3390/app131910599

12. **Qiang J., Qian Z., Li Y., Yuan Y., Wu X.** Short Text Topic Modeling Techniques, Applications, and Performance: A Survey. *IEEE Transactions on Knowledge and Data Engineering*, 2022, Vol. 34, No. 2, Pp. 1427–1445. DOI: 10.1109/TKDE.2020.2992485

13. **Wang Y., Zou P.X.W.** Decoding Construction Accident Causality: A Decade of Textual Reports Analyzed. *Buildings*, 2025, Vol. 15, No. 21, Art. no. 3859. DOI: 10.3390/buildings15213859

14. **Cao Y., Qu Z., Wu S., Chen Y., Skitmore M., Ma X., Wang J.** Analyzing OSHA Construction Accident Reports Using BERTopic Topic Modeling for Thematic Insights. *Buildings*, 2026, Vol. 16, No. 1, Art. no. 10. DOI: 10.3390/buildings16010010

15. **Markarian A.O., Meshcheryakov D.A., Gordeev G.Ya.** Structure and algorithm of the semantic analysis system for text data in the investigation of accidents and incidents at industrial facilities. *Legal Informatics*, 2025, Vol. 3, Pp. 57–68. DOI: 10.24412/1994-1404-2025-3-00-06

16. **Shrestha S., Morshed S.A., Pradhananga N., Lv X.** Leveraging Accident Investigation Reports as Leading Indicators of Construction Safety Using Text Classification. *ASCE Construction Research Congress* (*CRC*), 2020, Pp. 490–498. DOI: 10.1061/9780784482872.053

17. **Andrade S.R., Walsh H.S.** Machine learning framework for Hazard Extraction and Analysis of Trends (HEAT) in wildfire response. *Safety Science*, 2023, Vol. 167, Art. no. 106252. DOI: 10.1016/j.ssci.2023.106252

18. **Erfani A., Khanjar H.** Large Language Models for Construction Risk Classification: A Comparative Study. *Buildings*, 2025, Vol. 15, No. 18, Art. no. 3379. DOI: 10.3390/buildings15183379

19. **Zhang L., Hou Y., Ren F.** AIR Agent: A GPT-Based Subway Construction Accident Investigation Report Analysis Chatbot. *Buildings*, 2025, Vol. 15, No. 4, Art. no. 527. DOI: 10.3390/buildings15040527

20. **Du G., Chen A.** Coal Mine Accident Risk Analysis with Large Language Models and Bayesian Networks. *Sustainability*, 2025, Vol. 17, No. 5, Art. No. 1896. DOI: 10.3390/su17051896

21. **Rodionov D.G., Polyakov P.A., Yakob P.A., Konnikov E.A.** A scenario-optimisation method for semantic processing of textual data on accidental incidents at industrial enterprises. *Soft Measurement and Computing*, 2025, Vol. 95, No. 10, Pp. 117–129. DOI: 10.36871/2618-9976.2025.10.009

22. **Woźniak Z., Hoła B.** Analysing Near-Miss Incidents in Construction: A Systematic Literature Review. *Applied Sciences*, 2024, Vol. 14, No. 16, Art. no. 7260. DOI: 10.3390/app14167260

23. **Guan J., Xu Y., Chan A.P.C., Choi T., Yang Y.** Factors affecting learning from incidents: A cross-industry review. *Journal of Loss Prevention in the Process Industries*, 2024, Vol. 89, Art. no. 105297. DOI: 10.1016/j.jlp.2024.105297

24. **Suh Y.** Identifying Safety Technology Opportunities to Mitigate Safety-Related Issues on Construction Sites. *Buildings*, 2025, Vol. 15, No. 6, Art. no. 847. DOI: 10.3390/buildings15060847

INFORMATION ABOUT AUTHORS / СВЕДЕНИЯ ОБ АВТОРАХ

Viacheslav P. Shkodyrev
Шкодырев Вячеслав Петрович
E-mail: shkodyrev@mail.ru

Dmitry G. Rodionov
Родионов Дмитрий Григорьевич
E-mail: drodionov@spbstu.ru
ORCID: https://orcid.org/0000-0002-1254-0464

Evgenii A. Konnikov
Конников Евгений Александрович
E-mail: konnikov.evgeniy@gmail.com
ORCID: https://orcid.org/0000-0002-4685-8569

Submitted: 26.12.2025; Approved: 13.03.2026; Accepted: 17.03.2026.
Поступила: 26.12.2025; Одобрена: 13.03.2026; Принята: 17.03.2026.

Computing, Telecommunication and Control, 2026, Vol. 19, No. 1, Pp. 103–115.
Информатика, телекоммуникации и управление. 2026. Том 19, № 1. С. 103–115.

Research article
DOI: https://doi.org/10.18721/JCSTCS.19110
UDC 622.271:621.31:004.8

MONITORING AND DIAGNOSTICS OF ELECTROMECHANICAL SYSTEMS BASED ON MACHINE LEARNING

Yu.N. Kozhubaev ✉

Peter the Great St. Petersburg Polytechnic University,
St. Petersburg, Russian Federation

✉ um-urii@mail.ru

Abstract. Induction motors, widely used in electromechanical equipment of mining enterprises, are susceptible to failure due to frequent starts, overloads, and wear, leading to accidents and economic losses. Induction motors are one of the main sources of kinetic energy in industry and agriculture. Motor failure leads to shutdown of the technological process and reduced efficiency, requiring regular monitoring. Traditional diagnostic methods based on the analysis of individual signals and classic machine learning with manual feature selection are insufficiently reliable under variable operating conditions and are highly susceptible to human factor. This paper proposes an approach to diagnosing induction motor faults based on a deep residual network using signal analysis, deep and transfer learning, and information fusion. Various three-phase current input strategies are implemented, and a model capable of automatically extracting informative deep features from the current signal is constructed. The experimental results confirm that the proposed deep learning-based model provides higher diagnostic accuracy compared to traditional machine learning algorithms.

Keywords: motor fault diagnosis, deep residual network, information fusion theory, machine learning, induction motors

Citation: Kozhubaev Yu.N. Monitoring and diagnostics of electromechanical systems based on machine learning. Computing, Telecommunications and Control, 2026, Vol. 19, No. 1, Pp. 103–115. DOI: 10.18721/JCSTCS.19110

Научная статья
DOI: https://doi.org/10.18721/JCSTCS.19110
УДК 622.271:621.31:004.8

МОНИТОРИНГ И ДИАГНОСТИКА ЭЛЕКТРОМЕХАНИЧЕСКИХ СИСТЕМ НА ОСНОВЕ МАШИННОГО ОБУЧЕНИЯ

Ю.Н. Кожубаев ✉

Санкт-Петербургский политехнический университет Петра Великого,
Санкт-Петербург, Российская Федерация

✉ um-urii@mail.ru

Аннотация. Асинхронные двигатели, широко применяемые в электромеханическом оборудовании горных предприятий, подвержены отказам из-за частых пусков, перегрузок и износа, что ведет к авариям и экономическим потерям. Асинхронные двигатели являются одним из основных источников кинетической энергии в промышленности и сельском хозяйстве. Отказ двигателя приводит к остановке технологического процесса и снижению эффективности, поэтому его состояние требует регулярного контроля. Традиционные методы диагностики, основанные на анализе отдельных сигналов и классическом машинном обучении с ручным выбором признаков, недостаточно надежны в переменных условиях эксплуатации и сильно зависят от человеческого фактора. В статье предлагается подход к диагностике неисправностей асинхронных двигателей на основе глубокой остаточной сети с использованием методов анализа сигналов, глубокого и трансферного обучения, а также слияния информации. Реализованы различные стратегии ввода трехфазного тока и построена модель, способная автоматически извлекать информативные глубинные признаки из токового сигнала. Экспериментальные результаты подтверждают, что предложенная модель на основе глубокого обучения обеспечивает более высокую точность диагностики по сравнению с традиционными алгоритмами машинного обучения.

Ключевые слова: диагностика неисправностей двигателя, глубокая остаточная сеть, теория слияния информации, машинное обучение, асинхронные двигатели

Для цитирования: Kozhubaev Yu.N. Monitoring and diagnostics of electromechanical systems based on machine learning // Computing, Telecommunications and Control. 2026. Т. 19, № 1. С. 103–115. DOI: 10.18721/JCSTCS.19110

Introduction

Induction motors are one of the main sources of kinetic energy in industry and agriculture. The failure of the engine leads to a shutdown of the process and a decrease in efficiency; therefore, its condition requires regular monitoring.

Traditionally, performance is assessed by routine inspections and threshold methods of signal analysis, which often leads to “blind” maintenance and late detection of defects. The development of sensor technologies and computing tools makes it possible to implement online diagnostics based on recorded current and other signals, and the use of intelligent algorithms increases the accuracy and stability of diagnostics compared to simple threshold approaches [1]. Motor fault diagnosis technologies can be divided into four groups: based on signals, mechanical theory, models and digital modeling [2–4].

Algorithms based on signals and traditional machine learning are developed by improving the methods of signal detection and processing, but require manual selection of features and a large volume of data [5–7]. Modeling-based approaches use physically justified models of the motor and make it possible to obtain responses in terms of current, vibration, and acoustic parameters that reflect its condition [8–10]. Deep learning, which has become one of the main directions in the processing of technical data, is being actively studied and used in the tasks of diagnosing electric motors [11–13]. At the same time,

existing intelligent algorithms remain sensitive to cross-domain differences and imbalanced samples. In this regard, this paper discusses a method for diagnosing and classifying induction motor states based on deep learning, focused on improving accuracy under various operating conditions with a limited amount of training samples.

Materials and methods

Types of engine faults

If the engine starts and stops frequently, the rotor rods may break due to uneven force [14]. Load changes and voltage drops can also affect the service life, which will lead to rotor failure (Fig. 1).

When a fault occurs, the characteristic frequency expression of the rotor is as follows:

$$f_{bb} = \left(1 \pm 2ks\right) f_1, \tag{1}$$

where s is the sliding speed; f_1 is the power frequency; k is a positive integer.

Air gap between rotor and motor stator is unevenly distributed (Fig. 2).

The simplified expression of the frequency of the fault characteristic is as follows:

$$f_{ag} = f_1 \pm mf_r, \tag{2}$$

where m is a positive integer, m is the rotor speed, and the expression has the form:

$$f_r = \frac{\left(1-s\right) f_1}{p}, \tag{3}$$

where p is the number of pairs of poles of the magnetic field of the motor.

One type of the stator failure is the stator turn-to-turn failure – a common fault in induction motors [15]. It consists of damage to the insulation between two or more adjacent turns of the stator winding, which leads to a current leakage.

When this fault occurs, the stator current waveform is distorted, and harmonic components appear [16–18]. The specific expression of the harmonic component characteristic of the fault is as follows:

$$f_{st} = \left[\frac{n}{p}\left(1-s\right) \pm z\right] f_1 = nf_r \pm zf_1, \tag{4}$$

where $z = 1, 2, 3,...,(2p - 1)$; $n = 1, 3, 5,...$

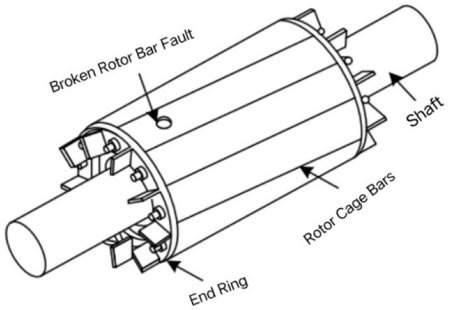

Fig. 1. Broken bar rotor fault diagram

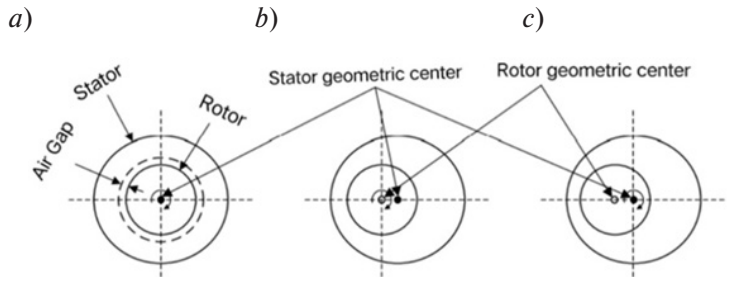

Fig. 2. Air gap eccentricity fault diagram: normal state (*a*), static eccentricity (*b*), dynamic eccentricity (*c*)

Bearings often operate under undesirable conditions, such as prolonged operation, overload, corrosion, and wear, which can easily lead to the failure of various parts of the bearing. At this time, the motor undergoes abnormal vibrations, causing changes in the magnetic field, thereby generating harmonics in the stator current.

Faults in different parts of the bearing will generate vibration information at specific frequencies, and their vibration characteristics differ from one another [19].

Failure of internal ring f_{bi}:

$$f_{bi} = \frac{Nn}{120}\left(1+\frac{d}{D}\cos\alpha\right). \tag{5}$$

Destruction of the outer ring f_{bo}:

$$f_{bo} = \frac{Nn}{120}\left(1-\frac{d}{D}\cos\alpha\right). \tag{6}$$

Failure of rolling elements f_{br}:

$$f_{br} = \frac{n}{120}\left(1-\frac{d}{D}\cos\alpha\right). \tag{7}$$

Cell breakdown f_{bc}:

$$f_{bc} = \frac{Dn}{120d}\left[1-\left(\frac{d}{D}\right)^2\cos^2\alpha\right]. \tag{8}$$

Traditional current signal analysis method

A fast Fourier transform (FFT) analysis of the stator current spectrum is used to identify frequency features. Based on the measured three-phase current, a spectrum is constructed, in which components appear at frequencies corresponding to the types of faults described in the previous section.

Next, a standard sequence of coordinate transformations is applied. First, the Clarke transform is performed, which converts the three-phase stator current into a two-phase orthogonal signal i_α, i_β. Then, using the Park transform, this signal is converted into a synchronously rotating coordinate system *d-q* with an electric angle θ, determined by rotor position. In the *d-q* coordinates, components i_d, i_q and their spectral components at diagnostic frequencies are analyzed, and they are used in the traditional model as fault features.

Convolutional neural networks

Deep learning refers to neural network machine learning methods and is distinguished by the fact that it automatically extracts complex features from data without manual specification. One of the main options is a convolutional neural network (CNN) – a sequence of convolutional and pooling layers followed by fully connected layers. In this article, a CNN is used to extract informative features from the current signals of an induction motor and then diagnose its faults.

CNNs share parameters and employ local receptive field strategies to reduce computation time. Initially, they were used in the field of motor fault diagnostics, either to extract and recognize features, or directly as a classifier. The most typical CNN is LeNet-5 [20].

In addition to the classical LeNet, other convolutional network architectures have been developed, such as AlexNet, VGG, and ResNet, which differ in depth and organization of layers. In this paper, a ResNet network was chosen as the basic model, using residual blocks (skip connections) for sustainable training of deep structures and reducing the risk of overfitting. Such a network includes a series of convolutional layers, multi-level residual modules, and an output fully coupled layer performing motor state classification.

There are eight residual modules in the entire network, and their structure is shown in Fig. 3.

The residual block design is divided into a non-downsampling module and a downsampling module, depending on whether a convolution step change is used. With input X and output Y, the block actually learns the residual mapping (Y–X), which reduces the problem of gradient disappearance with increasing network depth and helps preserve information about the input data.

Residual blocks use batch normalization (BN), which normalizes layer outputs over a small group of training examples. This accelerates convergence, reduces the spread of activation values and increases the network's resistance to changing the distribution of input data.

Engine fault diagnosis system based on deep residual mains

In the diagnosis of electric motors, methods of information fusion are widely used, where data from several sensors or different representations of the same signal are combined. This approach allows expanding the set of failure features and obtaining more reliable classification compared to the analysis of a single data source. A distinction is made between fusion at the data level, feature level, and decision level. This paper uses fusion at the feature level: informative characteristics are extracted from the initial signals, after which they are combined and sent to the classifier input.

Traditional information fusion systems in motor diagnostics usually use shallow networks and do not allow obtaining deep signal features. Here, a deep ResNet-based residual network is applied, that extracts features from current signals and performs classification using a Softmax output layer.

The shapes of stator currents for different types of faults (rotor rod failure, air gap eccentricity, stator turn-to-turn short circuit, bearing defects etc.) differ in amplitude, phase, and waveform structure.

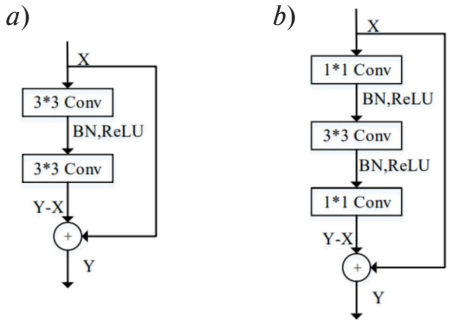

Fig. 3. Residual module architecture (*a*), residual module architecture downsampling (*b*)

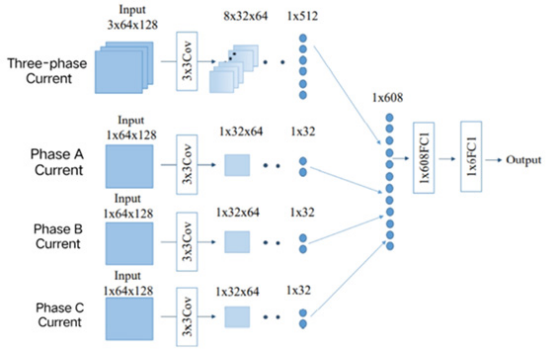

Fig. 4. Third strategy: three-phase current + single-phase current

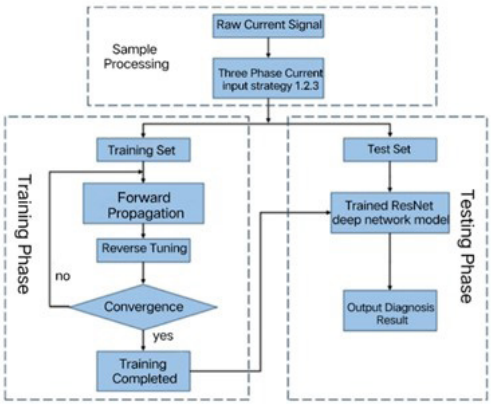

Fig. 5. ResNet deep learning motor fault diagnostic flowchart

These differences are reflected in both time and frequency domains and can be used as features for deep network training.

To assess the effect of the signal representation method, three strategies for introducing three-phase current into the network are considered. In the first strategy, the three-phase current is used as a three-channel input of a single convolutional branch of the network. In the second strategy, phase A, B and C currents are fed to three separate network branches, after which the extracted features are combined. In the third, combined strategy, the three-phase current and the sum of the A+B+C phases are processed by three-channel and single-channel branches, respectively, and then the features are fused in a fully connected layer (the structure is shown in Fig. 4).

The ResNet-based deep learning algorithm for fault diagnosis includes three main stages (Fig. 5). At the first stage, pre-processing and normalization of recorded current signals are performed, and training and test samples are formed for the selected input strategy. At the second stage, ResNet is trained on a training set using a loss function based on the classification results. At the third stage, the trained model is tested on independent data, and the motor state is determined from the output of the Softmax layer and the diagnostic accuracy is evaluated.

Results and discussions

In order to analyze the diagnostic effect of the above diagnostic model, three-phase normal motor stator currents, stator turn-to-turn short circuit, rotor failure, air gap eccentricity, imbalance and bearing failure are collected during stable operation, and 8192 consecutive sampling points are taken as one

sample of current signals. 200 samples of three-phase stator currents are collected for each state at 1200, 1500 and 1800 rpm, and 100 samples are randomly selected to construct a training set. 100 samples are randomly selected to construct a training sample, and the remaining 100 samples are used as a test sample, in which the categories of samples are presented in Table 1.

Rotor rod break, air gap eccentricity, stator turn-to-turn short circuit, bearing defects etc.

Table 1

Description of the experimental sample of the tag

Motor status	Training set	Test kit	Category
Normal	100	100	0
Rotor rod failure	100	100	1
Air gap eccentricity	100	100	2
Stator turn-to-turn short circuit	100	100	3
Power supply imbalance fault	100	100	4
Bearing failure	100	100	5

To verify the efficiency of the proposed algorithms, a three-speed fault classification model is used and three series of experiments are performed:

1. Traditional machine learning: 71 statistical features are extracted from the training and test datasets and fed into an SVM classifier to obtain the results.

2. Deep learning: the diagnostic performance of different current input strategies is compared, the network is trained on processed samples, the results of deep and classical models are compared under three-phase and single-phase current input conditions.

3. Variable modes of operation: 1500 → 1800, 1800 → 2100, and 1500 → 2100 rpm: the results of diagnostics of traditional and deep learning are compared, while the proposed algorithm uses a three-phase current input strategy.

Experimental analysis of a machine learning model

To analyze the capabilities of machine learning to recognize the state of motor failure, 71 statistical features were selected in the article, each feature was fed into SVM for classification after normalization, and, finally, an accuracy indicator was obtained (Table 2).

Table 2

Motor fault diagnosis results based on traditional machine learning

Speed	1500 rpm	1800 rpm	2100 rpm
Diagnostic accuracy	92.17%	92.67%	93.83%

As shown in Table 2, when using traditional machine learning for classification, the diagnostic accuracy depends on the rotation speed, and its values are 92.17% and 93.83%. at 1500 rpm and 2100 rpm, respectively.

When using machine learning for classification, there is a large number of errors in diagnosing motor imbalance faults, errors in diagnosing air gap eccentricity, and errors in diagnosing stator turn-to-turn short circuit for individual samples, while for all other states they can be distinguished directly.

Experimental analysis of deep learning models

Implementing deep learning in the context of motor fault diagnosis does not require signal processing. Feature extraction and other operations may be performed directly on the original current samples as training and test sets for deep learning.

In the training phase, the training sets are used as input to a deep learning network, and the diagnostic results of the current network for the training set are verified by minimizing the loss function. The test phase iteratively calculates the loss function for the test set and determines the accuracy of fault diagnosis for the test set. When the training set losses converge, it means that the network for testing is trained, and the diagnostic accuracy for the test set is the final diagnostic accuracy. Using the example of a speed of 2100 rpm, the parameters and weights of the ResNet deep network model are initialized, a training set at a speed of 2100 rpm is used to train the model, and a test set at the same speed is fed to the network for prediction and diagnosis. The curves of the loss function during the training and testing phases and the accuracy of the model diagnostics are shown in Fig. 6.

As shown in Fig. 6, the training set loss function begins to converge at the 31st iteration, the network loss is close to 0, and the training set validation effect reaches 100%. While the network losses of the test set tend to be stable and the diagnostic accuracy reaches 95.17% after a small fluctuation, i.e., the accuracy of the selected model of diagnosing motor faults based on ResNet deep learning for faults at 2100 rpm reaches 95.17%. Under these conditions, the final classification results from the confusion matrix are shown in Fig. 7. The horizontal coordinate is the real mark of the sample, and the vertical coordinate is the predicted mark.

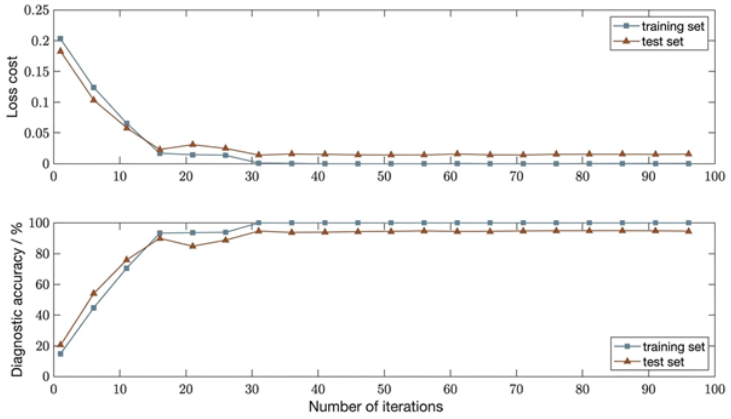

Fig. 6. ResNet deep network model at 2100 rpm

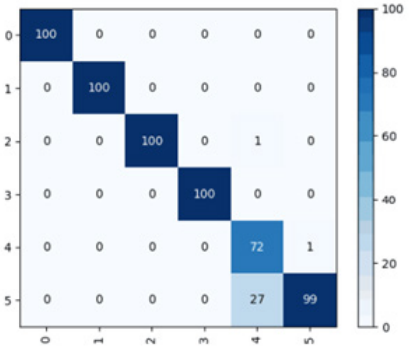

Fig. 7. ResNet deep network model results confusion matrix at 2100 rpm

As shown in Fig. 7, the deep learning model is able to fully identify four motor states: normal, open-circuit faul, eccentricity fault and turn-to-turn short circuit. For bearing failure, very few misclassified examples were observed, and for stator winding imbalance faults, only 72 out of 100 examples were classified correctly, with 27 examples were misdiagnosed as bearing failures.

In deep learning, evaluation metrics for multi-classification fault diagnosis models include micro-averaging (Micro-F1) and macro-averaging (Macro-F1), as well as accuracy and the confusion matrix. In the former case, the Micro-F1 value is calculated based on the total accuracy and metrics across all categories, and in the latter case, the Macro-F1 value is obtained by averaging the F1-Score values for each category. Taking the diagnosis at 2100 rpm as an example, the precision P and the recall R for each category should be calculated first, and the formula is as follows:

$$P = \frac{TP}{TP + FP}; \tag{9}$$

$$R = \frac{TP}{TP + FN}, \tag{10}$$

where TP is true positive, meaning "predicted positive, actual positive"; FP is false positive, meaning "predicted positive, actual negative"; FN is false negative, meaning "predicted negative, actual positive".

The value of F1-Score can be calculated from precision and recall, and the formula is as follows:

$$F_1 = \frac{2}{\frac{1}{P} + \frac{1}{R}} = \frac{2 * P * R}{P + R}. \tag{11}$$

It can be seen that the Micro-F1 is calculated taking into account the number of each category in the sample, which is suitable for imbalanced samples, and also affects classes with a large sample size; while Macro-F1 accounts for each category equally and is influenced by precision and recall rates for different categories. From the above equation, Micro-F1 and Macro-F1 can be calculated as shown in Table 3.

Table 3

Deep learning model score at 2100 rpm

Failure category	TP	FP	FN	P	R	F1
0	100	0	0	100%	100%	1
1	100	0	0	100%	100%	1
2	100	1	0	99%	100%	0.995
3	100	0	0	100%	100%	1
4	72	1	28	99%	72%	0.8324
5	99	27	1	79%	99%	0.8761
General indicators	571	29	29	95%	95%	–

The Micro-F1 and Macro-F1 values of the diagnostic model for this rotation speed are 0.9517 and 0.9506, respectively, which exceeds 0.95, indicating that the constructed deep learning model has excellent performance in multi-classification of motor faults and strong generalizability.

Diagnostic results for different current injection strategies

A diagnostic system with different current input strategies is used to diagnose motor faults at three speeds: 1500 rpm, 1800 rpm and 2100 rpm, and the accuracy of the results is shown in Table 4.

Table 4

Diagnostic results of motor faults based on deep learning at different values of input current

Current input strategy	1500 rpm	1800 rpm	2100 rpm
Three-phase current	94.17%	95.00%	95.17%
Single-phase current (A/B/C)	92.50%	95.50%	94.50%
Three-phase current + single-phase current (A/B/C)	94.67%	95.33%	95.83%

As shown in Table 4, the diagnostic effect of the diagnostic network at 2100 rpm is generally better than under the other two conditions, indicating that motor fault features are more apparent at 2100 rpm. When comparing circuits with different current strategies, the diagnostic accuracy when using three-phase currents and single-phase currents as input for different deep learning networks is higher than when using single-phase currents as input, but the difference in diagnostic results of the first two is small. The diagnostic result of 95.83% is achieved at 2100 rpm, which corresponds to the real requirements for fault diagnosis, and the specific diagnostic results are given in Table 5, which indicates the number of samples with correct prediction results from 100 samples for each condition.

Table 5

Diagnostic results for different current injection strategies at 2100 rpm

Fault type	Three-phase current	Single-phase current (A/B/C)	Three-phase current + single-phase current (A/B/C)
0	100	100	100
1	100	100	100
2	100	99	100
3	100	100	100
4	72	71	76
5	99	97	99
Medium accuracy	95.17%	94.50%	95.83%

As can be seen from Table 5, all current input strategies better differentiate the normal state of the motor, rotor rod failure and stator turn-to-turn short circuit, while for other faults, three-phase and single-phase currents can be fully differentiated in diagnosing air gap eccentricity faults and bearing failures by feeding them into a deep learning network, respectively, and in the case of stator windings, misdiagnosis still occurs, even though the rate of fault diagnosis has improved. For the stator winding, even though the fault diagnosis rate has improved, there are still misdiagnoses, and for the fault winding imbalance in the best diagnostic result of 100 samples, there are 24 misdiagnosed samples, of which 22 samples are predicted as bearing faults.

Comparison of diagnostic outcomes between machine learning and deep learning

For the diagnostic process of machine learning, extraction of the original signal features and extraction of the Park fusion current features correspond to the deep feature extraction of the single-phase and three-phase current in the third deep learning current input strategy, and therefore the results in this

state can be used to directly compare the fault diagnosis results of machine learning and deep learning for motor faults. The results of the comparison are shown in Table 6.

Table 6

Comparison of diagnostic results between traditional machine learning and deep learning model

	1500 rpm	1800 rpm	2100 rpm
Traditional machine learning	92.17%	92.67%	93.83%
Deep learning	95.17%	96.33%	96.83%

As shown in Table 6, the effects of traditional machine learning and deep learning are similar for the three speeds, and the diagnostic accuracy increases as it approaches the rated speed. The diagnostic accuracy of both traditional machine learning and deep learning is lowest at 1500 rpm, while the diagnostic accuracy of deep learning is higher than that of traditional machine learning for all speeds. For traditional machine learning, effective features must be selected manually, and diagnostic accuracy is easily dependent on the selected features, but the deep ResNet model can avoid this disadvantage. Thus, the deep ResNet network has potential for practical application in the diagnosis of numerous faults in electrical machines.

Conclusion

Induction motors are used in various industries and their safe operation affects the stability of the entire system. However, due to frequent starts and stops, as well as long-term use, the probability of faults increases; therefore, diagnosing failures and determining the state of induction motors is of great importance. With the development of diagnostic technologies, AI methods are being increasingly used in the field of equipment diagnostics. This article considers an induction motor with a squirrel-cage rotor as an object of research, the current state of motor fault diagnosis and the problems it faces are analyzed, and the method for recognizing the state of an induction motor under variable operating conditions based on deep learning methods and information fusion of current signals is investigated.

The article provides an analysis of causes of various faults and characteristic frequencies of faults in motors. On the basis of FFT and Park conversion, the manifestation of faults in current signals is considered. A stand with a real induction motor was built, current signals were collected in six different states. Deep learning theory is then generalized, and ResNet-based deep network is considered as the primary tool for motor state classification, utilizing the fact that several residual modules allow reduced network learning complexity and improved feature extraction.

It is evident that conventional signal analysis and machine learning methodologies require expert knowledge to extract a variety of statistical features that describe fault information. In this regard, this paper proposes a method for diagnosing faults in electric motors based on a deep residual network. It is shown that three-phase current carries different diagnostic information; therefore, several three-phase current input strategies have been developed. These strategies are used in combination with a deep ResNet network for deep feature extraction and state classification. Based on the deep ResNet network, a model for diagnosing motor faults is built, which combines the processing of three-phase current and its single-phase combination. The results of the experiments show that the diagnostic accuracy of entering three-phase and single-phase current data into the ResNet multi-branch deep learning network, which performs feature extraction and fusion, outperforms alternative strategies. The accuracy of diagnostics at three speeds is 94.67%, 95.33% and 95.83%, respectively, which confirms the effectiveness of using deep learning for fault diagnosis of induction motors.

REFERENCES

1. **Koteleva N.I., Korolev N.A., Zhukovskiy Y.L.** Identification of the technical condition of induction motor groups by the total energy flow. *Energies*, 2021, Vol. 14, No. 20, Art. no. 6677. DOI: 10.3390/en14206677

2. **Zhang F., Chen L., Dai Y., Kou L., Ji P., Liu Y.** Bearing fault diagnosis based on convolution neural network with logistic chaotic map. *Advanced Theory and Simulations*, 2024, Vol. 7, No. 5, Art. no. 2301090. DOI: 10.1002/adts.202301090

3. **Lan Y., Wang Y.** Application of sparse representation based on novel K-SVD algorithms in mechanical fault diagnosis. *2019 Prognostics and System Health Management Conference* (*PHM-Qingdao*), 2019, Pp. 1–5. DOI: 10.1109/phm-qingdao46334.2019.8942808

4. **Wang X., Liu X., Song P., Li Y., Qie Y.** A novel deep learning model for mechanical rotating parts fault diagnosis based on optimal transport and generative adversarial networks. *Actuators*, 2021, Vol. 10, No. 7, Art. no. 146. DOI: 10.3390/act10070146

5. **Klyuev R.V., Morgoeva A.D., Gavrina O.A., Bosikov I.I., Morgoev I.D.** Forecasting planned electricity consumption for the united power system using machine learning. *Journal of Mining Institute*, 2023, Vol. 261, Pp. 392–402.

6. **Zemenkova M.Yu., Chizherskaya E.L., Zemenkov Yu.D.** Intelligent monitoring of the condition of hydrocarbon pipeline transport facilities using neural network technologies, *Journal of Mining Institute*, 2022, Vol. 258, Pp. 933–944. DOI: 10.31897/PMI.2022.105

7. **Zhukovskiy Yu.L., Korolev N.A., Malkova Ya.M.** Monitoring of grinding condition in drum mills based on resulting shaft torque. *Journal of Mining Institute*, 2022, Vol. 256, Pp. 686–700. DOI: 10.31897/PMI.2022.91

8. **Manap M., Nikolovski S., Skamvin A., Karim R., Sutikno T., Jopri M.H.** An analysis of voltage source inverter switches fault classification using short time Fourier transform. *International Journal of Power Electronics and Drive Systems* (*IJPEDS*), 2021, Vol. 12, No. 4, Pp. 2209–2220. DOI: 10.11591/ijpeds.v12.i4.pp2209-2220

9. **Nayana B.R., Geethanjali P.** Analysis of statistical time-domain features effectiveness in identification of bearing faults from vibration signal. *IEEE Sensors Journal*, 2017, Vol. 17, No. 17, Pp. 5618–5625. DOI: 10.1109/JSEN.2017.2727638

10. **Dang Z., Lv Y., Li Y., Wei G.** A fault diagnosis method for one-dimensional vibration signal based on multiresolution tlsDMD and approximate entropy. *Shock and Vibration*, 2019, Vol. 2019, No. 1, Art. no. 262818. DOI: 10.1155/2019/3262818

11. **Muratbakeev E., Kozhubaev Yu., Yao Y., Shehzad U.** Symmetrical modeling of physical properties of flexible structure of silicone materials for control of pneumatic soft actuators. *Symmetry*, 2024, Vol. 16, No. 6, Art. no. 750. DOI: 10.3390/sym16060750

12. **Efimov I., Gabdulkhakov R.R., Rudko V.A.** Fine-tuned convolutional neural network as a tool for automatic microstructure analysis of petroleum and pitch cokes. *Fuel*, 2024, Vol. 376, Art. no. 132725. DOI: 10.1016/j.fuel.2024.132725

13. **Zhao R., Yan R., Chen Z., Mao K., Wang P., Gao R.X.** Deep learning and its applications to machine health monitoring: A survey. *arXiv:1612.07640*, 2016. DOI: 10.48550/arXiv.1612.07640

14. **Nor N.M., Hassan C.R.C., Hussain M.A.** A review of data-driven fault detection and diagnosis methods: applications in chemical processes. *Reviews in Chemical Engineering*, 2020, Vol. 36, Pp. 513–553. DOI: 10.1515/revce-2017-0069

15. **Krylov S., Makhovikov A., Korobitcyna M.** Novel approach to collect and process power quality data in medium-voltage distribution grids. *Symmetry*, 2021, Vol. 13, Pp. 460–460. DOI: 10.3390/sym13030460

16. **Van Tung L., Long P.T., Van An N., Vasilev B.** Compare the efficiency of the active filter and active rectifier to reduce harmonics and compensate the reactive power in frequency controlled electric drive systems. In: *Advances in Engineering Research and Application* (*ICERA 2020*) (eds. KU. Sattler, D.C. Nguyen, N.P. Vu, B.T. Long, H. Puta), 2021, Vol. 178, Pp. 242–253. DOI: 10.1007/978-3-030-64719-3_28

17. **Shklyarskiy Ya.E., Lobko K.K., Kuznetsova Yu.N., Vorobyov M.S.** Investigation of the Composite Motor Load in the Presence of Higher Harmonics in the Electrical Network. *ENERGETIKA. Proceedings of CIS higher education institutions and power engineering associations*, 2024, Vol. 67, No. 4, Pp. 285–299. DOI: 10.21122/1029-7448-2024-67-4-285-299

18. **Sychov Yu.A., Aladin M.E., Serikov V.A.** Developing a hybrid filter structure and a control algorithm for hybrid power supply. *International Journal of Power Electronics and Drive Systems* (*IJPEDS*), 2022, Vol. 13, No. 3, Pp. 1625–1634. DOI: 10.11591/ijpeds.v13.i3.pp1625-1634

19. **Serikov V.A., Kostin V.N., Sychev Yu.A., Haidar Samet.** Evaluation method of power quality in mine supply systems with high-powered high-voltage variable frequency drives. *Mining Informational and Analytical Bulletin*, 2024, Vol. 12, Pp. 162–177. DOI: 10.25018/0236_1493_2024_12_0_162

20. **Wei D., Miura T.** A super-zoom algorithm for envelope peak position resolution using discrete Fourier transform with multiple-warped time-sampling point calculations. *Results in Optics*, 2023, Vol. 11, Art. no. 100422. DOI: 10.1016/j.rio.2023.100422

INFORMATION ABOUT AUTHOR / СВЕДЕНИЯ ОБ АВТОРЕ

Yuriy N. Kozhubaev
Кожубаев Юрий Нургалиевич
E-mail: um-urii@mail.ru
ORCID: https://orcid.org/0009-0006-1822-7117

Submitted: 10.01.2026; Approved: 06.03.2026; Accepted: 27.03.2026.
Поступила: 10.01.2026; Одобрена: 06.03.2026; Принята: 27.03.2026.